

Resistance mechanism to Notch inhibition and combination therapy in human T cell acute lymphoblastic leukemia

Présentée le 20 avril 2023

Faculté des sciences de la vie
Unité du Prof. Radtke
Programme doctoral en approches moléculaires du vivant

pour l'obtention du grade de Docteur ès Sciences

par

Linlin CAO

Acceptée sur proposition du jury

Prof. E. Oricchio, présidente du jury
Prof. F. Radtke, directeur de thèse
Dr A. Trumpp, rapporteur
Dr J. Meijerink, rapporteur
Dr B. Deplancke, rapporteur

Abstract

T cell acute lymphoblastic leukemia (T-ALL) is an aggressive hematological malignancy caused by acquisition of genetic alterations during T-cell development. The 5-year overall survival of pediatric T-ALL patients has improved considerably over the past 30 years, largely attributed to improved risk-based stratification and the application of aggressive combination chemotherapies. Classical chemotherapy treatment, however, proves inadequate when treating relapsed and refractory T-ALL, necessitating the development of novel therapeutic strategies.

NOTCH1 was identified as one of the most frequently mutated genes in T-ALL and was found often mutated in other cancers. This finding boosted the development of a spectrum of Notch-targeting therapies. These include neutralizing antibodies against Notch receptors and ligands as well as γ -secretase inhibitors (GSI) that prevent NOTCH receptor cleavage. Previously, we identified and validated a novel orally active small molecule (CB-103) that efficiently blocks the Notch transcription activation complex.

Although novel therapeutics blocking Notch signaling show promising outcomes, it is well-known that the use of mono-therapies often results in relapse due to tumor heterogeneity or therapy-induced resistance. Thus, a better understanding of resistance mechanisms to Notch inhibitors and the development of combination therapies will facilitate effective treatment of T-ALL patients.

Here, we performed a genome-wide CRISPR-Cas9 screen in human T-ALL cells and identified the *Phosphoinositide-3-Kinase regulatory subunit 1* (*PIK3R1*) as a key player in NOTCH-targeting treatment response. Mutational loss of *PIK3R1* activity confers resistance to pharmacological Notch inhibition. Unbiased transcriptomic and proteomic analyses in *PIK3R1*-deficient T-ALL cells revealed PI3K-AKT mediated upregulation of pro-survival and proliferation pathways, along with alterations of the spliceosome machinery in response to Notch inhibition. Moreover, we identified and validated a variety of combination therapies, which resulted in reduced tumor burden and prolonged survival in a preclinical xenograft T-ALL model. Overall, our study identified novel resistance mechanisms to pharmacological Notch inhibition and

combination strategies capable of more efficient treatment of refractory or relapsed T-ALL patients.

Keywords: Notch1, T-ALL, PIK3R1, resistance mechanism, combination therapy.

Résumé

La leucémie lymphoblastique aiguë de type T (LLA-T) est une maladie cancéreuse hématologique agressive, causée par l'acquisition d'altérations génétiques pendant le développement des cellules T. L'espérance de vie des patients pédiatriques atteints de LLA-T au cours des 5 ans suivant le diagnostic s'est grandement améliorée au cours des 30 dernières années, en grande partie grâce à une meilleure stratification des risques et à l'application de chimiothérapies combinées agressives. Cependant, les traitements de chimiothérapie classiques se montrent moins efficaces pour le traitement de LLA-T en rechute ou réfractaires, exigeant ainsi l'implémentation de nouvelles stratégies thérapeutiques.

NOTCH1 a été identifié comme étant l'un des gènes les plus fréquemment mutés dans la LLA-T, et est souvent muté dans d'autres cancers. Cette découverte a stimulé le développement d'une gamme de thérapies ciblant la voie de signalisation Notch. Ces thérapies comprennent des anticorps neutralisants contre les récepteurs et ligands Notch, ainsi que des inhibiteurs de la γ -sécrétase qui empêchent le clivage du récepteur NOTCH. Nous avons précédemment identifié et validé une nouvelle petite molécule active par voie orale (CB-103), qui bloque de manière efficace l'activation du complexe de transcription de Notch.

Bien que de nouvelles thérapies bloquant la signalisation Notch montrent des résultats prometteurs, il est bien connu que l'utilisation de monothérapies mène souvent à des rechutes dues à l'hétérogénéité des tumeurs ou à la résistance aux traitements. Par conséquent, une meilleure compréhension des mécanismes de résistance aux inhibiteurs de Notch et le développement de thérapies combinées faciliteront un traitement efficace des patients atteints de LLA-T.

Ici, nous avons effectué un criblage CRISPR-Cas9 ciblant l'entièreté du génome humain sur des cellules LLA-T humaines et avons identifié la sous-unité régulatrice 1 de la phosphoinositide 3-kinase (*PIK3R1*) comme étant un élément clé de la réponse aux traitements ciblant la voie de signalisation Notch. La perte de l'activité de la *PIK3R1* suite à une mutation de type perte de fonction confère aux cellules une résistance à l'inhibition pharmacologique de la voie Notch. Des analyses

transcriptomiques et protéomiques non biaisées effectuées sur des cellules LLA-T déficientes pour *PIK3R1* ont révélé des voies de survie et de prolifération régulées positivement par PI3K-AKT, ainsi que des altérations du mécanisme d'épissage en réponse à l'inhibition de la voie Notch. De plus, nous avons identifié et validé toute une série de thérapies combinées qui mènent à une réduction de la croissance tumorale et à augmentation de l'espérance de vie chez des modèles précliniques de xénogreffes de cellules LLA-T. En conclusion, notre étude nous a permis d'identifier de nouveaux mécanismes de résistance à l'inhibition pharmacologique de Notch, ainsi que des stratégies combinées permettant un traitement plus efficace des patients atteints de LLA-T qui sont en rechute ou réfractaires.

Mots-clés: Notch1, T-ALL, PIK3R1, résistances au traitement, thérapies combinées.

Table of Contents

Abstract	3
Résumé	5
List of Figures	10
List of Tables	12
Abbreviations	13
1. Introduction	16
1.1. Hematopoiesis and T cell development	16
1.1.1. Hematopoiesis.....	16
1.1.2. T cell development.....	18
1.2. The Notch signaling pathway	19
1.2.1. Notch signaling.....	19
1.2.2. Notch signaling in T cell development	22
1.2.3. Notch signaling in cancer.....	22
1.3. T cell acute lymphoblastic leukemia (T-ALL)	23
1.3.1. T-ALL disease.....	23
1.3.2. Genetic landscape of T-ALL	25
1.3.3. Notch signaling in T-ALL	26
1.3.4. T-ALL treatment options.....	27
1.4. Resistance to cancer therapy	32
1.4.1. General resistance mechanisms and solutions.....	32
1.4.2. Known resistance mechanisms to chemotherapy in T-ALL.....	35
1.4.3. Resistance to Notch-targeted therapy in T-ALL	36
2. Aims of the thesis	38
3. Materials and methods	39
3.1. Cell culture and cell lines	39
3.2. Lentiviral transduction	39
3.3. Stable cell line generation	39
3.2.1. Generation of knockout cell lines by CRISPR/Cas9 using lentiviral transduction.....	39
3.2.2. Generation of knockout cell lines by CRISPR/Cas9 through ribonucleoprotein (RNP) delivery.	40
3.2.3. Generation of stable knockdown cell lines through shRNA.....	40
3.3. Proliferation assay	40
3.4. Cell cycle assay	41
3.5. Apoptosis assay	41
3.6. Immunoblotting	41
3.7. <i>In vitro</i> synergy analyses	41
3.8. Animals and <i>in vivo</i> xenotransplantation	42
3.8.1. <i>In vivo</i> xenotransplantation.....	42
3.8.2. Animal treatment	42
3.9. CRISPR/Cas9 screen and analysis	43

3.9.1. CRISPR/Cas9 screen.....	43
3.9.2. Screen analysis.....	44
3.10. RNA-seq and analysis.....	44
3.10.1. RNA-seq and differential gene expression	44
3.10.2. Differential transcript expression	45
3.10.3. Differential exon usage	46
3.11. Proteomics and analysis.....	46
3.11.1. Sample preparation	46
3.11.2. Mass spectrometry analyses and data processing	47
3.11.3. Phosphosite visualization and pathway enrichment analysis.....	49
3.12. Software	49
3.13. Data Availability	50
4. Results	51
4.1. Genome-wide CRISPR screen identifies <i>PIK3R1</i> associated with resistance to pharmacological Notch inhibition in T-ALL	51
4.2. Loss of <i>PIK3R1</i> renders T-ALL cells resistant to pharmacological Notch inhibition	54
4.3. <i>PIK3R1</i> deficiency leads to elevated gene expression of proliferation and pro-survival pathways in response to Notch inhibition.....	57
4.4. Notch-inhibited <i>PIK3R1</i>-mutant T-ALL cells reveal major phosphorylation changes in the cell cycle and spliceosome machinery.....	60
4.5. Pharmacological Notch inhibitors synergize with targeted therapies in human T-ALL cells <i>in vitro</i>	69
4.6. Pharmacological Notch inhibitors synergize with targeted therapies in a human T-ALL cell line xenografted model	71
5. Conclusion and discussion	75
5.1. Mutation loss of <i>PIK3R1</i> induces resistance to Notch inhibition in T-ALL	75
5.2. Increased PI3K/AKT signaling regulates the cell cycle and spliceosome machinery at the transcriptional and post-translational level	77
5.3. Pharmacological Notch inhibition synergizes with CDK4/6 inhibitors in T-ALL	78
5.4. Limitations of this project	80
5.4.1. Identification of other potential biomarkers of response to Notch inhibition in clinics.....	80
5.4.2. Systematic analysis of alternative splicing upon increased PI3K signaling in T-ALL cells in response to Notch inhibition	81
5.4.3. Further exploration of molecular resistance mechanism by <i>PIK3R1</i> loss to Notch inhibition in T-ALL	82
5.4.4. Significance of <i>PIK3R1</i> loss to Notch inhibition in primary T-ALL cells.....	83
5.5. Future Perspectives	84
5.5.1. Further exploration of the mechanism how loss of <i>PIK3R1</i> may cause resistance to Notch inhibitor in T-ALL	84

5.5.2. Further exploration of the consequence of <i>PIK3R1</i> loss to Notch inhibitor resistance in primary T-ALL cells.	85
6. Annex.....	86
7. Bibliography.....	92
Acknowledgements.....	111
CV.....	113

List of Figures

Figure 1. Hematopoiesis in humans. _____	17
Figure 2. Early T cell development in mice. _____	19
Figure 3. Canonical Notch signaling pathway. _____	21
Figure 4. Stages of early T cell development and T-ALL subtypes. _____	24
Figure 5. Mutational landscape of pediatric T-ALL patients. _____	25
Figure 6. Schematic representation of <i>NOTCH1</i> mutations identified in T-ALL patients. ____	27
Figure 7. A simplified view of resistance mechanisms in cancers. _____	32
Figure 8. Functional genome-wide CRISPR screen identifies <i>PIK3R1</i> associated with resistance to Notch inhibition and druggable candidate pathways for combination therapies in T-ALL. 52	
Figure 9. Genome-wide CRISPR screen reveals key candidate pathways synergistic with Notch inhibition. _____	53
Figure 10. Total protein analyses in stable <i>PIK3R1</i> knockout or knockdown T-ALL cells. ____	54
Figure 11. Loss of <i>PIK3R1</i> leads to resistance to Notch inhibition in T-ALL cells. _____	55
Figure 12. Loss of <i>PIK3R1</i> protects T-ALL cells from cell cycle arrest induced by Notch inhibition. _____	56
Figure 13. Loss of <i>PIK3R1</i> protects T-ALL cells from apoptosis induced by Notch inhibitor CB-103. _____	56
Figure 14. Experimental design and overview results of RNA-seq study. _____	58
Figure 15. RNA-seq analysis of <i>PIK3R1</i> KO cells reveals responses to Notch inhibition at transcriptional level. _____	59
Figure 16. Experimental design and overview of total proteomics and phosphoproteomics study. _____	61
Figure 17. Pathway enrichment analysis reveals key signaling changes in <i>PIK3R1</i> deficient cells in response to Notch inhibition. _____	63
Figure 18. Kinase-Substrate-Enrichment-Analysis reveals differential kinase activities in <i>PIK3R1</i> deficient cells in response to Notch inhibition. _____	64
Figure 19. Loss of <i>PIK3R1</i> in T-ALL cells causes major phosphorylation changes in the cell cycle regulation pathway. _____	65
Figure 20. RNA splicing is altered in <i>PIK3R1</i> KO cells in response to Notch inhibition. ____	67
Figure 21. A proposed model summarizing the key nodes mediating resistance to Notch	

inhibition upon loss of <i>PIK3R1</i> . _____	69
Figure 22. <i>In vitro</i> synergy between Notch inhibitors and a CDK4/6 inhibitor. _____	71
Figure 23. Combination of Notch inhibitors and multiple targeted therapies lead to decreased tumor burden and prolonged survival in a human T-ALL cell line xenograft model. _____	72

List of Tables

Table 1. Classification of T-ALL risks _____	28
Table 2. A summary of promising targeted therapies in T-ALL currently under pre-clinical or clinical investigations. _____	29
Table 3. Challenges of immune checkpoint blockade (ICBs) and possible strategies to synergize with ICBs. _____	35
Table 4. <i>In vitro</i> synergy between Notch inhibitors and multiple targeted therapies identified from the CRISPR screen. _____	71
Annexed Table 5. List of oligos used in this study _____	86
Annexed Table 6. List of antibodies used in this study _____	89
Annexed Table 7. List of drugs used in this study _____	91

Abbreviations

- 7-AAD – 7-Aminoactinomycin D
- ANOVA – analysis of variance
- BlaR – Blasticidin resistant
- Cerebrospinal Fluid – CSF
- CI – Combination Index
- CLP – common lymphoid progenitor
- CMP – common myeloid progenitor
- CPM – counts per million
- CRISPR – Clustered Regularly Interspaced Short Palindromic Repeats
- DLL – delta-like ligand
- DMSO – Dimethyl sulfoxide
- DN – double negative (CD4⁻ CD8⁻)
- DNA – deoxyribonucleic acid
- DP – double positive (CD4⁺ CD8⁺)
- EDTA – Ethylenediaminetetraacetic acid
- EPFL – École Polytechnique Fédérale de Lausanne
- ETP – early thymic progenitor
- FACS – fluorescence-activated cell sorting
- FBS – Fetal bovine serum
- FDR – false discovery rate
- FWD – Forward
- GeCKO – Genome-Scale CRISPR Knock-out
- GFP – green fluorescent protein
- GOBP – Gene Ontology biological process
- GoF – Gain of function
- GSEA – Gene Set Enrichment Analysis

- GSI – γ -secretase inhibitor
- HD – heterodimeric domain
- HSC – hematopoietic stem cell
- KD – knockdown
- KEGG – Kyoto Encyclopedia of Genes and Genomes
- KO – knockout
- KSEA – Kinase-Substrate Enrichment Analysis
- LoF – Loss-of-function
- Luc – Luciferase
- mAb – monoclonal antibody
- MAML – mastermind-like
- MHC – Major Histocompatibility complex
- MPP – multipotent progenitor
- MS – Mass Spectrometry
- NGS – Next Generation Sequencing
- NICD – Notch intracellular domain
- NSG mice – NOD Scid Gamma (immunodeficient) mice
- NT – non-targeting sgRNA control
- ORA – over-representation analysis
- P2A – 2A self-cleaving peptides
- PBS – Phosphate-buffered saline
- PCR – polymerase chain reaction
- PEST – Proline/glutamic acid/serine/threonine-rich motif
- PI – Propidium Iodide
- REV – Reverse
- RNA – ribonucleic acid
- RNP - ribonucleoprotein

- RRA – Robust Rank Aggregation
- scr – scrambled shRNA control
- scRNA – small conditional RNA
- sgRNA – single-guide RNA
- shRNA – short-hairpin RNA
- SP – single positive
- STRING – Search Tool for the Retrieval of Interacting Gene/Proteins
- T-ALL – T cell acute lymphoblastic leukemia
- TBP – TATA-binding protein
- TCR – T cell receptor
- TF – transcription factor
- TMT – Tandem Mass Tag
- TPM – transcripts per million
- tracrRNA – Trans-activating CRISPR RNA
- WGS – Whole-genome Sequencing

1. Introduction

1.1. Hematopoiesis and T cell development

1.1.1. Hematopoiesis

Hematopoiesis is the formation of blood cells. In vertebrates, there are two developmental stages of hematopoiesis: primitive and definitive hematopoiesis¹. Primitive hematopoiesis starts on embryonic Day 7.5 (E7.5) in mice and around day 14 in humans^{2,3}. It occurs in the yolk sac and features the generation of abundant erythrocytes and small numbers of primitive macrophages, mainly to facilitate rapid growth in terms of oxygen needs during embryonic development⁴. On E10.5 in mice and around week 4-5 in humans, the transition from primitive to definitive hematopoiesis occurs^{3,5-7}. Definitive Hematopoietic Stem Cells (HSCs) emerge from the aorta-gonad-mesonephros (AGM) region, from which HSCs and progenitors subsequently colonize fetal liver, and eventually the bone marrow to support adult hematopoiesis^{5,7,8}. HSCs are multipotent stem cells that give rise to all types of blood cells constituting the entire definitive hematopoietic system⁹.

HSCs, by the definition of being stem cells, have the potential of both self-renewal and differentiation. In a classical view¹⁰ (Figure 1), HSC can give rise to Common Myeloid Progenitor (CMP) and Common Lymphoid Progenitor (CLP). CMP subsequently can develop into three lineages: 1) Megakaryoblasts that will develop into thrombocytes (platelets), which are involved in wound healing and blood coagulation; 2) Pro-erythroblasts that will generate erythrocytes through erythropoiesis; and 3) Myeloblasts that eventually give rise to basophils, neutrophils, eosinophils as well as macrophages and myeloid dendritic cells, which are involved in innate immunity. CLP, on the other hand, can produce T and B lymphocytes, which are predominantly involved in adaptive immunity, as well as Natural Killer (NK) and lymphoid dendritic cells.

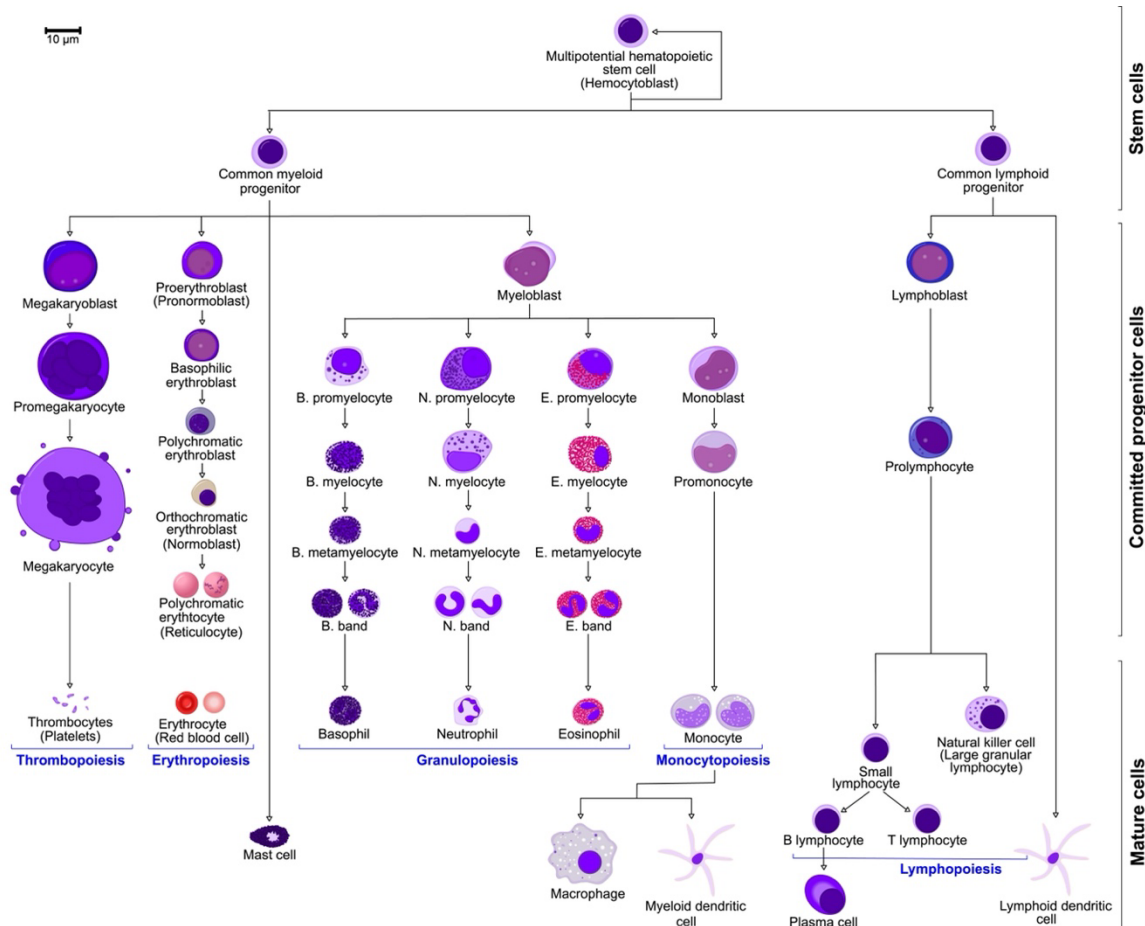


Figure 1. Hematopoiesis in humans.

A simplified model of human Hematopoiesis is shown. Hematopoietic Stem Cells can give rise to Common Myeloid Progenitors (CMPs) and Common Lymphoid Progenitors (CLPs). CMPs will eventually develop into thrombocytes, erythrocytes, basophils, neutrophils, eosinophils, macrophages, and myeloid dendritic cells. CLPs will give rise to T lymphocytes, B lymphocytes, Natural Killer cells and lymphoid dendritic cells. The figure is adapted from M. Häggström and A. Rad (Wikimedia Commons 2016)¹⁰.

HSCs can be further subdivided into Long-Term HSCs (LT-HSCs) and Short-Term HSCs (ST-HSCs). LT-HSCs possess a long lifespan and have the highest self-renewal potential, while ST-HSCs may retain self-renewal capacity for approximately 8-12 weeks^{11,12}. Further downstream of these are multipotent progenitors (MPPs)¹³, which are multipotent yet with diminished self-renewal capacity. A transposon-based analysis reports that MPPs are the main drivers of native hematopoiesis (at steady-state)¹⁴, yet other clonal analyses favor a model that homeostatic hematopoiesis may actually be polyclonal and originate from lineage-biased clonal pools^{15,16}. In the future, a combination of efficient clonal labelling (diverse clonal barcodes) and high-resolution tracing (for example via single-cell RNA-seq overtime) may provide more accurate views of clonality of the hematopoietic system^{12,17}.

In addition to the classical hierarchy model of hematopoiesis, which was largely developed by Weissman and colleagues, more recent studies helped to shape complementary views of hematopoiesis. One view based on single-cell transcriptome analyses is that hematopoiesis is likely to be a continuous differentiation process without clear developmental boundary in the hierarchy^{12,17,18}. Also, the boundary between myeloid and lymphoid lineages is less definitive¹².

1.1.2. T cell development

Our knowledge of early T cell development is mainly based on studies in mice and summarized in Figure 2¹⁹. When CLPs enter the thymus from blood vessel and encounter growth and survival signals including Notch ligands, FLT3 ligand, KIT ligand and IL-7, they develop into immature/early T cell progenitors (ETP, or DN1) and later enter a stage called double-negative2 (DN2) as the cells lack expression of both coreceptor CD4 and CD8. These pro-T cells then undergo T cell lineage commitment by expressing CD3 complexes and recombinases RAG1 and RAG2, followed by T cell receptor (TCR) rearrangement ($\gamma\delta$ chain, and V-DJ β gene arrangement). For $\alpha\beta$ precursors, a successful TCR β gene rearrangement is verified to ensure the formation of functional pre-TCR by pairing TCR β and pre-T α (β -selection). The DN3 cells that failed to do so will undergo apoptosis. Following β -selection, the thymocytes undergo a proliferation boost and progress to DN4 and immature single-positive (ISP) stage to the subsequent double-positive (DP) stage. At this point, CD4⁺CD8⁺ cells undergo TCR α gene rearrangement, and positive and negative selection based on their TCR $\alpha\beta$ specificity. The survival and further development of DP thymocytes is largely dependent on the interaction of the TCR and self-antigen presenting Major Histocompatibility Complex (MHC) molecules. DP cells bearing TCRs that do not recognize any antigen-MHC complexes, will undergo apoptosis, a process called death by neglect. DP thymocytes with TCRs that have too strong binding avidities to antigen-MHC complexes are negatively selected and eliminated by apoptosis, as they otherwise would cause autoimmunity. Only DP thymocytes bearing TCRs with intermediate binding avidities will be positive selected, survive and continue to differentiate into either CD8⁺ (cytotoxic) cells or CD4⁺ (helper) cell fates depending on

their interaction with MHC complexes: thymocytes recognizing MHC class I will downregulate CD4 to become CD8⁺ cells and the ones recognizing MHC class II will commit to CD4⁺ lineage. Regulatory T cells are considered to be derived from CD4⁺ cells²⁰.

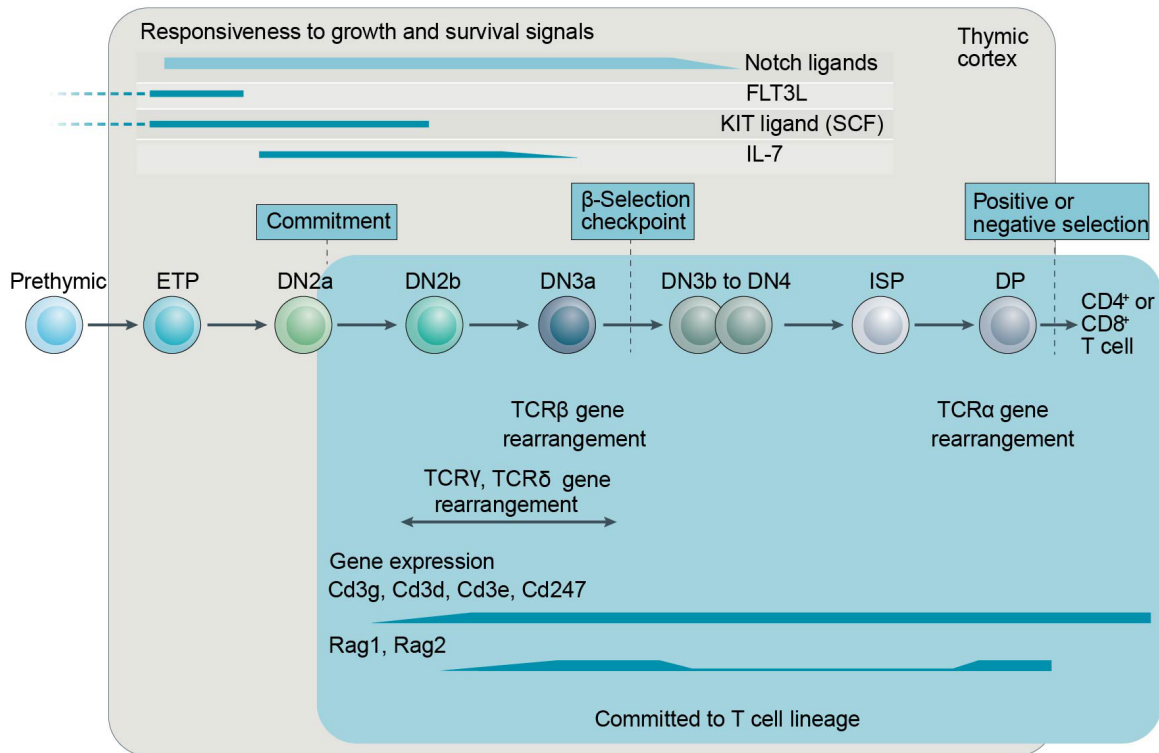


Figure 2. Early T cell development in mice.

Developmental stages of murine thymocytes are shown, including stages defining T cell commitment, β-selection, positive or negative selection. The approximate timeline of T Cell Receptor gene arrangements is shown, and expression of key genes are depicted. The figure is adapted from H. Hosokawa and E. Rothenberg (Nature Review Immunology 2021)¹⁹.

1.2. The Notch signaling pathway

1.2.1. Notch signaling

The Notch pathway is a highly conserved signaling cascade that mediates cell-to-cell signaling thereby regulating multiple processes during development and tissue homeostasis in the adult²¹. Notch signaling is involved in cell proliferation, differentiation and survival²¹.

Unlike other conserved signaling pathway, the Notch pathway requires initiation by ligand-receptor interaction between a signal-sending and a neighboring signal-

receiving cell (Figure 3). In mammals, the currently known Notch ligands are categorized as: 1) DSL (Delta/Serrate/LAG-2) ligands including Jagged1/Jagged2 and Delta-like (DLL) ligands; 2) DOS (Delta and OSM-11-like) ligands; and 3) non-canonical ligands.

While *Drosophila melanogaster* has one and *Caenorhabditis elegans* two Notch receptors, there are four Notch receptor paralogs (Notch1-4) in mammals. In brief, Notch receptor contains an extracellular domain consisting of EGF repeats (29-36) followed by a Negative regulatory region (NRR), a transmembrane domain (TMD), and the intracellular domain (NICD) harboring an RBP_J association module (RAM) domain, a domain with 6 ankyrin repeats (ANK), two nuclear localization sequences (NLS), and a C-terminal Proline/glutamic acid/serine/threonine-rich motifs (PEST). EGF repeats mediate ligand interactions. NRR contains Lin12-Notch repeats (LNR) and a heterodimerization domain (HD), which is important for preventing ligand-independent activation of the receptors. The RAM and ANK domain help to associate with the transcription factor RBP-J (also known as CSL). The PEST domain is recognized by E3 ubiquitin ligase and ensures a short half-life of the activated Notch intracellular domain.

In mammals, Notch proteins are first cleaved in the Golgi by Furin proteases at site 1 (S1) during their transport to the cell surface. This cleavage generates a heterodimeric receptor consisting of an extracellular subunit that is noncovalently linked to a second subunit containing the extracellular heterodimerization domain and the transmembrane domain followed by the cytoplasmic region of the Notch receptor. Upon ligand binding, a series of proteolytic cleavage events are triggered. The first of which is mediated by metalloproteases of the ADAM family (ADAM-10 or ADAM-17) at site 2 (S2), located 12-13 amino acids external to the transmembrane domain. Subsequently, the γ -secretase multi-protein complex cleaves the remaining Notch receptor within the transmembrane domain at site 3-4 (S3-4), resulting in the release of the intracellular cytoplasmic domain of Notch (NICD). NICD subsequently translocates to the nucleus. The RAM domain of Notch interacts with the DNA-binding protein RBP-J (also known as CSL), and the ANK domain of Notch associates with RBP-J to recruit other coactivators including mastermind like proteins (MAML1-3), p300 and many other proteins. Thus, the binding of NICD to RBP-J results in a short-

lived transcription activation complex to induce transcription of downstream target genes²¹⁻²³.

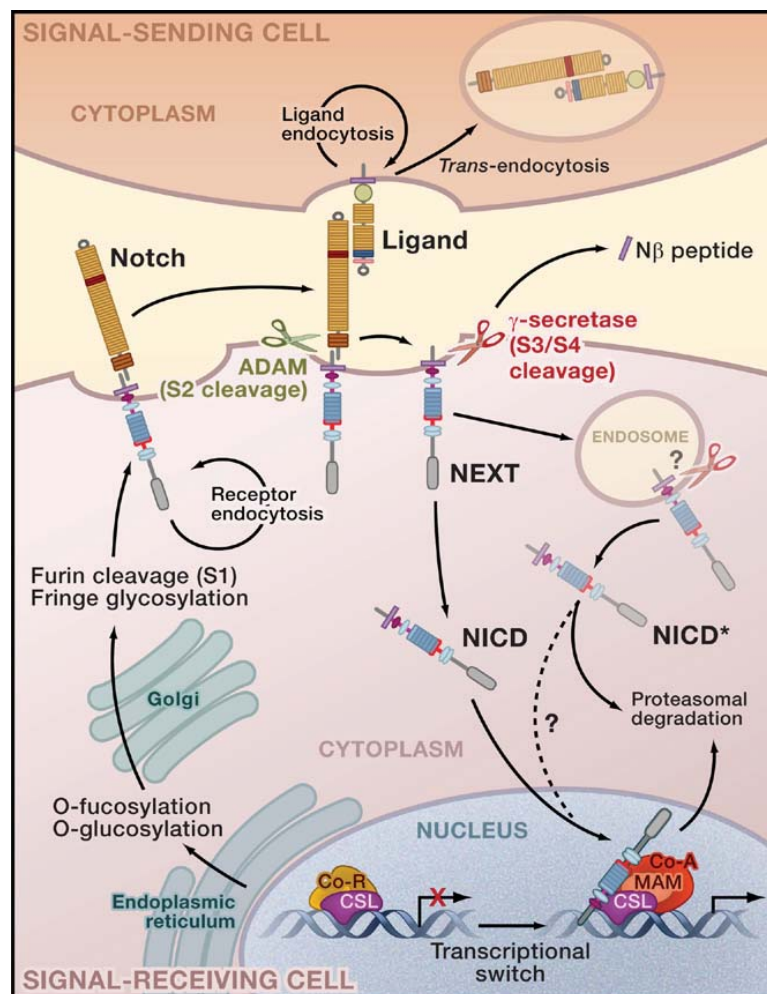


Figure 3. Canonical Notch signaling pathway.

The Notch receptors are modified in ER and Golgi and then translocate to the cell membrane. The canonical Notch signaling pathway is dependent on ligand-receptor interaction. Upon ligand binding, Notch receptors undergo a series of proteolytic cleavage events after which the Notch intracellular domains translocate to the nucleus and induce expression of downstream target genes. The figure is taken from R. Kopan and M. Ilagan (Cell, 2009)²¹.

Notch signaling plays critical roles in embryonic and tissue development²⁴, including somitogenesis²⁵, the development of skeletal muscle²⁶, cardiovascular system²⁷, heart²⁸, pancreas²⁹, hematopoietic system³⁰⁻³², and nervous system³³. Notch signaling is also crucial for maintenance of homeostasis in tissues including skin³⁴, liver³⁵, vascular system³⁶, intestine³⁷, and lung³⁸. Specifically, in hematopoietic system, Notch signaling controls marginal zone B-cell (MZB) differentiation and T cell development^{21,24}.

1.2.2. Notch signaling in T cell development

Notch signaling is essential for early T cell development in the thymus. Conditional inactivation of either Notch1 in bone marrow progenitors or of the Notch ligand Dll4 in thymic epithelial cells results in a complete block of T cell development at the earliest stages of T-cell lymphopoiesis. This developmental block of thymocytes is accompanied by ectopic B-cell development in the thymus^{31,39}. Conversely, constitutive expression of active Notch1 ICD in bone marrow progenitor cells leads to ectopic T-cell development and failure of B lymphopoiesis^{32,40}. These reciprocal loss- and gain-of-function experiments strongly indicate that Notch1 signaling in mice is essential and sufficient for T cell lineage commitment.

Besides the key role in the cell fate decision of T-cell lineage, NOTCH1 signaling is indispensable throughout multiple stages of early T-cell development including DN1, DN2 and DN3 stages of thymocyte maturation. Single-cell analysis revealed that Notch signaling is responsible for the activation of the expression of genes such as *Gata3*, *Tcf7*, *Bcl11b*⁴¹, which encode key transcription factors involved in T cell specification⁴². *Gata3* and *Tcf7* are upregulated in ETPs and important for initiating T cell program^{43–45}, and they further regulate T cell lineage genes including the activation of *Bcl11b*⁴⁶, finalizing the T cell lineage commitment process⁴². On the other hand, Notch signaling can also lead to the expression of transcription repressors such as HES family transcription factor genes including *Hes1*. *Hes1* expression has been shown to be important in T cell commitment and pro-T cell survival⁴⁷. Notch signaling has also been linked to the regulation of TCR β rearrangement⁴⁸.

1.2.3. Notch signaling in cancer

Adequate signaling pathway output is crucial for cellular homeostasis and development. Aberrant signaling output might lead to cellular dysfunction or even tumor formation. Dysregulated Notch signaling has been associated with certain developmental disorders and is one of the commonly activated signaling pathways in cancer²⁴. Aberrant activation or expression of several members of the Notch receptor and ligand family has been implicated in various cancers, including breast cancer⁴⁹, adenoid cystic carcinoma⁵⁰, colorectal cancer⁵¹, pancreatic ductal adenocarcinoma⁵²,

and multiple lymphomas⁵³ and leukemias^{54,55}. On the other hand, loss-of-function mutations in Notch genes have been associated with tumor suppressive functions⁵⁶ such as for squamous cell carcinoma⁵⁷, Head and neck squamous cell carcinoma⁵⁸, and small-cell lung cancer⁵⁹. Thus, whether Notch pathway functions as oncogenic or tumor suppressive is tissue and cell context dependent⁶⁰⁻⁶².

The role of Notch pathway in T cell acute lymphoblastic leukemia will be discussed in detail in the following chapter 1.3.

1.3. T cell acute lymphoblastic leukemia (T-ALL)

1.3.1. T-ALL disease

Overview

T cell acute lymphoblastic leukemia (T-ALL) is an aggressive hematological malignancy caused by genetic lesions in immature thymocytes. T-ALL accounts for 10-15 % of pediatric and about 25% of adult ALL cases. The cure rate of T-ALL in children improved considerably from less than 30% to a current estimated 5-year overall survival of >80%, while in adults it remains around 40%^{63,64}. The increased survival rate is largely due to risk-based stratification and applying aggressive combination chemotherapy⁶⁵. Although the five-year survival of T-ALL has been improved, primary resistant and relapsed T-ALL patients yet have a poor prognosis.

T-ALL Subtype

Nowadays, the determination of gene expression profiles and the identification of genomic abnormalities allows the classification of the T-ALL cases into four major subtypes (figure 4):

- 1) ETP-ALLs, or immature ALLs, present high expression of self-renewal genes resembling the profile of HSCs or progenitor cells. This group shows high mutational load yet with rare mutation in *NOTCH1*, and clinically associates with the worst outcome compared to the other groups.
- 2) The TLX-rearranged group, lacks functional TCR, or in some cases presents $\gamma\delta$ TCR, much like the DN2 stage of T cell development. This group is driven by ectopic expression of transcription factor *TLX3 (HOX11L2)* or *HOXA* and often presents activating mutations of *NOTCH1*.

3) The TLX1/NKX2.1-rearranged group, possesses a feature of differentiation arrest at DN3-DP stage of T cell development. This group is driven by transcription factor *TLX1* (*HOX11*) or *NKX2.1* (*NK2 Homeobox 1*) aberrations, and associates with good treatment outcomes.

4) The TAL/LMO subgroup, features immunophenotypes similar to CD4⁺ or CD8⁺ SP cells. This group is characterized by the aberrant expression of transcription factors *TAL1/TAL2* and *LMO1/LMO2/LMO3*, and often carry *PTEN* or *PIK3R1* loss-of-function mutations.

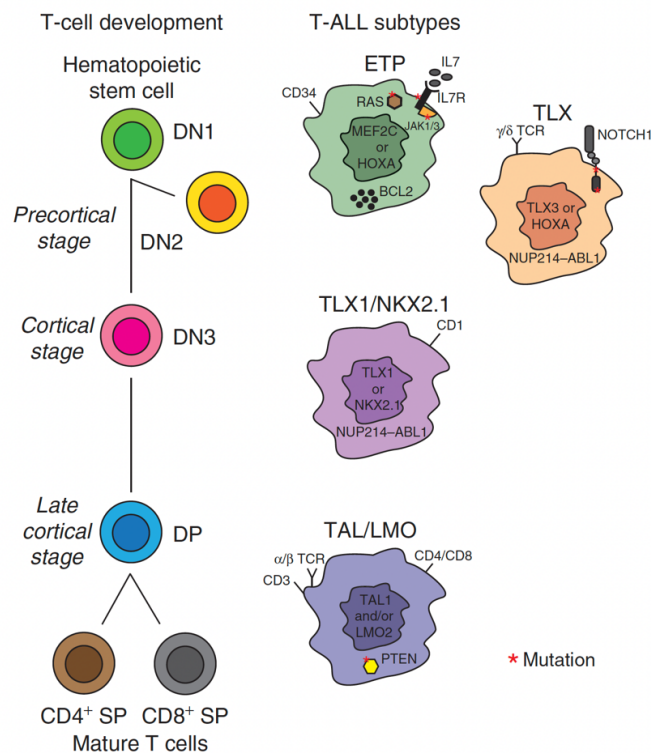


Figure 4. Stages of early T cell development and T-ALL subtypes.

Four T-ALL subtypes (ETP, TLX, TLX1/NKX2.1, TAL/LMO) are illustrated with corresponding aberrant gene expression profiles or mutational events (on the right), in analogy to the developmental stages of thymocytes (on the left). The figure is taken from V. Cordo *et al.* (Blood Cancer Discovery 2021)⁶⁶.

Diagnosis and prognosis:

Typical symptoms for T-ALL are anemia, shortness of breath, tiredness, frequent or long infections, small bruises in skin, bleeding. T-ALL is diagnosed by laboratory tests. These include blood and bone marrow sample test for leukocytes count, chest scan to identify swollen lymph nodes, and examination of Cerebrospinal fluid (CSF) to investigate if ALL cells entered the nervous system already.

1.3.2. Genetic landscape of T-ALL

The progress in Next Generation Sequencing and diagnostic genomics of ALL patient samples have provided us a panoramic view of oncogenic pathways in pediatric T-ALLs^{67–69} (Figure 5).

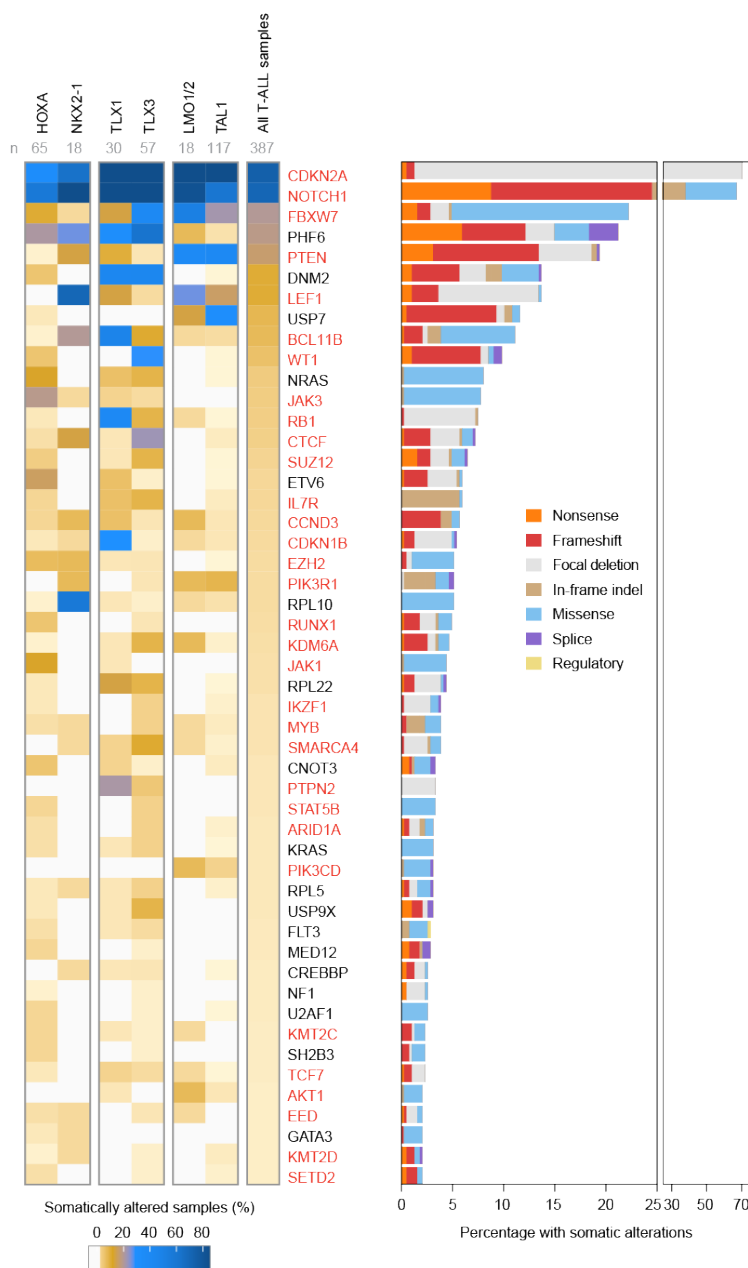


Figure 5. Mutational landscape of pediatric T-ALL patients.

Characterization of somatic SNVs/Indels and copy alterations in 387 pediatric T-ALL samples are shown. Heatmap (on the left panel) shows the percentage of somatically altered samples in each T-ALL subtype (column) in all genes (row). The percentage of altered samples are depicted and the types of alterations are indicated (on the right panel). The figure is adapted

from S. Brady *et al.* (Nature Genetics 2022)⁶⁷.

Figure 5 illustrates the most frequently mutated genes throughout T-ALL subtypes of pediatric cancer patients. These include:

- 1) NOTCH1 and the FBXW7 pathway: *NOTCH1* is one of the most frequently mutated genes in T-ALL disease. *FBXW7*, which encodes an E3 ligase that regulates half-lives of proteins such as NOTCH1, C-MYC and CYCLIN E through ubiquitin-mediated degradation, is also frequently mutated.
- 2) Cell cycle regulation: such as *CDKN2A* (the most frequently mutated gene), *RB1*, *CCND3*, *CDKN1B*.
- 3) PI3K-AKT-mTOR pathway: including *PTEN*, *PIK3R1*, *PIK3CD*, *AKT1*.
- 4) IL7R-JAK-STAT pathway: including *IL7R*, *JAK3*, *STAT5B*.
- 5) gene transcription: such as *BCL11B*, *MYB*, *LEF1*, *RUNX1*, *IKZF1*, *TCF7*, *WT1*.
- 6) protein translation: such as *RPL10*, *RPL22*, *RPL5*.
- 7) epigenetic regulation: such as *CTCF*, *SUZ12*, *EZH2*, *KDM6A*, *SMARCA4*, *ARID1A*, *KMT2C*, *EED*, *KMT2D*, *SETD2*.

Analysis of the genomic landscape not only provides an overview of the main pathways impacted by mutations, but also sheds light on the possible evolutionary occurrence of mutation events. Through the analysis of driver mutation clonality on pediatric T-ALL sequencing profiles, kinase-related alterations (including in *JAK3* and *NRAS*) were revealed to likely occur as early events; on the contrary, mutations in *PIK3R1*, *AKT1*, *PTEN* may happen at a later timepoint in the tumor evolution⁶⁷.

1.3.3. Notch signaling in T-ALL

The *NOTCH1* gene was first described in human leukemogenesis by the identification of the chromosomal translocation t(7;9) (q34;q34.3) in cells derived from a T-ALL patient⁷⁰. Yet, the frequency of such translocations in cancer patients was revealed as very low in subsequent analysis, putting a stall on further explorations on the relationship between aberrant Notch signaling and T-ALL^{71,72}. This was overcome by the discovery from the Aster group more than a decade later. They identified activating mutations in the HD and PEST domains of NOTCH1 in approximately 60% of human T-ALL patients⁵⁵. Mutations in the HD domain causes ligand-independent activation of

the signaling pathway, and those in the PEST domain will block ubiquitin-mediated degradation of the activated functional Notch domain (Figure 6)^{55,61,71,72}.

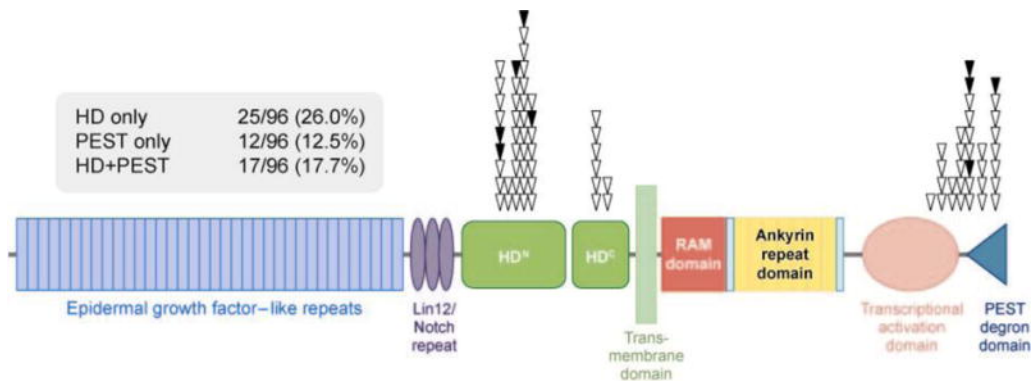


Figure 6. Schematic representation of *NOTCH1* mutations identified in T-ALL patients.

Frequencies and locations of mutations in *NOTCH1* in pediatric T-ALL patients are shown. Heterodimer domain and PEST domain are frequently mutated in *NOTCH1* in T-ALL. The figure is adapted from A. Weng *et al.* (Science, 2004)⁵⁵ and J. Aster *et al.* (Annu Rev Pathol, 2008)⁶¹.

Since this landmark paper, multiple publications reported that activating Notch mutations were identified in 50-70% of pediatric T-ALL samples⁶⁷⁻⁶⁹, which makes the *NOTCH1* gene one of the most frequently mutated genes in this disease.

NOTCH1 mutations were shown to associate with a favorable outcome in the TLX3 T-ALL subtype^{67,73}. Yet, whether this correlation is true for all T-ALL subtypes is not clear⁷⁴⁻⁷⁸ and needs future clinical investigations.

1.3.4. T-ALL treatment options

1.3.4.1 Standard of care treatment

The standard of care for T-ALL is usually an immediate treatment with chemotherapy upon diagnosis, which consists of three phases⁷⁹:

1) induction phase, which lasts about 4-6 weeks. The agents used for this phase are: glucocorticoid (dexamethasone or prednisone), microtubule-destabilizing agents (vincristine), hydrolyzing enzymes (L-asparaginase), with or without the addition of a fourth drug anthracycline.

2) consolidation phase, which lasts for a few months. The agents used for this phase are: alkylating agents (cyclophosphamide), nucleoside analogues (cytarabine and

mercaptopurine).

3) maintenance phase, which typically lasts more than one year. The agents typically used for this phase are: mercaptopurine, antimetabolites (methotrexate), or with vincristine and steroid pulses.

Patients are typically assigned to risk-based chemotherapies based on response to standard treatment^{66,79,80}. The current classification of risk groups is summarized in Table 1. End-of-consolidation Minimal Residue Disease (MRD) indicating early response to chemotherapy is a key prognostic parameter for T-ALL. The patients who achieve MRD negativity at the end of treatment have favorable outcomes with conventional chemotherapy^{66,73,79,80}.

Risk	Children's Oncology Group T-ALL risk definitions
Standard	Day 29: <5% blasts, MRD<0.01%; <5WBC/ μ L and no blasts in the cerebrospinal fluid; no testicular disease; no steroid pretreatment
Medium	Day 29: <25% blasts, MRD \geq 0.01%; end-of-consolidation MRD<0.1%;
High	Day 29: >25% blasts or end-of-consolidation MRD \geq 0.1%;

Table 1. Classification of T-ALL risks

The table summarizes the current classification of risk groups used in T-ALL treatments. MRD, minimal residue disease. The information listed here is summarized based on E. Raetz, D. Teachey (Hematology Am Soc Hematol Educ Program, 2016)⁸⁰.

For 10-15% of patients with Central Nervous System (CNS) disease or persistent MRD positivity, allogenic hematopoietic stem cell transplantation might be given, and sometimes a Cranial Radiation Therapy (CRT) is considered.

Yet, classical chemotherapy treatment proves inferior when treating relapsed and refractory T-ALL. Approximately 20% of pediatric patients die from relapsed or refractory disease within 5 years. This calls for the identification and implementation of novel therapeutic strategies.

1.3.4.2 Targeted therapies

Next generation sequencing and related diagnostic genomics of ALL patient samples have not only provided unprecedented insight into different T-ALL subgroups

associated with different mutation and gene expression signatures, but also identified potentially actionable targets⁶⁷.

Table 2 summarizes the targeted therapies inspired from these studies, which have been tested in preclinical or clinical settings^{66,80}:

Signaling pathways	Property of Drugs	Drugs
apoptosis	BH3 memetics	Venetoclax, Navitoclax, AZD-5991
MEK	MEK inhibitors	Selumetinib, Trametinib
PI3K-AKT-mTOR	PI3K/AKT/mTOR inhibitors	Buparlisib, Dactolisib, MK-2206, Sirolimus, Everolimus, Temsirolimus
IL7R-JAK	JAK1/2 inhibitors	Ruxolitinib
PIM	PIM1 inhibitors	AZD-1208
P53-MDM2	P53 activators, MDM2 inhibitors	APR-246, Idasanutlin, NVP-HDM201
Protein degradation	Proteasome inhibitors	Bortezomib
Notch	Notch inhibitors	Monoclonal antibodies against Notch receptors or ligands, GSIs, CB-103
CXCR4	CXCR4 antagonists	Plerixafor, BL8040
ABR/SRC	ABL/SRC inhibitors	Imatinib, Dasatinib
Cell cycle	CDK4/6 inhibitors	Palbociclib, Ribociclib
BRD4	BET inhibitors	OTX015, JQ1
Nuclear Trafficking	XPO1 inhibitors	Selinexor

Table 2. A summary of promising targeted therapies in T-ALL currently under pre-clinical or clinical investigations.

A non-exhaustive list of drugs that have been tested in preclinical and clinical trials are shown here. The information listed here is summarized based on V. Cordo *et al.* (Blood Cancer Discovery, 2021)⁶⁶, and E. Raetz, D. Teachey (Hematology Am Soc Hematol Educ Program, 2016)⁸⁰.

These promising therapeutic targets and drugs await or undergo further investigations in clinical trials. In practice, the goal would be to establish routine tumor profiling so that each patient can receive customized treatment or so-called precision medicine to achieve the best outcome.

1.3.4.3 Notch-targeting therapies

The crucial role of Notch signaling in the pathophysiology of various cancers and its potential link to cancer stem cells positioned the pathway as a potential therapeutic target for cancer management. Given the well-documented role of hyperactivated Notch signaling in T-ALL, as well as its implication in a plethora of other solid and blood born tumors, multiple companies have developed inhibiting molecules to block this pathway.

Mono-clonal antibodies

Genentech, Oncomed and Regeneron developed blocking antibodies against specific Notch receptors or ligands, which inhibit ligand-receptor interactions^{81–83}.

GSI

Other companies including Roche, Merck Eli Lilly and others developed small molecule γ -secretase inhibitors (GSIs) as Notch inhibitors⁸⁴, which prevent the proteolytic cleavage and release of the Notch intracellular domain. Yet, most GSIs failed in clinical trials due to gut toxicity and insufficient efficacy⁸⁴. A preclinical study demonstrated that a combination of GSI and dexamethasone help relieve gut toxicity and improve the antitumor efficacy⁸⁵, so currently this strategy is being tested in clinical trials^{86,87}.

Recently, it was been shown that a PSEN1 inhibitor can safely and selectively target Notch1 signaling in T-ALL in a preclinical study. It was found that T-ALL cells are exclusively positive for PSEN1, while intestinal epithelial cells express both PSEN1 and PSEN2. Thus, this PSEN1 specific inhibitor demonstrates antileukemic activity with no intestinal toxicity in PDX model⁸⁸.

CB-103

Our lab has previously discovered and developed a novel, orally active small molecule CB-103 that can efficiently block the Notch transcription activation complex. CB-103 does not cause dose limiting intestinal toxicities, which is often observed with therapeutics that interfere with Notch receptor activation at proximal points of the pathway⁸⁹. Additionally, CB-103 inhibits the Notch pathway at the transcriptional level whereas the other agents are acting at the level of the cell surface. Consequently, CB-103 can also block Notch pathway in situations where the Notch pathway is activated due to chromosomal translocations leading to the loss of the extracellular portion of the receptors^{90,91}.

CB-103 has successfully been evaluated in a recent phase I/II clinical trial⁹² and resulted in a complete response in a patient with relapsed and refractory T-ALL⁹³.

1.3.4.4 Immunotherapy

Antibody-based therapy

CD38 was found to be expressed in multiple hematopoietic malignancies including T-ALL, in which it is expressed at highly levels throughout all stages (diagnosis, treatment and relapse) of the disease⁶⁶. Thus, anti-CD38 monoclonal antibodies (Daratumumab, Isatuximab)^{94–96} can be considered for T-ALL as they were shown to inhibit tumor cell growth through complement-dependent cytotoxicity (CDC), antibody-dependent cytotoxicity (ADCC), and antibody-dependent macrophage phagocytosis (ADCP)⁹⁶. Anti-CD38 monoclonal antibodies are currently evaluated in clinical trials^{97–99}. In addition, a preclinical study shows CD3 might be another promising target in T-ALL¹⁰⁰, which requires further studies.

Cellular therapy

Multiple Chimeric Antigen Receptor T (CAR T) cell therapies, including anti-CD5, anti-CD7, anti-CD1 and anti-CD38 have been proposed⁶⁶. Anti-CD5 and Anti-CD7 CAR T therapies are currently being investigated in clinical trials in T-ALL patients^{101,102}.

Yet, the development of immunotherapies in T-ALL is challenged by the demand for

improved safety and efficacy. The surface markers targeted by these therapies can be expressed not only on tumor cells but also on all thymocytes, thus immunodeficiency and T cell depletion are potential side effects to avoid when developing such therapies.

1.4. Resistance to cancer therapy

1.4.1. General resistance mechanisms and solutions

Despite the success of chemotherapies, a not negligible percentage of cancer patients develop drug resistance and relapse after having initially responded to standard of care therapy. Combining different forms of chemotherapies has proven to be more efficacious and have increased overall survival in various cancers including lymphoma¹⁰³, testicular cancer¹⁰⁴ and breast cancer¹⁰⁵. However, once patients relapse or are refractory to the initial treatment, changing chemotherapy regimens is often unsuccessful. In such situations a combination of targeted therapies eventually combined with immunotherapies is the only hope for these patients. But targeted therapy is also often subject to the development resistance mechanisms. Drug resistance mechanisms can occur at various levels^{106,107} (Figure 7):

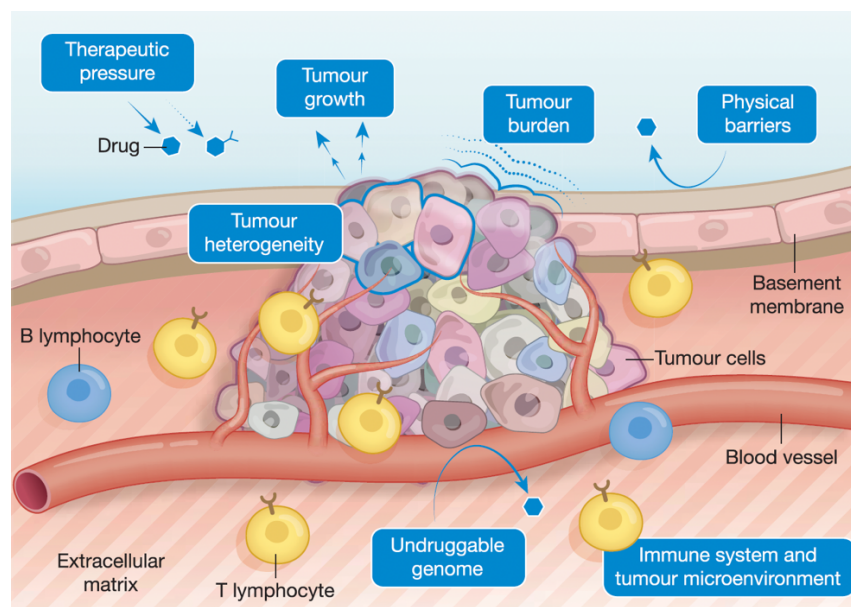


Figure 7. A simplified view of resistance mechanisms in cancers.

A simplified schematic view of determinants of drug resistance in cancer is shown, such as tumor burden and growth, tumor heterogeneity and therapeutic pressure, tumor microenvironment. The figure is taken from N. Vasan, J. Baselga, D.M. Hyman (Nature 2019)¹⁰⁷.

Let me briefly summarize some variables that may account for or influence drug response and the development of treatment resistance.

1. Tumor burden and tumor growth kinetics:

The size of a tumor matters in terms of predicting treatment response and outcome of disease, as large tumors associate with higher metastatic risk¹⁰⁸. Also, the growth kinetics of tumors may vary: while indolent cancers associate with long survival, they are less sensitive to chemotherapy or targeted therapies. Conversely, aggressive fast-growing tumors can be remarkably sensitive to treatment.

A model that tries to explain the tumor growth kinetics in response to drug treatment is the so-called Norton-Simon model. According to this model, solid tumors grow in a sigmoidal way. They grow fast when the tumor is small, and slow down their growth rates and even plateau as the tumor size increases^{109,110}. Thus, chemotherapeutic treatment of the tumor will induce tumor shrinkage resulting in a smaller tumor size, the smaller tumor may then change its growth kinetics by adapting to an accelerated or even exponential growth. Should this concept be true, the chances of eliminating a tumor would be maximized by preventing the rapid growth phase that may occur due to the drug-induced shrinkage of the tumor. This reflection resulted in the development of a “dose-dense chemotherapy”, meaning that the effective dose of chemotherapy should be administered with shortest interval possible, so that that smaller tumors cannot return to its exponential growth phase again¹¹¹.

2. Tumor heterogeneity and therapeutic selection:

Tumors represent in most cases a heterogenous mass of cells exhibiting cellular and genetic diversity. Some of these cancer cells might be resistant from the very beginning to a given form of therapy. In this case these resistant cells do not respond to the presence of therapeutic pressure and there is no benefit for the patient. This was exemplified by resistance to BRAF inhibitors of BRAF-mutant colorectal cancer via activation of EGFR signaling^{112,113}. Another form of resistance is the acquired resistance of cancer cells upon treatment. In this case the initial form of therapy is partially successful by eliminating targeted clones, which results in the shrinkage of the tumor mass. One way of acquired resistance is through the acquisition of genomic alterations. Acquired mutations can alter the drug binding pocket of a targeted drug exemplified by threonine mutations induced resistance to tyrosine kinase inhibition¹¹⁴.

Another mode is through up or downregulations of alternative signaling pathways to compensate for the pathways being inhibited by the cancer therapy. For example, loss of PTEN will upregulate the PI3K β signaling in response to PI3K α inhibitors¹¹⁵. Additionally, cancer cells under drug treatment can even undergo histological phenotype switching, showcased in anti-androgen treated prostate cancer, which adopt an aggressive neuroendocrine phenotype¹¹⁶. Mechanistically the cell fate plasticity in enzalutamide-resistant prostate cancer has been shown to be induced by the upregulation of transcription factor SOX2¹¹⁶.

To understand and counteract resistance caused by tumor heterogeneity, recent efforts have focused on exploring synthetic lethality through screening and computational analysis of tumor evolution. The ultimate goal would be to identify and utilize effective combinations of therapies to address multiple cancer dependencies, either to avoid tumor growth relapse, or to anticipate a targeted follow-up treatment in case of relapse to standard of care.

3. Tumor microenvironment

Tumors, when growing rapidly, consume large amount of nutrients and depend on blood supply. To support this, tumors promote angiogenesis by secretion of VEGF and other angiogenic growth factors. These newly formed tumor associated blood vessel are distorted in their vascular structure and function, and thereby create a physical barrier that hinders the exposure of the tumors to drugs as well as impairs T cell extravasation¹¹⁷. One possible solution to overcome this resistance mechanism is to combine anti-angiogenic agents, which have been shown to normalize tumor associated vasculature¹¹⁸, with immune checkpoint blockade^{119,120} and targeted therapies¹²¹ (also in Table 3).

Furthermore, solid tumors may exhibit an “immune-desert” phenotype (“cold-tumor”) often featured by the exclusion or absence of immune cells. Specifically, tumors may adapt intrinsically or utilize extrinsic clues for immune escape, through affecting one or several processes of the “priming, circulation, infiltration, survival, antitumor activity” of T cells¹²². Such tumors usually end up responding poorly to immune checkpoint blockade (ICB). For example, tumor cells may downregulate the MHC proteins, which are essential for presenting tumor antigens to T cells, via mutations of *B2M* or *JAK1/2*

genes, thus becoming resistant to immunotherapy¹²³.

To tackle these resistance mechanisms, there are different strategies to combine with immune checkpoint blockades (ICBs), to convert “cold-tumor” to “hot-tumor” (“immune-inflamed”) and improve the outcomes of treatments in patients. For example, the combination of chemotherapy and anti-PD-1 has shown promising responses in NSCLC, TNBC patients in clinical trials^{124,125}. A non-exhaustive list of resistance mechanisms and treatment strategies are summarized in Table 3.

Resistance mechanisms	strategies to combine with Immune checkpoint blockade	Examples of Therapies
Lack of neoantigens	increase immunogenicity	chemotherapy, radiotherapy, oncolytic virus, epigenetic modulators
antigen presentation deficiency	increase antigen presentation	DNA repair inhibitors, cytokines, immune modulators and co-stimulators
impaired T cell trafficking and infiltration	improve circulation and infiltration of T cells	targeted therapies, anti-angiogenesis reagents
immunosuppressive microenvironment	reprogram immunosuppressive microenvironment	epigenetic modulators, reagents that target immunosuppressive cells
lack of antitumor activity	increase cytotoxic T cells	Adoptive cell therapies, vaccines

Table 3. Challenges of immune checkpoint blockade (ICBs) and possible strategies to synergize with ICBs.

A non-exhaustive list of resistance mechanisms to ICBs and promising treatment strategies to combine with ICBs treatments are summarized here. The information is gathered from J. Zhang *et al.* (Trends in Immunology, 2022)¹²².

1.4.2. Known resistance mechanisms to chemotherapy in T-ALL

As illustrated in 1.4.1, tumors can acquire mutations upon treatment pressure. In response to conventional chemotherapy in T-ALL, mutations in *NR3C1* and *NT5C2* have been identified as mediators of resistance^{126,127}. *NR3C1* encodes a corticosteroid receptor, loss of which can affect the response to glucocorticoids¹²⁸. *NT5C2* encodes a nucleotide metabolism enzyme crucial for purine/pyrimidine synthesis, and activation mutations of this gene are associated with resistance to purine analog

treatments such as mercaptopurine¹²⁹.

Additionally, multiple studies have shown that activation of JAK/STAT signaling can lead to upregulation of pro-survival genes such as *BCL2* and *PIM1*, and thus contribute to resistance in response to steroids^{130,131}. A combination of Ruxolitinib and dexamethasone may benefit patients with T-ALL and ETP-ALL to overcome IL7-induced steroid resistance^{130,131}.

1.4.3. Resistance to Notch-targeted therapy in T-ALL

The identification of Notch pathway as being crucial for T-ALL oncogenesis has boosted the development of Notch-targeting therapies. Yet, besides one major drawback of gut toxicity induced by GSIs, the response to the treatment is also transient and not sufficient. Multiple resistant mechanisms have been proposed to explain this.

The Ferrando group, was among the first to report that mutational loss of *PTEN* is associated with resistance to pharmacological Notch inhibitors in T-ALL¹³². In a subsequent study they demonstrated that, besides activation of AKT signaling, *PTEN* loss also upregulates glycolysis in support of leukemic cell metabolism and thus rendering the cells resistant to Notch inhibition¹³³.

The same group also put forward a combination of GSI and an antitumor agent withaferin A that could work synergistically in treating T-ALL patients¹³⁴. Although it's controversial if loss of *PTEN* is responsible for resistance to GSIs *a priori* in T-ALL¹³⁵ (which will be discussed in detail in Discussion 5.1 session), it is certain that its loss is associated with high risk of disease relapse^{136,137}.

Epigenetic mechanisms have also been implicated in the resistance to GSI in T-ALL. *BRD4*, which encodes the Bromodomain-containing protein 4, can modify histones and remodel the chromatin and thereby affect gene transcription. In response to GSI, *BRD4* can recruit new enhancer elements to re-establish expression of critical T-ALL genes including *MYC* and *BCL2*¹³⁸, thereby mediating resistance to GSI. Yet, these

GSI-resistant cells remain sensitive to the BRD4 inhibitor JQ1, providing a clinical opportunity of applying indicating BET inhibitor treatment in NOTCH1-driven T-ALLs.

A recent phospho-proteomics study focused on dissecting the differential signaling modules between sensitive and resistant T-ALL cell lines and PDXs. They highlighted several pathways, including the activation of Protein Kinase C family signaling, can converge on MYC and protein translation thus responsible for resistance to GSI¹³⁹. It was further demonstrated that a combination of Notch inhibitor and PKC inhibitor reach synergy in a T-ALL preclinical setting.

Admittedly, we have gained some insights into potential resistance mechanisms to Notch inhibitors in T-ALL. Yet, none of the mentioned Notch inhibitors (chapter 1.3.4) has been approved or administrated to patients long enough to experience resistance mechanisms. To anticipate such resistance mechanisms, the establishment of a systematic research at molecular level is needed. Thus, understanding how cells develop resistance against the GSI or CB-103 treatment will be of great benefit to help predicting potential resistance scenarios. Moreover, the identification of Notch inhibitor driven resistance mechanisms on the molecular level will help to refine the selection of patients with the highest chance to respond to targeted therapies in clinical trials. Moreover, identifying targets that sensitize the cancer cells to specific treatments will promote the development of dual or multi-target therapies.

2. Aims of the thesis

T-cell acute lymphoblastic leukemia (T-ALL) is an aggressive hematological malignancy caused by genetic alterations during T-cell development. Despite the improvement of current cure rates, classical chemotherapy treatment proves inferior when treating relapsed and refractory T-ALL, demanding the implementation of targeted therapies. The identification of NOTCH1 as one of the most frequently mutated genes in T-ALL has boosted the development of Notch-targeting therapies, such as γ -secretase inhibitor (GSI) and a recent discovery of CB-103 in the lab. Yet, patients with initial promising responses to mono-therapies will likely experience relapse due to tumor heterogeneity and acquired resistance. Thus, a better understanding of resistance mechanisms to Notch inhibitors and the development of combination therapies will facilitate effective treatment of T-ALL patients in the clinics. In this study, we aimed to:

- Identify candidate genes associated with resistance to Notch inhibitors by performing a genome-wide CRISPR-Cas9 knockout screening in human T-ALL cells.
- Perform genetic loss-of-function (LoF) approach to validate that loss of *Phosphoinositide-3-Kinase Regulatory Subunit 1 (PIK3R1)* causes resistance to pharmacological Notch inhibition in multiple human T-ALL cell lines.
- Dissect the LoF *PIK3R1*-mediated resistant mechanism(s) to Notch inhibition in T-ALL via transcriptomic and phosphoproteomic analysis.
- Identify and validate combination therapies to more efficiently treat Notch-driven T-ALL.

The major part of data presented here is posted on BioRxiv and under review in a scientific journal as a Research Article entitled 'Resistance mechanism to Notch inhibition and combination therapy in human T cell acute lymphoblastic leukemia' authored by Linlin Cao; Gustavo A. Ruiz Buendía; Nadine Fournier; Yuanlong Liu; Florence Armand; Romain Hamelin; Maria Pavlou; Freddy Radtke

3. Materials and methods

3.1. Cell culture and cell lines

All cell lines were maintained in a humidified atmosphere incubator with 5% CO₂ at 37°C. The lentiviral packaging cell line HEK293T (RRID: CVCL_0063) was obtained from D. Trono Lab maintained in DMEM GlutaMAX (Thermo Fisher, Cat#31966047) supplemented with 10% FBS (GIBCO), 10µg/mL Gentamicin (Life Technologies, Cat# 15710049). The human T-ALL cell lines DND-41 and RPMI-8402 were grown in RPMI 1640 GlutaMAX (GIBCO, Cat# 61870010) supplemented with 10% FBS. The human T-ALL cell line TALL-1 was grown in RPMI 1640 GlutaMAX (GIBCO, Cat# 61870010) supplemented with 15% FBS.

3.2. Lentiviral transduction

For lentiviral transduction of CRISPR vectors, HEK293T cells were seeded at 30-40% confluency in 10cm dishes in DMEM GlutaMAX (Thermo Fisher, Cat#31966047) supplemented with 10% FBS (GIBCO), and transfected the next day with the plasmid of interest and the packaging plasmids VSV-G (RRID: Addgene_8454), and dR8.74 (RRID: Addgene_22036) using Fugene (Promega) or Calcium Phosphate method¹⁴⁰. Media was changed 16 hours after transfection. Viral supernatant was collected twice, at 48 and 72hours post-transfection, pooled and precipitated overnight at 4°C using Polyethylene Glycol 8000 (PEG-8000) as resin, then centrifuged at 3000 rpm for 1 hour at 4°C. The pellet was resuspended in cold PBS and used to infect cells in presence of 4µg/µL polybrene (Millipore, Cat#TR-1003-G).

3.3. Stable cell line generation

3.2.1. Generation of knockout cell lines by CRISPR/Cas9 using lentiviral transduction.

For RPMI-8402 *PIK3R1* CRISPR/Cas9 knockout: RPMI-8402 cells were first transduced with lentiCas9-Blast (Addgene, Cat #52962) and selected using Blasticidin (Invivogen, Cat #ant-bl-1) to obtain stable a cell line expressing the Cas9 protein. Once stably transduced and selected, cells were transduced with a second lentiviral plasmid containing *PIK3R1*-targeting sgRNA (1 and 2, please see in Annexed Table 5, sgRNAs sequences were selected from the top 2 enriched sgRNAs from the screen result),

coupled with RFP (Addgene, Cat #57823). Cells were transduced and RFP⁺ cells were sorted in single cells into 96-well U-bottom plates. Single cells were expanded into clones and screened by Western Blot for loss of p85 expression. KO#1 and KO#2 lines were generated from *PIK3R1_sgRNA1*, KO#3 and KO#4 lines were generated from *PIK3R1_sgRNA2*.

3.2.2. Generation of knockout cell lines by CRISPR/Cas9 through ribonucleoprotein (RNP) delivery.

For DND-41 *PIK3R1* CRISPR/Cas9 knockout: DND-41 cells were delivered ribonucleoprotein complexes using IDT protocol (Neon Transfection System). In brief, cells were split one day prior for optimal growth at the time of transfection. Customized Alt-R CRISPR-Cas9 crRNAs and Alt-R CRISPR-Cas9 tracrRNA ATTO550⁺ (IDT, Cat #1075927) were annealed to duplex, and then introduced to cells together with Alt-R HiFi Cas9 Nuclease V3 (IDT, Cat #1081060) in Resuspension Buffer R (Neon System Kit). ATTO550⁺ cells were sorted 24hrs post-electroporation in single cells into 96-well plates. Single cells were expanded to colonies and clones were selected as described above. KO#1 and KO#2 lines were generated from *PIK3R1_crRNA1*, KO#3 and KO#4 lines were generated from *PIK3R1_crRNA2*. NT lines were generated from Alt-R® CRISPR-Cas9 Control Kit (Cat #1072554), Human with same procedure. (Oligo sequences are listed in Annexed Table 5).

3.2.3. Generation of stable knockdown cell lines through shRNA.

For TALL-1 *PIK3R1* knockdown: TALL-1 cells were transduced with hU6_mir30-shRNA-hPGK_GFP-P2A-Luc2-P2A-BlaR (gift from Dr. J. Huelsken Lab), GFP⁺ cells were sorted in bulk and cell lines were screened by Western Blot for loss of p85 expression. The KD#5 line was generated from *PIK3R1_shRNA5*, KD#8 was generated from *PIK3R1_shRNA3/4/5/6* in combination. shRNAs sequences were chosen based on previous published data¹⁴¹ and Sigma Mission Human shRNA website (oligo sequences are listed in Annexed Table 5).

3.3. Proliferation assay

Cells were seeded at same numbers in appropriate media (vehicle or drug treated) and cultured in 96-well U-shaped plates for 6 days, in 3-4 replicates. At indicated time

points, live cell numbers were counted using Attune NxT (ThermoFisher) and data was analyzed using FlowJo v.10.8.1.

3.4. Cell cycle assay

Cells were permeabilized with 0.01% Triton-X100 on ice for 3 hours, fixed and stained with FxCycle PI/RNase staining solution (Invitrogen, Cat #F10797) overnight at 4°C. Data acquisition was performed on Gallios (Beckman Coulter) and analyzed using FlowJo v.10.8.1.

3.5. Apoptosis assay

Cells were stained with the anti-Cy5-Annexin V (1:100, BD Biosciences, Cat#559934, RRID: AB_2869267) and 7-aminoactinomycin D (7-AAD) (1:20, BD Bioscience, Cat #559925, RRID: AB_2869266) in AnnexinV binding Buffer (Biolegend, Cat #422201). Data acquisition was performed on Gallios (Beckman Coulter) and analyzed using FlowJo v.10.8.1.

3.6. Immunoblotting

Cells were washed twice with 1x PBS and resuspended in RIPA buffer (50mM Tris-HCl, pH 7.5, 150mM NaCl, 1% Nonidet P-40, 0.5% sodium deoxycholate and 0.1% SDS) supplemented with PhosSTOP (Sigma Aldrich, Cat #4906837001) and Protease inhibitor (Sigma Aldrich, Cat #P8340). Whole cell lysates were separated on 10% Tris-Glycine (SDS) gel and transferred to polyvinylidene difluoride (PVDF; Sigma Aldrich, Cat #3010040001) membranes. Membranes were incubated with the indicated primary antibodies overnight at 4°C (Annexed Table 6). Washed membranes were incubated with secondary antibody for 1 hour at room temperature. Membranes were developed using Pierce ECL Western Blotting Substrate (Thermo Fisher Scientific, Cat# 32209).

3.7. *In vitro* synergy analyses

A total of 5,000 cells per well were seeded in a final volume of 100µL with the indicated amount of each drug either alone or in combination in 96-well flat bottom plates. Each treatment was carried out in 3-4 replicates for 3 days. 10µL of AlamarBlue (Life

Technologies, Cat #DAL1025) was added to each well and incubated for 4 hours followed by plate reading using Infinite F500 multimode reader (Tecan). Values were normalized to those of no treatment controls and analyzed in GraphPad Prism 7.0 applying non-linear regression dose-response curve calculations to obtain the IC50 values.

Combination index (CI) was calculated according to the Chou-Talalay algorithm¹⁴² using the formula: $CI = [D]1/[Dx]1 + [D]2/[Dx]2$. [D]1 and [D]2 are the concentrations of drug 1 and drug 2 to show a certain effect when treated with two drugs together. [Dx]1 and [Dx]2 are the concentrations that show the same effect with a combination of drug 1 and drug 2 when treated with each drug alone. Synergism can be defined as follows: $CI < 1$ indicates a synergistic effect; $CI = 1$ indicates an additive effect; $CI > 1$ indicates an antagonistic effect.

3.8. Animals and *in vivo* xenotransplantation

3.8.1. *In vivo* xenotransplantation

NSG (NOD.Cg-Prkdz^{scid} IL2rg^{tm1Wjl}/Szj; SN 005557) mice were originally purchased from Jackson laboratory. RPMI-8402 cells were engineered to express luciferase by lentiviral transduction using mPGK-Luciferase-hPGK-eGFP plasmid. One million cells were intravenously injected through the tail vein into female NSG mice. Tumor growth was measured twice a week using an *in vivo* imaging system (IVIS, Caliper Life Sciences). Briefly, 12 min after intraperitoneal administration of 150mg/Kg of D-luciferin (Biosynth, Cat #L-8220), mice were anesthetized in an induction chamber (O₂ and 2% isoflurane) and transferred to the imager. Images were acquired and analyzed using Living Image Software v4.4 (Caliper Life Sciences). Upon tumor establishment (~14 days post xenograft transplantation), animals were randomized based on tumor burden into either vehicle or drug treatment groups. Tumor growth was continuously monitored at indicated time points until endpoint.

3.8.2. Animal treatment

CB-103, dissolved in castor oil by sonication, was administrated intraperitoneally once per day (40mg/Kg). LY3039478, dissolved in solvent (93% water, 5% ethanol and 2% Tween80) and administrated intraperitoneally once per day (20mg/Kg). PD-0332991,

dissolved in 50mM sodium lactate at pH4, was administrated by oral gavage once per day (150mg/Kg). MK-2206, dissolved in 30% Captisol, was administrated by oral gavage twice a week (120mg/Kg). Venetoclax, dissolved in 35% PEG400, 0.5% Tween80 and 64.5% water, was administrated by oral gavage once per day (35mg/Kg). Drugs were administrated for 14 days and mice were monitored for tumor development according to scoresheet. (For detailed vendor information please see in Annexed Table 7.)

All animal work was carried out in accordance with Swiss national guidelines. This study (VD3323, VD3665) was reviewed and approved by the cantonal veterinary service (Service vétérinaire cantonal de Vaud).

3.9. CRISPR/Cas9 screen and analysis

3.9.1. CRISPR/Cas9 screen

The Human GeCKOv2 CRISPR knockout libraries A and B (Addgene #1000000048, #1000000049) were pooled and used to identify genes responsible for Notch resistance in T-ALL cells. In brief, a stable Cas9-expressing T-ALL cell line (DND-41-Cas9) was established by lentiviral transduction of DND-41 cells with LentiCas9-Blast (Addgene, Cat #52962) and selected using 10ug/mL Blasticidin (Invivogen, Cat #ant-bl-1). Stable expression of Cas9 protein in the DND-41-Cas9 T-ALL cell line was verified by Western Blot analysis. Subsequently, these cells were transduced with GeCKO v2A library containing 123,411 unique sgRNA sequences targeting 19,050 human genes at a low MOI (~0.3) to ensure effective barcoding of individual cells. Next, transduced cells were selected with 1µg/mL of puromycin (Life Sciences, Cat #A1113803) for 6 days to generate a mutant cell pool. A cell aliquot was frozen as Day0 sample. Cells were cultured and treated with either vehicle (DMSO), γ -secretase inhibitor (GSI) (N-[N-(3,5-Difluorophenacetyl)-L-alanyl]-S-phenylglycine t-butyl ester) (DAPT, 10µM) or CB-103 (5µM) for 3 weeks for sgRNA selection with each condition done in triplicates.

At endpoint, at least 3×10^7 cells per replicate were collected for genomic DNA extraction to ensure over 400-fold coverage of library using ZymoResearch Quick-gDNA MidiPrep Plus Kit (Zymo Research, Cat #ZYM-D4075-25TST). sgRNA

sequences were amplified in two rounds: first round by GeCKO-F1/R1 primers using Herculase II Fusion DNA polymerase (Agilent Technologies, Cat #600679); second round by NGS-Lib_Fwd/Rev 1-10 indexed primer using NEBNext® High-Fidelity 2X PCR Master Mix (Cat #M0544L). PCR products were purified (Qiagen gel purification kit, Cat #28706, and Qiagen PCR purification kit, Cat #28106), quantified by Qubit (Thermo Fisher Scientific), and profiled by Fragment Analyzer.

Samples were sequenced in one run on Illumina NextSeq 500 Instrument (Illumina) according to the manufacturer instructions, yielding 20 to 48 million single-end 75 nucleotide reads per sample.

3.9.2. Screen analysis

MAGeCK¹⁴³ (v.0.5.9.2) was used to analyze the data. Reads were trimmed of their adapters with bcl2fastq v2.19 (Illumina) and quality-controlled with FastQC v0.11.5. Read count tables were obtained using the MAGeCK count command with default parameters on the Human GeCKOv2 combined library of A and B¹⁴³. Treatments were compared to untreated DMSO/vehicle samples using the MAGeCK test command with default parameters and pooling all replicates. Robust Rank Aggregation (RRA) tables were generated. Genes with an adjusted $P < 0.001$ and a \log_2 fold-change > 1 or < -1 were considered as positive and negative significant hits, respectively.

Gene set enrichment analysis (GSEA)¹⁴⁴ was performed by ranking genes according to their RRA values in descending order. GSEA was performed with the clusterProfiler R package (v4.0.5)¹⁴⁵ using 10,000 permutations, minimum gene set size = 10, maximum gene set size = 1,000, and hallmark gene sets¹⁴⁶ from the msigdb package (7.4.1)¹⁴⁷. Pathways with an adjusted $P < 0.05$ were deemed as significantly enriched. If more than 20 pathways were significantly enriched, the top 20 are shown in the corresponding dot plots.

3.10. RNA-seq and analysis

3.10.1. RNA-seq and differential gene expression

RNA was extracted from cell lines using RNeasy Mini Kit (QIAGEN, Cat#74104). RNA quality was assessed on a Fragment Analyzer (Agilent) or TapeStation 4200 (Agilent)

to proceed to the PolyA-based stranded mRNA library prep method (scores > 7.2). Libraries for mRNA-seq were prepared with the Stranded mRNA Ligation method (Illumina) starting from 1µg RNA, according to manufacturer's instructions. Libraries, all bearing unique dual indices, were subsequently loaded at 250pM in a HiSeq 4000 instrument (Illumina) and sequenced according to manufacturer's instructions, yielding paired-end reads of 75 nucleotides. Reads were trimmed of their adapters with bcl2fastq v2.20 (Illumina) and quality-controlled with FastQC v0.11.9.

Reads were aligned to the human genome build hg38 using HISAT2 (v2.2.1)¹⁴⁸. Transcript-level counts and transcripts per million (tpm) were estimated using Salmon (v1.4.0). Counts were then summarized at the gene level with the tximport R package (v1.20.0)¹⁴⁹. Genes with an average expression per condition less than counts per million reads mapped (cpm) = 1, and a coefficient of variation per condition higher than 100% were removed from all conditions with the filtered.data() function from the NOIseq R package (v2.36.0)¹⁵⁰ using the following parameters: cv.cutoff = 100, cpm = 1. Reported log₂ fold-change values are the average of the log₂ fold-changes computed by edgeR (v.3.34.0)^{151,152}, DESeq2 (v.1.32.0)¹⁵³ and voom from the limma R package (v.3.48.1)¹⁵⁴. Three differential gene expression analysis methods were run in parallel with the consensusDE R package (v1.14.0)¹⁵⁵.

Differentially expressed genes were defined as genes with Benjamini-Hochberg-adjusted $P < 0.05$. Genes were ranked according to their log₂ fold-change in descending order and GSEA was performed with the GSEA() function from the clusterProfiler R package with the following parameters: minGSSize = 10, maxGSSize = 1000, eps = 0, pvalueCutoff = 0.05. Pathways with an adjusted $P < 0.05$ were deemed as significantly enriched. If more than 20 pathways were significantly enriched, the top 20 are shown in the corresponding dotplots.

3.10.2. Differential transcript expression

Transcript expression was quantified with Salmon (v.1.4.0). Transcript-level quantification estimates were imported to R with the tximport package (v.1.22.0). Low-expression transcripts with less than 10 reads were filtered from dataset. Subsequent differential transcript expression analysis was performed with DESeq2 (v.1.34.0) and

significantly differentially expressed transcripts were considered as those with an adjusted $P < 0.01$ and an absolute \log_2 fold-change > 1 .

Pathway enrichment analysis was performed by selecting the top 100 most significant up- and downregulated transcripts, obtaining the genes they correspond to and using that unique set of genes in an over-representation analysis (ORA) with the `enricher()` function from `clusterProfiler` (v.4.2.2) and gene sets obtained with the `msigdb` package (v.7.5.1). Pathways with an adjusted $P < 0.05$ were considered as significantly enriched. If more than 20 pathways were significantly enriched, the top 20 are shown in the corresponding plots.

3.10.3. Differential exon usage

Differential exon usage analysis using RNA-seq data was performed with the `DEXSeq` package (v.1.40.0). For each sample, BAM files were converted to SAM format with `samtools` (v.1.9). The python script available with `DEXSeq` called “`dexseq_prepare_annotation.py`” was used to prepare a flattened annotation file in GFF format by using the same GTF file used in the alignment step. Next, the number of reads overlapping each exon counting bin defined in the GFF file was obtained with the python script provided with `DEXSeq` called “`dexseq_count.py`” using the following parameters: `-p yes`, `-r pos` to indicate respectively that the data was from a paired-end sequencing run, and that the alignment data was sorted by position. For each comparison, the corresponding count files were used to proceed with the downstream analysis steps where a `DEXSeqDataSet` object was constructed and used for the normalization, dispersion estimation, and differential exon usage steps with default parameters. The parameter “`design = ~ sample + exon + condition:exon`” was used each time to define the full model formula. Significant differentially used exons were considered as those with a false discovery rate of 10%. Exon usage plots from significantly differentially used exons were obtained with the `DEXSeqHTML()` function.

3.11. Proteomics and analysis

3.11.1. Sample preparation

Proteolytic digestion was performed with Lys-C (FUJIFILM Wako Pure Chemical Corporation) in an enzyme/protein ratio of 1:100 (w/w) for 4 hours followed by a 6-fold

dilution with 50mM (NH₄)HCO₃ pH 8 (Sigma) to 1M GndCl. Samples were further digested with Trypsin gold (Promega) 1:40 overnight at 37°C. Resulting peptides were desalted using a 100mg SEP-PAK C18 cartridge (Waters) and vacuum centrifuged. For Tandem Mass Tag (TMT) labeling, dried peptides from each sample (250µg) were first reconstituted in 30µL 100mM HEPES pH 8 and 12µL of TMT solution (66,6µg/µL in pure acetonitrile) was then added. TMT labeling was performed at room temperature for 1.5h and reactions were quenched with hydroxylamine to a final concentration of 0.4% (v/v) for 15min. TMT-labeled samples were then pooled at a 1:1 ratio across all samples. A single shot control LC-MS run was performed to ensure similar peptide mixing across each TMT channel to avoid the need of further excessive normalization. The combined samples were then desalted using a 500mg SEP-PAK C18 cartridge (Waters) and vacuum centrifuged. For proteome analysis of TMT-labeled samples, 5% of the pooled samples were fractionated into 12 fractions using an Agilent OFF-Gel 3100 system following the manufacturer's instructions. Resulting fractions were desalted on SDBRPS StageTips¹⁵⁶ and dried by vacuum centrifugation. Phosphopeptides were enriched using the sequential metal oxide affinity chromatography (SMOAC) strategy using two consecutive High Select TiO₂ enrichments and a Fe-NTA enrichment (Thermo Scientific). Eluates were immediately acidified, combined and dried by vacuum centrifugation. Resulting phosphopeptides were fractionated with the Pierce High pH Reversed-Phase Peptide Fractionation Kit (Thermo Scientific). All fractions were dried by vacuum centrifugation and stored at -20°C until the day of mass spectrometry assessment and analysis.

3.11.2. Mass spectrometry analyses and data processing

Mass spectrometry assay and analysis were performed to standard protocol (Ref here). Shortly, each individual fraction was resuspended in 2% acetonitrile; 0.1% formic acid and nano-flow separations were performed on a Dionex Ultimate 3000 RSLC nano UPLC system on-line connected with a Lumos Fusion Orbitrap Mass Spectrometer interfaced with FAIMS Pro. A capillary precolumn (Acclaim Pepmap C18; 3µm-100Å; 2cm x 75µm ID) was used for sample trapping and cleaning. Analytical separations were performed at 250nl/min over a 150-min biphasic gradient on a 50cm long in-house packed capillary column (75µm ID; ReproSil-Pur C18-AQ 1.9µm silica beads; Dr. Maisch). Acquisitions were performed through Top Speed Data-Dependent

acquisition mode using 3 seconds cycle time. First MS scans were acquired at a resolution of 120'000 (at 200m/z) and the most intense parent ions were selected and fragmented by High energy Collision Dissociation (HCD) with a Normalized Collision Energy (NCE) of 37.5% using an isolation window of 0.7m/z. Fragmented ions scans were acquired with a resolution of 50'000 (at 200m/z) and selected ions were then excluded for the following 120s.

Raw data were processed using SEQUEST, Mascot, MS Amanda¹⁵⁷ and MS Fragger¹⁵⁸ in Proteome Discoverer v.2.4 against the Uniprot Human reference proteome (77027 canonical and isoform Sequences - Last Modified 21/01/29). Enzyme specificity was set to Trypsin and a minimum of six amino acids was required for peptide identification. Precursor tolerance and ion fragment tolerance were set at 10 ppm and 0.02 Da, respectively. Up to two missed cleavages were allowed and a 1% FDR cut-off was applied both at peptide and protein identification levels. For the database search, carbamidomethylation (C) and TMT tags (K and Peptide N termini) were set as fixed modifications whereas oxidation (M) and phosphorylation (S, T, Y) were considered as a variable. Proteome Discoverer node ptmRS was used for analysis and mapping of peptide/protein phosphorylation sites.

The resulting data were processed through in-house written R scripts (v.4.1.2)¹⁵⁹. The Proteome Discoverer proteins and peptide tables were processed separately. Common contaminants and proteins with a low FDR confidence were filtered out so that the proteins were not quantified in all the TMT channels. The TMT abundances were log₂ transformed.

Proteins with less than 2 peptides were discarded. A first normalization step was applied according to the Sample Loading normalization¹⁶⁰. Assuming that the total protein abundances were equal across the TMT channels, the reporter ion intensities of all spectra were summed and each channel was scaled according to this sum, so that the sum of reporter ion signals per channel equals the average of the signals across samples. Following this, a trimmed M-mean (TMM) normalization step was also applied using the package EdgeR¹⁵¹ (v.3.34.1). The normalization factors obtained from each step were used for the normalization of the phosphopeptide sets. Differential protein expression analysis was performed using R Bioconductor package

Limma (v.3.50.0)¹⁵⁴, followed by Benjamini-Hochberg multiple-testing method¹⁶¹.

The peptides with phosphosite(s) assigned with a confident localization probability greater or equal to 0.75 were retained. The intensities of phosphopeptides carrying different PTMs (apart from the common phosphorylation) were summed. The TMT abundances of the phosphopeptides were then normalized using the normalization factors originating from the proteome analysis. Differential protein expression analysis was performed using R Bioconductor package Limma (v.3.50.0)¹⁵⁴, followed by Benjamini-Hochberg multiple-testing method¹⁶¹.

3.11.3. Phosphosite visualization and pathway enrichment analysis

A protein was defined as differentially expressed with a threshold of adjusted $P < 0.05$ and $\text{abs}(\log_2 \text{fold-change}) > 0.5$. Differentially phosphorylated sites were defined with a threshold of 1) being situated on Class I phosphopeptides, 2) adjusted $P < 0.05$, and $\text{abs}(\log_2 \text{fold-change}) > 1$, and 3) either its absolute differentially expression level is higher than that at the corresponding proteome level or its fold-change is on the opposite direction than total proteome change.

Protein-protein interactions were retrieved from the STRING database (v11.5)¹⁶². Only those interactions having active interaction sources from “Experiments” were kept. Minimum required interaction score is 0.700. Network nodes were colored by the average \log_2 fold-change of displayed phosphosites.

We performed pathway enrichment analysis for differentially expressed proteins and for differentially phosphorylated proteins. We used the clusterProfiler R package (4.0.5)¹⁴⁵ on Gene Ontology (GO) and KEGG terms separately. Pathways with an adjusted $P < 0.05$ were deemed as significantly enriched.

3.12. Software

Quantitative data and statistical analysis were performed with GraphPad Prism v.9.4.1 (RRID: SCR_002798). Flow cytometric data were analyzed with FlowJo v10.8.1 (RRID: SCR_008520). Representation of data was generated in Adobe Illustrator 2021 (RRID: SCR_010279).

3.13. Data Availability

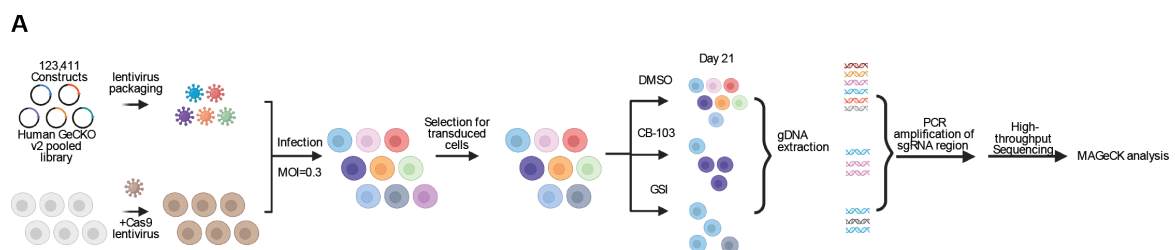
CRISPR screen data (GSE221576) and RNA-seq data (GSE221577) were deposited to Gene Expression Omnibus database repository. Proteomics data (PXD038908) were deposited to the ProteomeXchange Consortium via the PRIDE partner repository.

4. Results

4.1. Genome-wide CRISPR screen identifies *PIK3R1* associated with resistance to pharmacological Notch inhibition in T-ALL

The efficacy of targeted therapies for treatment of cancer patients is often limited by development of drug resistance¹⁰⁶. Potential resistance mechanisms to pharmacological Notch1 inhibition mediated by GSI or CB-103 in T-ALL are currently unclear. CRISPR screening is a powerful tool enabling the identification of mediators of drug resistance and sensitivity¹⁶³. Thus, we performed a genome-wide loss-of-function (LoF) CRISPR/Cas9 screen to identify genes responsible for resistance to Notch inhibition and novel combination therapies for efficient treatment of human T-ALL.

We used a Notch-dependent human T-ALL cell line, DND-41, which responds moderately to both GSI and CB-103 treatment *in vitro*⁸⁹. DND-41 cells stably expressing Cas9 were infected with human GeCKO v2 CRISPR libraries, containing 123,411 sgRNAs targeting 19,050 genes and treated with either vehicle, GSI or CB-103 for 21 days enabling both positive and negative selection of sgRNAs (Figure 8A).



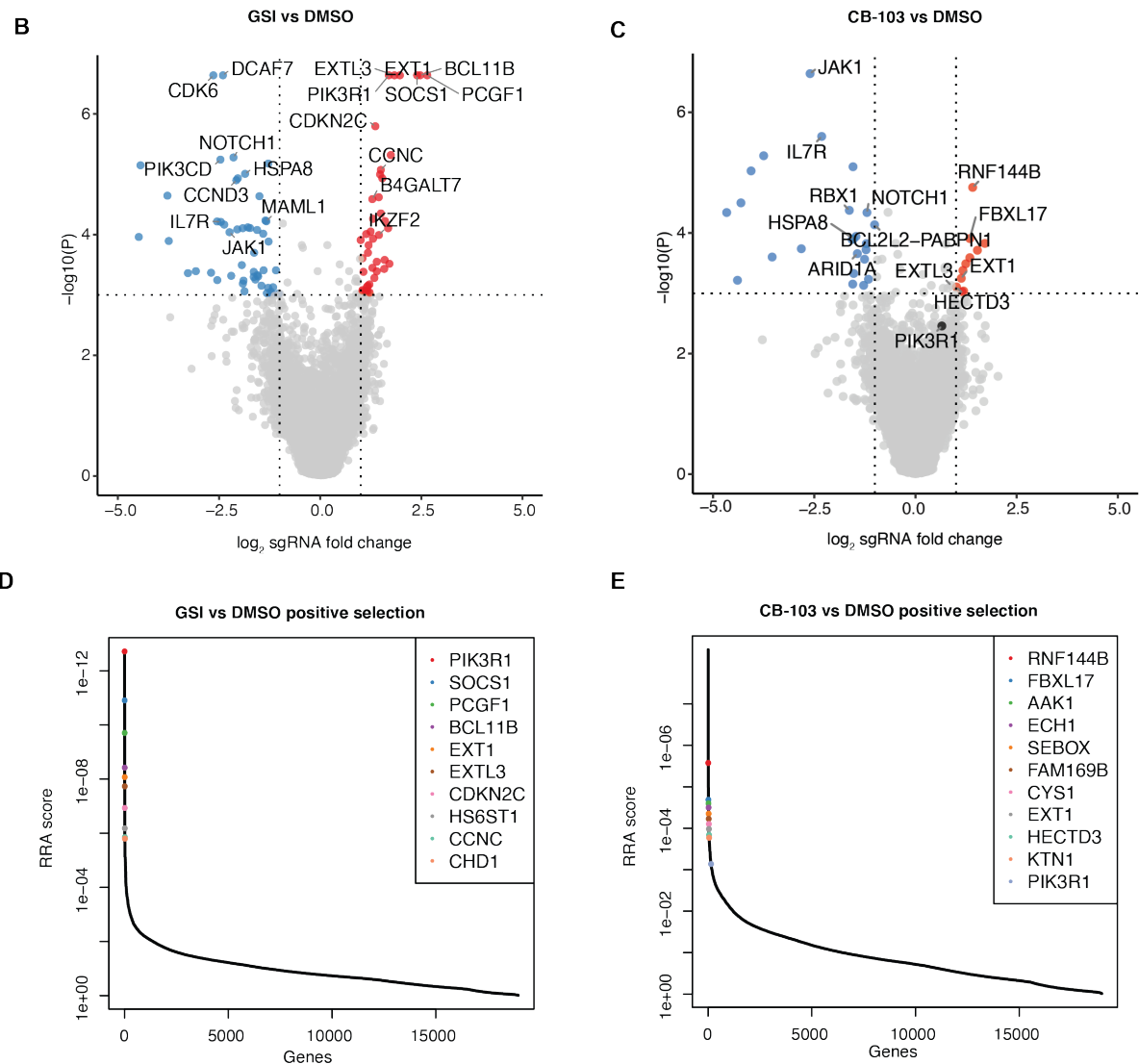


Figure 8. Functional genome-wide CRISPR screen identifies *PIK3R1* associated with resistance to Notch inhibition and druggable candidate pathways for combination therapies in T-ALL.

(A) Schematic representation of the genome-wide loss-of-function CRISPR screen. (B) Volcano plots depicting gene-targeting sgRNAs negatively or positively selected comparing γ -secretase inhibitor (GSI) vs DMSO treatment. Red, adjusted $P < 0.001$, \log_2 fold-change > 1 ; blue, adjusted $P < 0.001$, \log_2 fold-change < -1 . (C) Volcano plots showing gene targeting sgRNAs negatively or positively selected comparing CB-103 vs DMSO treatment. Red, adjusted $P < 0.001$, \log_2 fold-change > 1 ; blue, adjusted $P < 0.001$, \log_2 fold-change < -1 . (D) Robust rank aggregation (RRA) plots displaying the top 10 enriched sgRNAs comparing GSI vs DMSO treatment. (E) RRA plots displaying top enriched sgRNAs comparing CB-103 vs DMSO treatment.

sgRNAs targeting 293 (GSI-treated) and 131 (CB-103-treated) genes were identified as significantly depleted ($P < 0.05$, $\log_2FC < -1$) in GSI- and CB-103-treated T-ALL cells compared to vehicle control (Figure 8B-C). Negatively selected sgRNAs indicate

genes that, when inhibited, might function synergistically with Notch inhibition to effectively eradicate T-ALL cells. Pathway analysis revealed that significantly depleted genes were regulating MYC- and E2F signaling, as well as G2M checkpoint and mTOR signaling pathways (Figure 9).

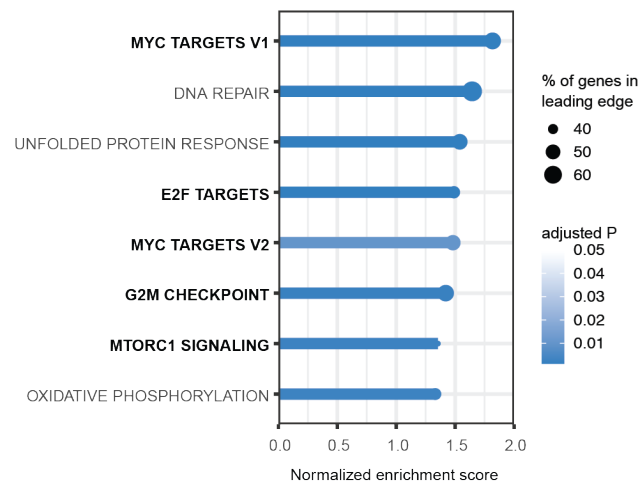


Figure 9. Genome-wide CRISPR screen reveals key candidate pathways synergistic with Notch inhibition.

Gene set enrichment analysis (GSEA) for negative-selection genes both in CB-103 and γ -secretase inhibitor (GSI) treatment in the CRISPR screen based on gene ranking (Robust rank aggregation score) in descending order. Significantly enriched (adjusted $P < 0.05$) hallmark pathways (y-axis) are shown as normalized enrichment score (x-axis). The solid line color scale resembles adjusted P , dot size of the leading-edge displays percentage of genes enriched in corresponding pathways.

Conversely, sgRNAs targeting 178 (GSI-treated) and 76 (CB-103) genes were identified as significantly enriched ($P < 0.05$, $\log_2FC > 1$) in GSI- and CB-103-treated cells compared to vehicle control, indicating that the loss of these genes could confer resistance to Notch inhibition (Figure 8B-C). Robust rank aggregation (RRA) method was used to identify genes preferentially lost in response to Notch inhibition (Figure 8D-E). Among these genes, *Phosphoinositide-3-Kinase regulatory subunit 1 (PIK3R1)* was identified at the top of the list in the GSI versus DMSO screen and was also identified in the screen of CB-103 versus DMSO-treated T-ALL cells.

The *PIK3R1* gene encodes for the p85 α regulatory subunit of PI3K, which contains an SH2 domain that binds to and inhibits the catalytic subunit (p110) of PI3Ks. Interestingly, *PIK3R1* mutations were identified as drivers of tumorigenesis in ovarian cancer¹⁴¹, endometrial cancer¹⁶⁴ and breast cancer¹⁶⁵. *PIK3R1* hotspot mutations in the SH2 domain were also recently reported in pediatric T-ALL patients^{67,68}. In addition,

we noticed that the positive regulatory subunit of PI3K (*PIK3CD*, leukocyte-restricted catalytic p110 δ subunit) was depleted in Notch inhibitor treated cells. Taken together, these observations suggested a key role of PI3K signaling in acquired resistance to Notch1 inhibition.

4.2. Loss of *PIK3R1* renders T-ALL cells resistant to pharmacological Notch inhibition

To validate the screening results, we generated multiple *PIK3R1* knockout clones in two different NOTCH1-driven T-ALL cell lines (DND-41, RPMI-8402) and stable knockdown clones in the NOTCH3-driven cell line TALL-1 (Figure 10).

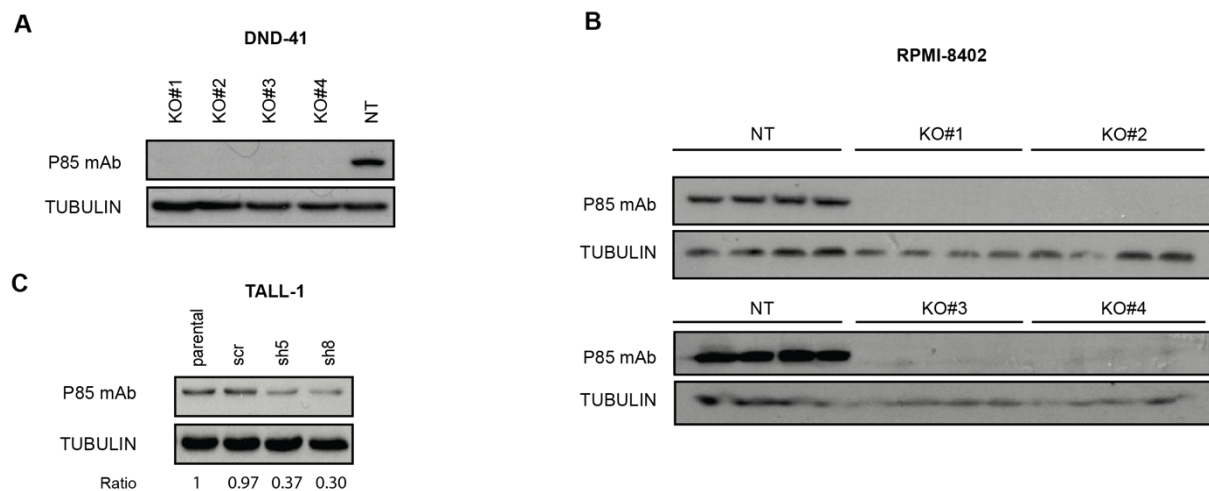


Figure 10. Total protein analyses in stable *PIK3R1* knockout or knockdown T-ALL cells.

(A) Total protein analyses of p85 expression in four different DND-41 *PIK3R1* knockout clones as well as Non-Target (NT) clone are shown. (B) Total protein analyses of p85 expression in four different RPMI-8402 *PIK3R1* knockout clones as well as NT clone are depicted. (C) Total protein analyses of p85 expression in two different TALL-1 *PIK3R1* knockdown cell lines as well as scrambled-hairpin control (scr) line were assessed. TUBULIN was used as loading control.

Loss of *PIK3R1* in several T-ALL cell lines led to no or a mild growth advantage compared to non-targeting control sgRNA clones (NT) or scrambled shRNA controls (scr). In contrast, cell growth of all GSI- and CB-103-treated *PIK3R1* knock-out (KO) or knock-down (KD) clones was significantly enhanced compared to NT or scr (Figure 11).

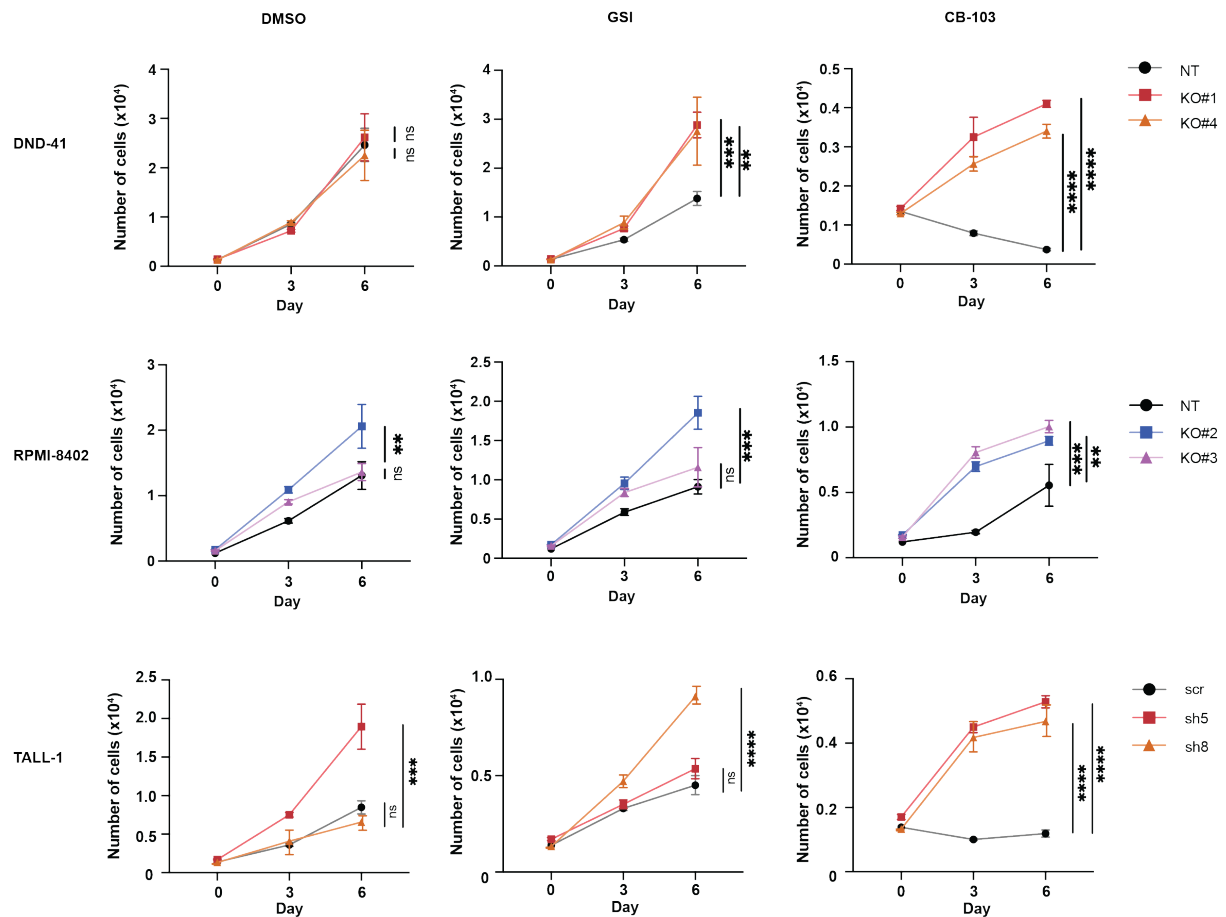


Figure 11. Loss of *PIK3R1* leads to resistance to Notch inhibition in T-ALL cells. Cell proliferation assays of T-ALL *PIK3R1* knockout or knockdown cell lines under DMSO, CB-103 or GSI treatment conditions. Black connected dots, Non-Target control (NT) or scrambled-hairpin control (scr); colored dots, representative *PIK3R1* knockout or knockdown cell lines. The values shown are mean \pm SD (n=3 biologically independent samples, two independent experiments). One-way ANOVA, non-significant (ns), **P* value < 0.0332, ***P* value < 0.0021, ****P* value < 0.0002, *****P* value < 0.0001.

We observed a significant decrease in the percentage of cells in S phase in NT or scr T-ALL clones when treated with GSI, confirming that GSI induces cell cycle arrest in T-ALL cells⁵⁵. However, this effect was alleviated in all *PIK3R1* KO and KD cell lines under the same treatment conditions (Figure 12). Interestingly, we also observed cell cycle arrest in RPMI-8402 and TALL-1 control lines treated with CB-103 and the effect was significantly decreased when *PIK3R1* was lost (Figure 12).

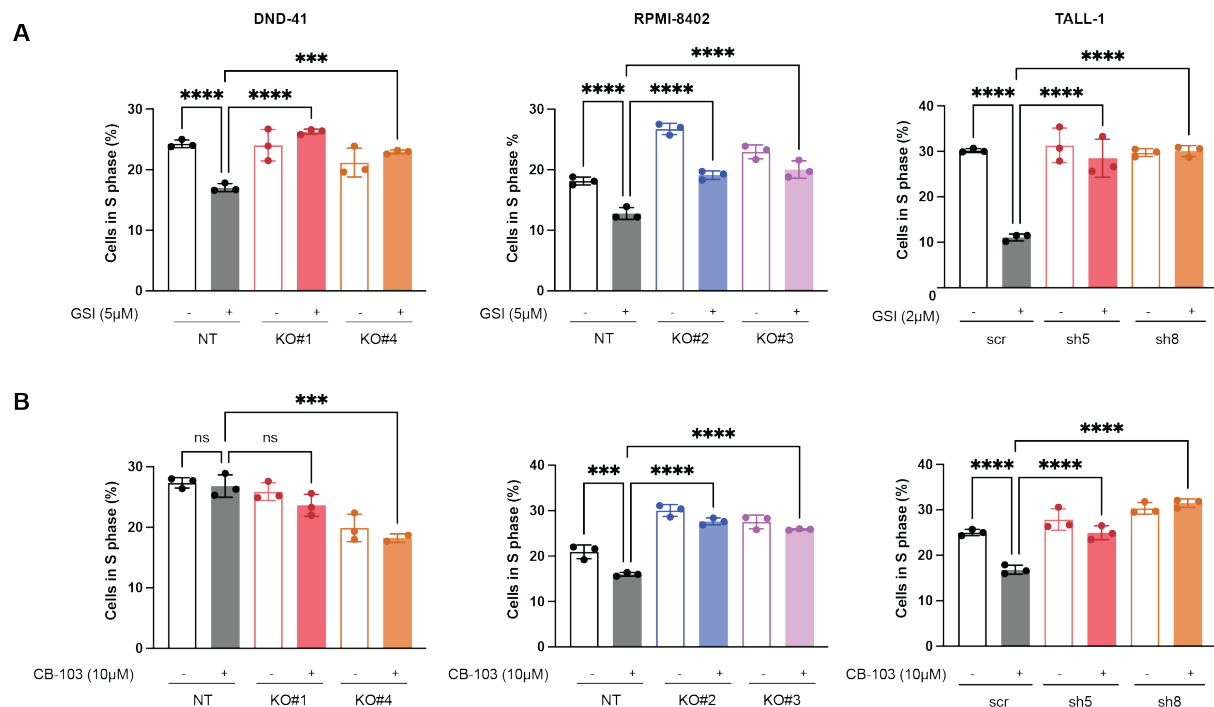


Figure 12. Loss of *PIK3R1* protects T-ALL cells from cell cycle arrest induced by Notch inhibition.

(A) Cell cycle analyses of *PIK3R1* knockout or knockdown cell lines performed 6 days post DMSO or GSI treatment at indicated concentrations. (B) Cell cycle analyses of *PIK3R1* knockout or knockdown cell lines 24hrs post DMSO or CB-103 treatment at indicated concentrations. The values shown are mean \pm SD (n=3 biologically independent samples, two independent experiments). One-way ANOVA, non-significant (ns), **P* value < 0.0332, ***P* value < 0.0021, ****P* value < 0.0002, *****P* value < 0.0001.

Previously, we showed that CB-103 induces apoptosis in T-ALL cells⁸⁹. Correspondingly, CB-103 treatment for three days induced substantial apoptosis significantly in all three control cell lines. However, loss of *PIK3R1* significantly ablated this effect (Figure 13). Altogether, these results suggest that loss of *PIK3R1* confers resistance of T-ALL cells to Notch inhibition by protecting them from both drug-induced apoptosis and cell cycle arrest.

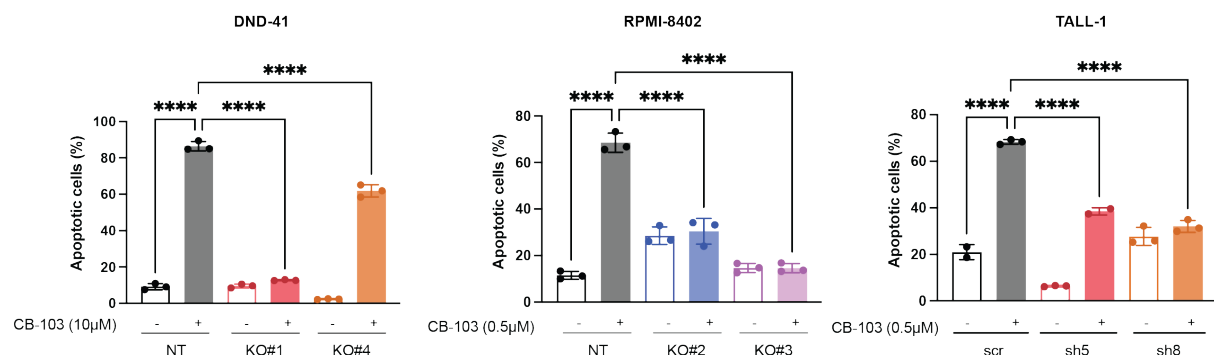


Figure 13. Loss of *PIK3R1* protects T-ALL cells from apoptosis induced by Notch

inhibitor CB-103.

Apoptosis assays of *PIK3R1* knockout or knockdown cell lines performed 3 days post DMSO or CB-103 treatment at indicated concentrations. The values shown are mean \pm SD (n=3 biologically independent samples, two independent experiments). One-way ANOVA, non-significant (ns), **P* value < 0.0332, ***P* value < 0.0021, ****P* value < 0.0002, *****P* value < 0.0001.

4.3. *PIK3R1* deficiency leads to elevated gene expression of proliferation and pro-survival pathways in response to Notch inhibition

To gain insight into how loss of *PIK3R1* confers resistance to pharmacological Notch inhibition in T-ALL cells, we performed gene expression analysis (Figure 14A). Treatment of RPMI-8402 cells for 24hrs with CB-103 resulted in significantly downregulation of genes associated to hallmark pathways including NOTCH signaling, MYC targets, and E2F targets (Figure 14B) as previously reported⁸⁹, whereas GSI treatment resulted in significantly downregulated MYC targets and MTOR signaling (Figure 14B). We did not observe significant enrichment of hallmark pathways when analyzing the gene expression differences of RPMI-8402 *PIK3R1* KO versus NT cells, albeit a moderate trend of increased expression of PI3K-AKT and KRAS hallmark pathway genes (Figure 14C). This might explain the no or mild growth advantage observed under normal culture conditions due to loss of *PIK3R1* in T-ALL cells (Figure 11). Interestingly, Gene Set Enrichment Analysis (GSEA) from CB-103-treated KO versus NT cells revealed enrichment in multiple hallmarks including E2F targets, MYC targets, PI3K-AKT-MTOR signaling, G2M checkpoint and Apoptosis pathways (Figure 14D). Increased expression of MYC target genes was also observed in GSI-treated KO versus NT cells (Figure 14D).

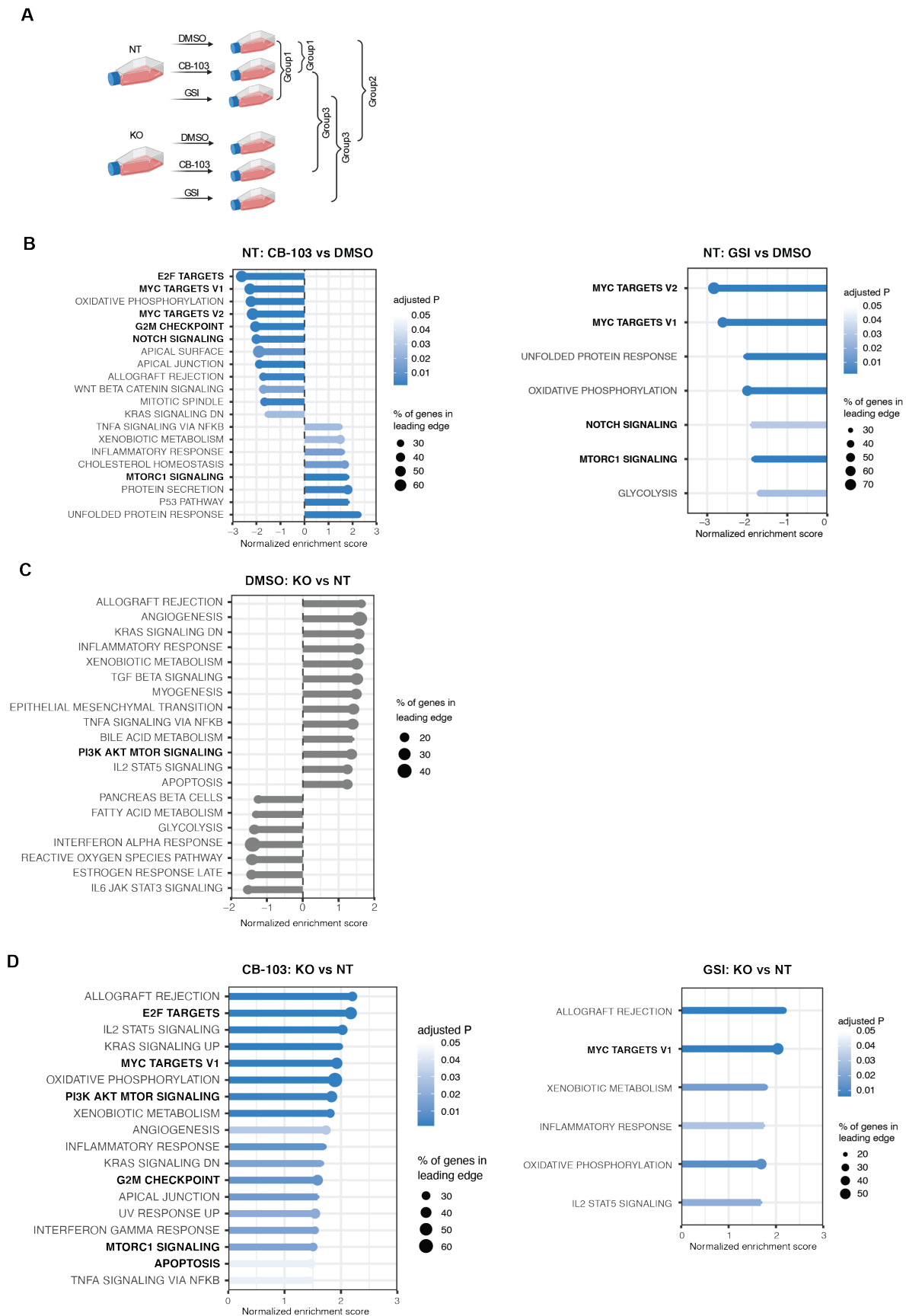


Figure 14. Experimental design and overview results of RNA-seq study. (A) Experimental set-up and three comparison groups to assess the effect of loss of *PIK3R1* to Notch inhibition in RPMI-8402 cell line at transcriptional level are depicted. (B) Top

significantly enriched Hallmark pathways of gene expression level changes comparing CB-103 vs DMSO treated (left panel), GSI vs DMSO treated (right panel) T-ALL cells. (C) Enriched Hallmark pathways of gene expression level changes comparing *PIK3R1* KO vs NT cells. (D) Top significantly enriched Hallmark pathways of gene expression level changes comparing *PIK3R1* KO CB-103 treated vs NT CB-103 treated (left panel), *PIK3R1* KO GSI treated vs NT GSI treated (right panel) T-ALL cells. Significantly enriched (adjusted $P < 0.05$) hallmark pathways (y-axis) are shown as normalized enrichment score (x-axis). The solid line color scale resembles adjusted P (grey, non-significant), dot size of the leading-edge displays percentage of genes enriched in corresponding pathways.

Specifically, upregulation of key E2F family transcriptional activators including E2F1, E2F2, E2F3, cell cycle regulators *CCND2*, *CCND3*, and downregulation of the transcriptional repressor E2F5 were observed. In addition, we detected significant upregulation of anti-apoptotic genes such as *BCL2* and *BCL-xL* (Figure 15A-B). In contrast, typical Notch target genes including *MYC*, *HES1* or *DTX1* were equally downregulated in CB-103-treated *PIK3R1* KO and NT cells (Figure 15C).

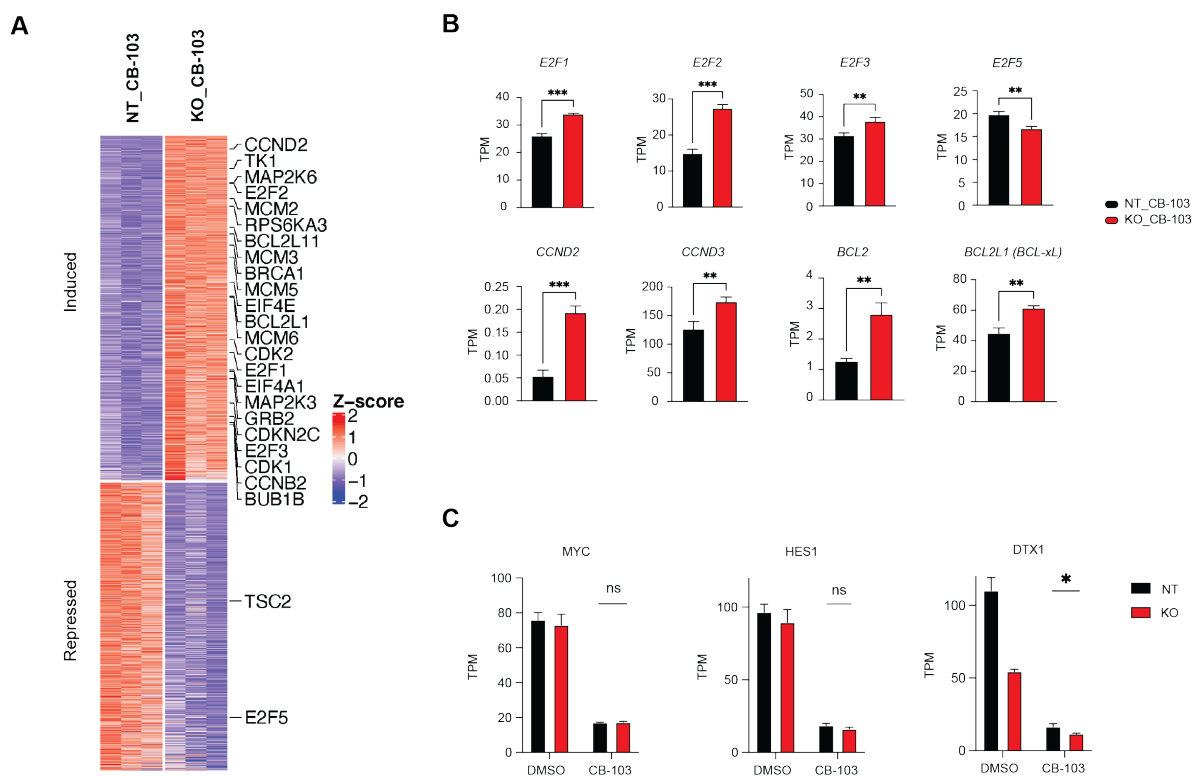


Figure 15. RNA-seq analysis of *PIK3R1* KO cells reveals responses to Notch inhibition at transcriptional level.

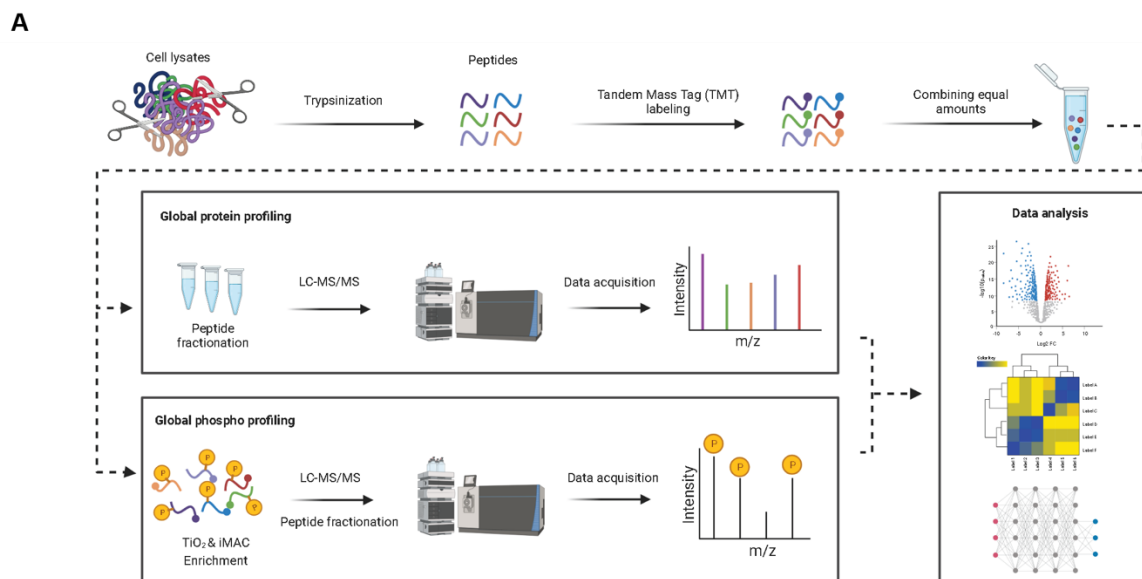
(A) Heatmap plot showing unbiased clustering of gene expression level changes comparing *PIK3R1* KO CB-103-treated vs NT CB-103-treated T-ALL cells, highlighting key genes involved in E2F targets, PI3K-AKT-mTOR signaling and apoptosis pathway. (B) Expression of a subset of differentially expressed genes measured as transcripts per million (TPM) comparing *PIK3R1* KO CB-103-treated vs NT CB-103-treated T-ALL cells. (C) Expression of indicated genes measured as TPM comparing *PIK3R1* KO (red bars) vs NT (black bars) cells with or without CB-103 treatment. Values shown are mean \pm SD. One way ANOVA test, * P

value < .0332, ***P* value < 0.0021, ****P* value < 0.0002, *****P* value < 0.0001.

These results are consistent with the increased proliferation and survival observed in drug-treated *PIK3R1* KO vs NT cells (Figure 12-13), and provide some mechanistic insight for Notch inhibitor resistance.

4.4. Notch-inhibited *PIK3R1*-mutant T-ALL cells reveal major phosphorylation changes in the cell cycle and spliceosome machinery

The p85 protein, which is encoded by *PIK3R1*, is an essential component of a key kinase signaling complex. Loss of this protein can cause rapid changes in signaling events. Therefore, we performed total- and phospho-proteome analysis of RPMI-8402 NT and *PIK3R1* KO cells treated with DMSO or CB-103 (Figure 16A-B).



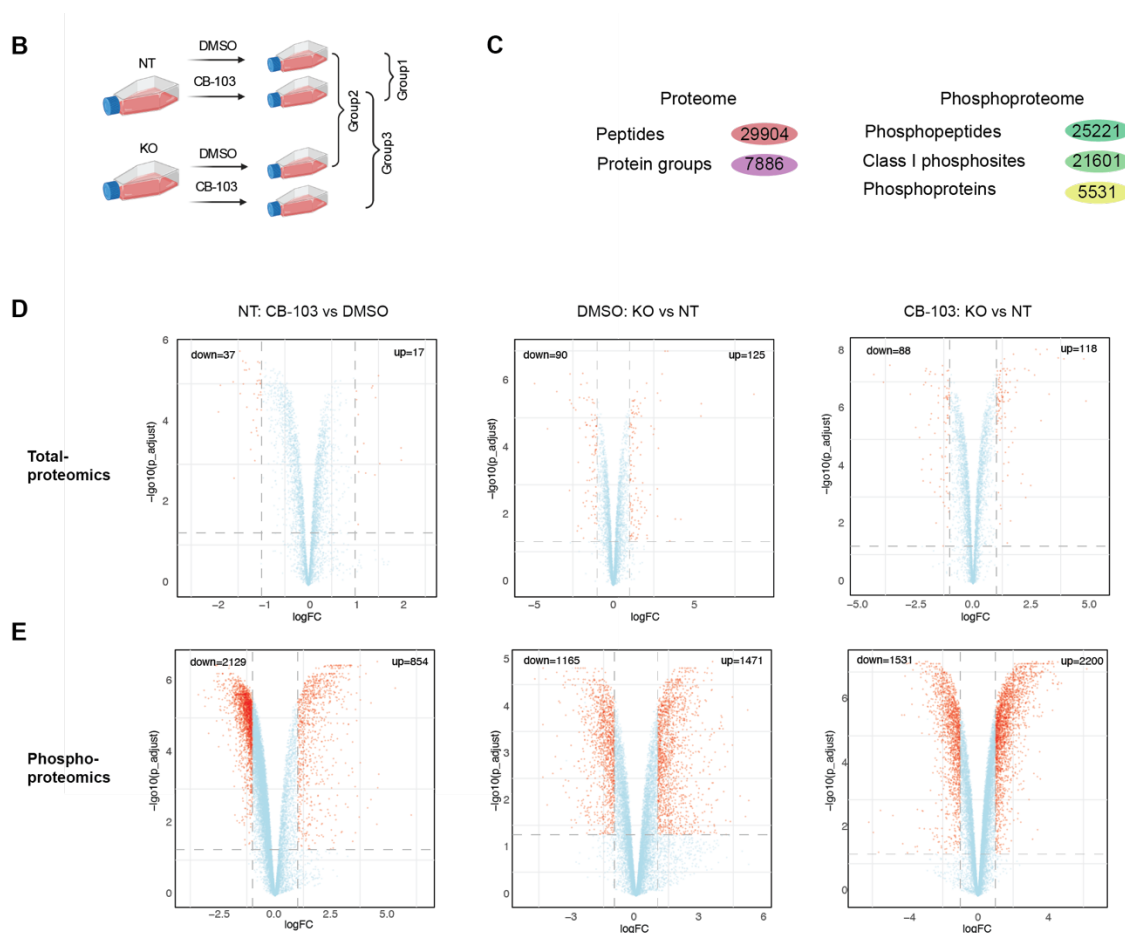


Figure 16. Experimental design and overview of total proteomics and phosphoproteomics study.

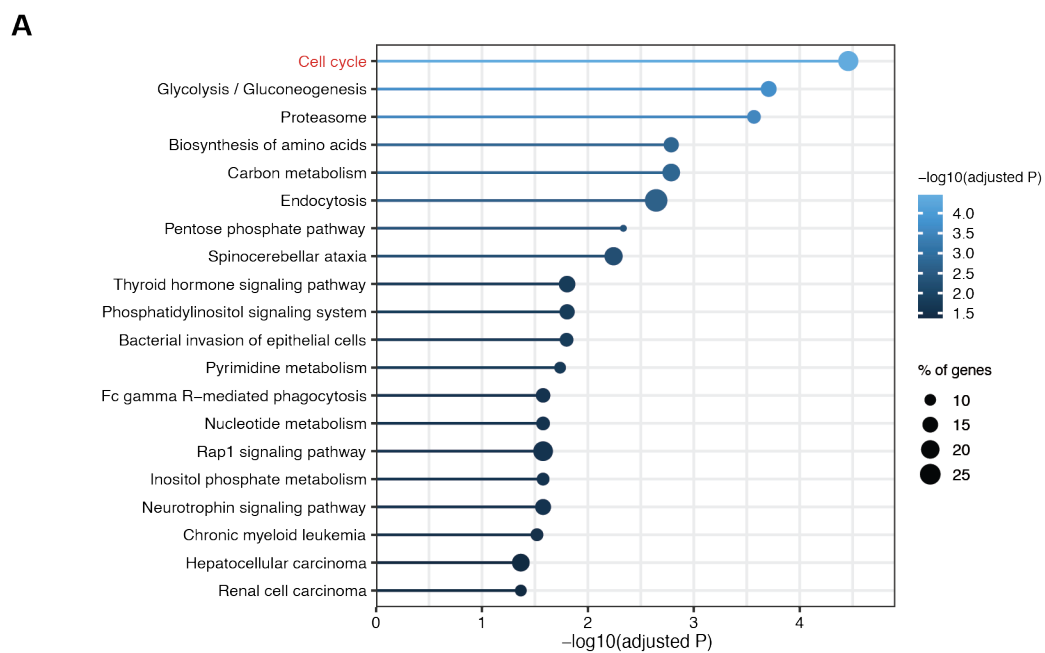
(A) Workflow of total proteomics and phosphoproteomics study. (B) Experimental set-up and three comparison groups to assess the effect of loss of *PIK3R1* to CB-103 in RPMI-8402 T-ALL cell line. (C) Overview of results from proteome and phosphoproteome analysis. (D) Volcano plot depicting protein level changes for each comparison. Red, significant, $FDR < 0.05$, $abs(\log_2 \text{fold-change}) > 1$; blue, non-significant (ns). (E) Volcano plot displaying phosphorylational level changes for each comparison. Red, significant, $FDR < 0.05$, $abs(\log_2 \text{fold-change}) > 1$; blue, non-significant (ns).

Across samples, we quantified 29904 peptides corresponding to 7886 protein groups and 25221 phosphopeptides, of which 21601 were categorized as class I phosphosites¹⁶⁶ originating from 5531 phosphoproteins (Figure 16C).

At the total protein level, we observed 54 (NT, CB-103 versus vehicle), 215 (*PIK3R1* KO versus NT) and 206 (*PIK3R1* KO CB-103 versus NT CB-103) significant changes (Figure 16D). The comparisons at the phosphorylation level revealed 2983 (NT, CB-103 versus vehicle), 2636 (*PIK3R1* KO versus NT) and 3731 (*PIK3R1* KO CB-103 versus NT CB-103) significant changes (Figure 16E). Thus, changes occurring at the level of phosphorylation profiles are much more pronounced compared to changes of

the total proteome.

KEGG analysis of total protein changes of CB-103-treated *PIK3R1* KO versus NT cells, identified cell cycle regulation as the most significantly affected pathway (Figure 17A), which corroborated observations from the RNA-seq data. Similar analysis at the phosphoproteome level pointed to cell cycle and spliceosome as the most significant alterations (Figure 17B).



B

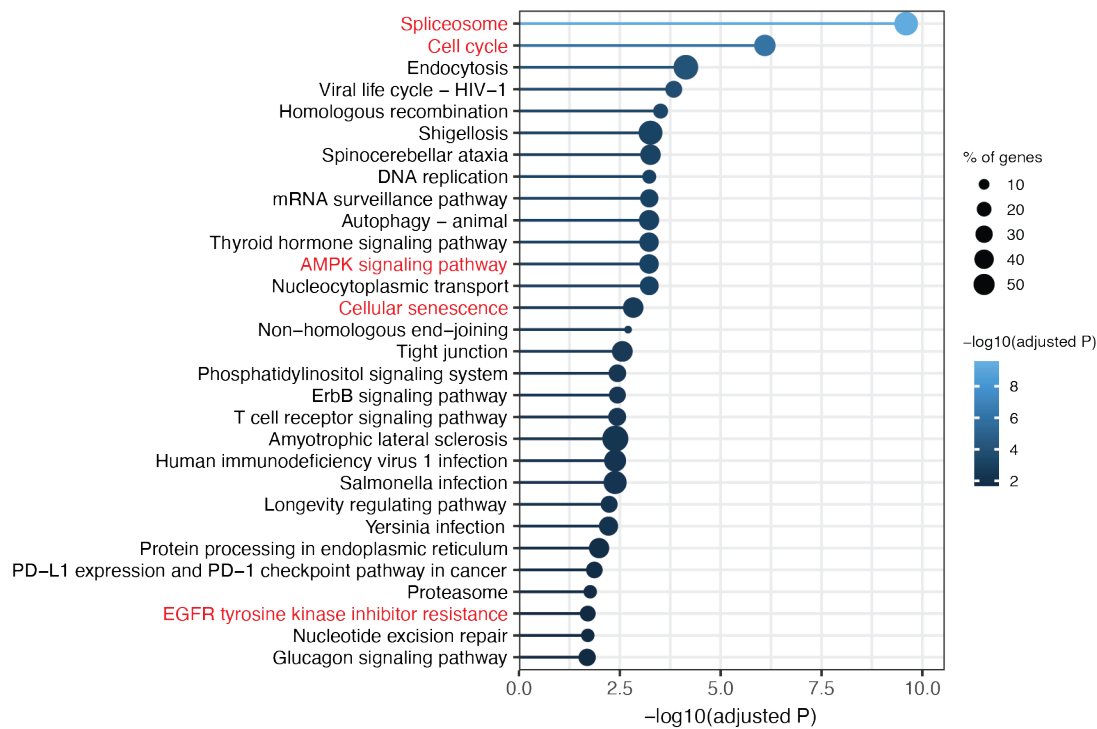


Figure 17. Pathway enrichment analysis reveals key signaling changes in *PIK3R1* deficient cells in response to Notch inhibition.

Significantly enriched KEGG pathways of proteins with altered total protein level changes (A) or with altered level of phosphorylations (B) comparing *PIK3R1* KO CB-103-treated vs NT CB-103-treated T-ALL cells. Top 20 (A) or 30 (B) pathways are shown, the solid line color scale resembles adjusted *P*, dot size of the leading-edge displays percentage of genes enriched in corresponding pathways.

To dissect kinase regulation in more detail, we performed Kinase-substrate Enrichment Analysis (KSEA) on the differential phosphorylation profiles of our comparison groups (Figure 18). The analysis of CB-103 versus vehicle revealed that CB-103 treatment led to decreased AKT1, MTOR, and S6K signaling (Figure 18A), whereas the *PIK3R1* versus NT comparison showed the expected reciprocal outcome, with increased PKC family, AKT signaling, due to loss of p85, (Figure 18B). Importantly, comparison of *PIK3R1* KO CB-103-treatment versus NT CB-103-treatment showed increased activating phosphorylation events for AKT 1/2/3, PKC family, and S6K, which were maintained and no longer downregulated by CB-103 treatment (Figure 18C). This is comparable to a recent proteomics study, which showed the involvement of the PKC family and AKT signaling pathways in the resistance to GSI in DND-41 cells¹⁶⁷.

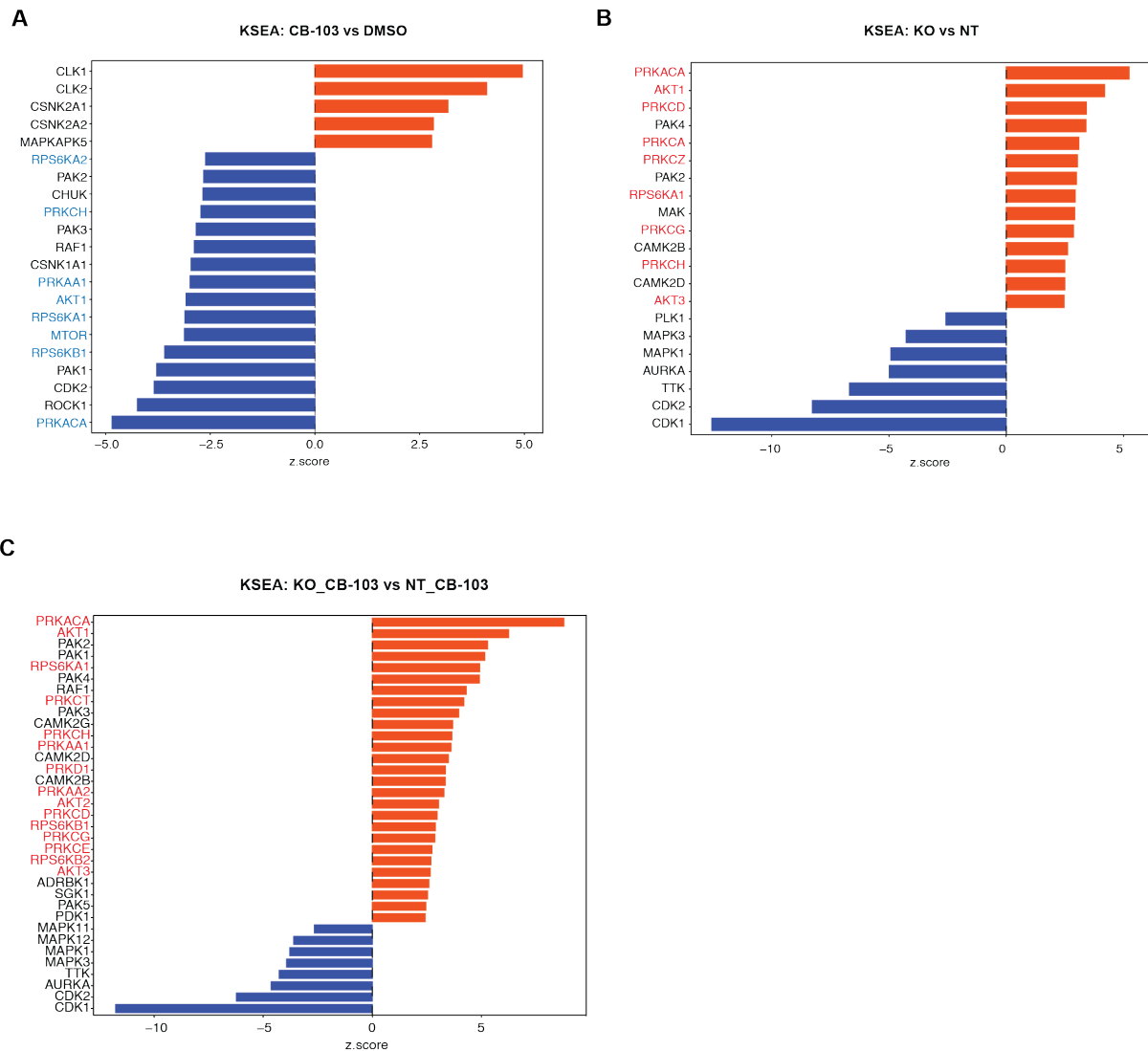


Figure 18. Kinase-Substrate-Enrichment-Analysis reveals differential kinase activities in *PIK3R1* deficient cells in response to Notch inhibition.

(A) Kinase-Substrate-Enrichment-Analysis (KSEA) of phosphorylation profiles comparing CB-103 vs DMSO treated RPMI-8402 cells. (B) KSEA of phosphorylation profiles comparing *PIK3R1* KO vs NT RPMI-8402 cells. (C) KSEA of phosphorylation profiles comparing *PIK3R1* KO CB-103-treated vs NT CB-103-treated RPMI-8402 cells. Red, kinases with positive z-score; blue, kinases with negative z-score.

Subsequently, we examined interactions among key proteins (Figure 17B) using experimentally validated knowledge from the STRING database (Figure 19A) and highlighted phosphorylation changes on these proteins (Figure 19B). This detailed phospho-mapping provides insights regarding functionally established phosphorylation events such as S780 for RB as well as less examined events including T451 on AKT2, which has previously been associated with oncogenic signaling (Figure 19B).

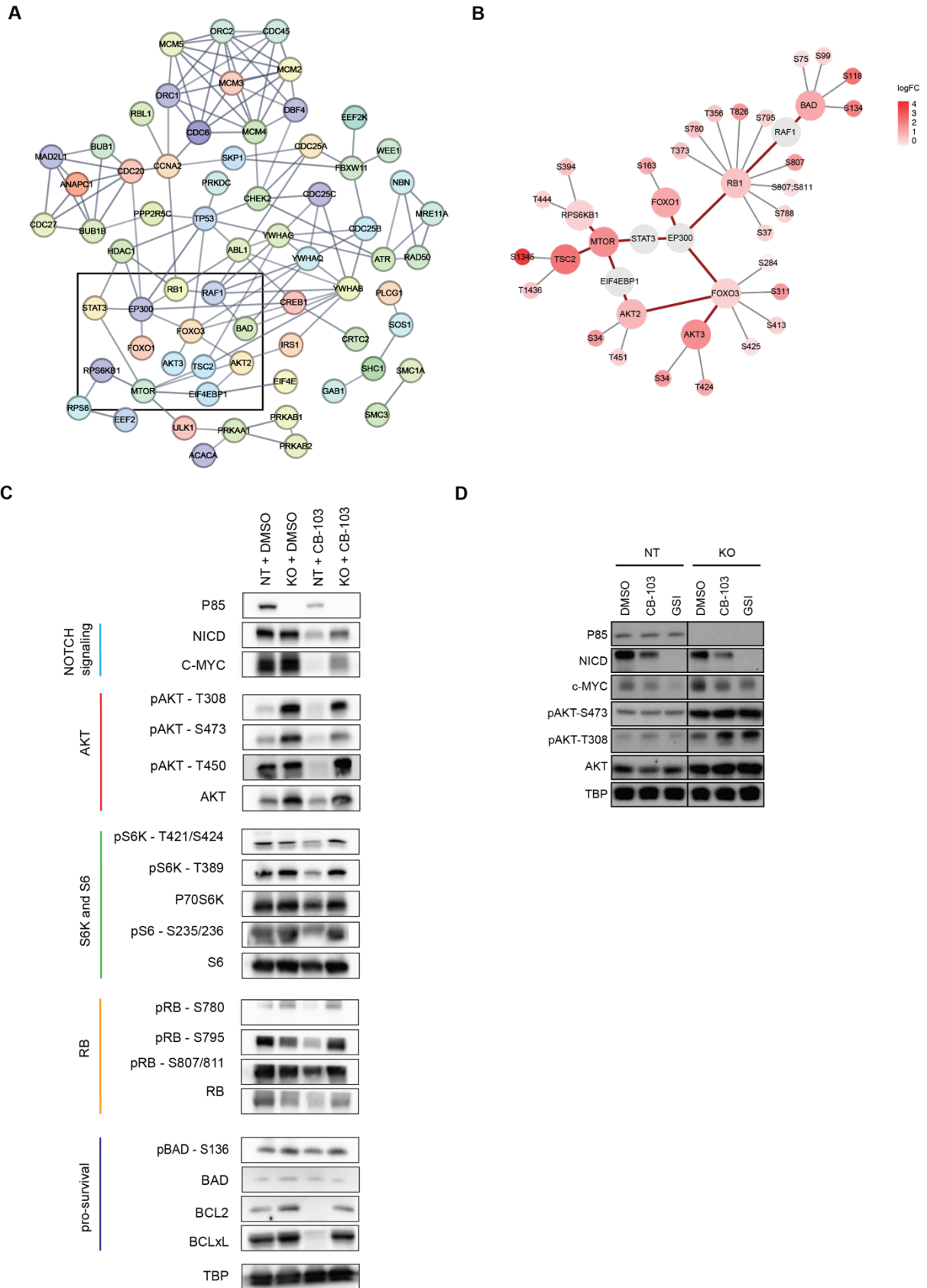


Figure 19. Loss of *PIK3R1* in T-ALL cells causes major phosphorylation changes in the cell cycle regulation pathway.

(A) Interactions among phosphoproteins within 4 of the top enriched KEGG pathways in Figure 17B: assessing cell cycle, AMPK signaling, cellular senescence, EGFR tyrosine kinase

inhibitor resistance pathways. Line color indicates the strength of interaction (“Confidence” from the STRING database). Key nodes are gated with black rectangle. (B) Detailed plots of key phosphoproteins with annotated phosphosites and corresponding fold changes from (A) rectangle area. Red circle, identifies phosphoproteins with phosphorylation changes as \log_2 fold-change >1 , FDR <0.05 . Grey circle, identifies phosphoproteins with phosphorylation sites omitted. Red connecting line, protein interaction from STRING database. Grey radiating line, detailed phosphorylation sites associated with phosphoproteins. (C) Total protein and phosphorylation level of indicated phosphosites by Western blotting for key proteins involved in indicated nodes or pathways: Notch signaling (Light blue); AKT (Red); S6K and S6 (Green); RB (Orange); pro-survival signaling (Dark Blue) in RPMI-8402 NT or *PIK3R1* KO cells. (D) Total protein and phosphorylation level of indicated phosphosites by Western blotting for key proteins involved in Notch and PI3K-AKT pathways in DND-41 NT or *PIK3R1* KO cells. TATA-box binding protein (TBP) was used as loading control.

Immunoblotting validated key phosphorylation events for AKTs, S6K, RB1 and BAD, which are important regulators of proliferation and cell survival (Figure 19C). CB-103 treatment resulted in marked downregulation of NICD and C-MYC⁸⁹, along with reduced total AKT levels and more pronounced reduced phosphorylation at residues T308, S473 and T450. Yet, these effects were largely ablated in p85-deficient cells (Figure 19C-D). Similarly, the phosphorylation of ribosome protein S6 kinase (p-S6K, T389, T421/S424) and its downstream substrate S6 (p-S6, S235/236) were downregulated by CB-103 treatment but not in p85-deficient cells. Thus, loss of *PIK3R1* indeed helps to maintain proteins involved in protein translation under CB-103 treatment. In addition, all phosphorylation sites of RB tested (S780, S795 and S807/811) were downregulated in CB-103 sensitive compared to the resistant cells (RB). The same holds true for BCL2 and BCL-xL, whereas BAD and p-BAD levels (pro-survival) remained comparable. These results confirm that p85-deficient T-ALL cells are able to cope with Notch inhibition through increased AKT signaling and maintain protein translation, cell proliferation and pro-survival pathways (Figure 19C).

Interestingly, LoF *PIK3R1* led to prominent phosphorylation changes in proteins involved in the spliceosome and RNA processing in cells treated with pharmacological Notch inhibitors (Figure 17B). This analysis allowed to establish changes in phosphorylation profiles of splicing factors upon altered PI3K signaling and highlighted a wide spectrum of so far uncharacterized phosphorylation sites (Figure 20A-B). A recent report linked oncogenic PI3K signaling with splicing alterations in breast cancer at transcriptional level¹⁶⁸. Thus, we reanalyzed our RNA-seq data for differentially expressed transcripts, which were indeed associated with genes involved in cell cycle and regulation of apoptosis signaling pathways (Figure 20C-D).

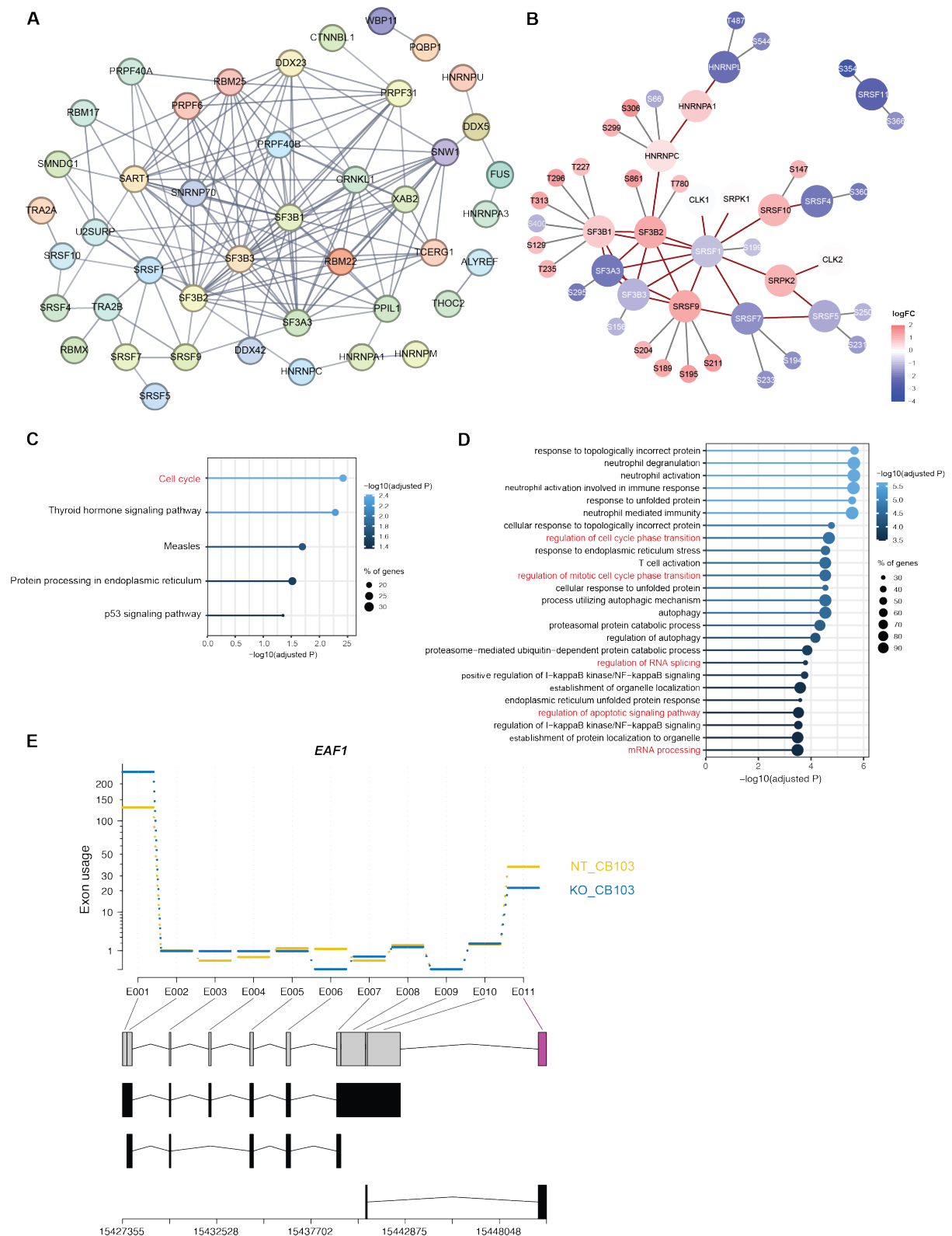


Figure 20. RNA splicing is altered in *PIK3R1* KO cells in response to Notch inhibition.

(A) STRING analysis of phosphoproteins within spliceosome pathway in Figure 4A. Line thickness indicates the strength of data support (“Confidence”), interaction source is

“Experiments”, minimum required interaction score is 0.700. (B) Detailed plots of key phosphoproteins with annotated phosphosites and corresponding fold changes from A. Red circles identified phosphoproteins with phosphorylational changes as fold-change > 2, FDR < 0.05. Grey circles identified phosphoproteins with phosphorylation sites omitted. Red connecting line, interaction with proteins demonstrated by String analyses, grey radiating line, depicting detailed phosphorylation sites associated with phosphoproteins. (C) Top significantly enriched KEGG pathways of transcripts with altered expression levels comparing *PIK3R1* KO CB-103 treated vs NT CB-103 treated T-ALL cells. The solid line color scale resembles adjusted *P*, dot size of the leading-edge displays percentage of genes enriched in corresponding pathways. (D) Top significantly enriched gene ontology biological process (GOBP) pathways of transcripts with altered expression levels comparing *PIK3R1* KO CB-103 treated vs NT CB-103 treated T-ALL cells. The solid line color scale resembles adjusted *P*, dot size of the leading-edge displays percentage of genes enriched in corresponding pathways. (E) Fitted splicing plot from DEXSeq analysis displaying differential exon usages of gene *ELL Associated Factor 1 (EAF1)* comparing *PIK3R1* KO CB-103 treated vs NT CB-103 treated T-ALL cells. Purple, altered exon usage.

Furthermore, we assessed the differential exon usage using DEXSeq and identified a spectrum of genes with alternative exon usage events in *PIK3R1* deficient cells in response to Notch inhibition compared to NT cells, including transcripts of *ELL Associated Factor 1 (EAF1)* (Figure 20E).

Our results show that loss of *PIK3R1* in T-ALL cells led to increased PI3K-AKT signaling, causing major phosphorylation changes in the cell cycle and spliceosome machinery that resulted in downstream activation of cell cycle progression, increased cell proliferation, E2F gene activation, increased protein synthesis and cell survival. Changes in the spliceosome at phosphorylation levels correlated also with differential splicing at the transcriptional level. Consequently, these mechanisms contribute to resistance to Notch inhibition in T-ALL (Figure 21).

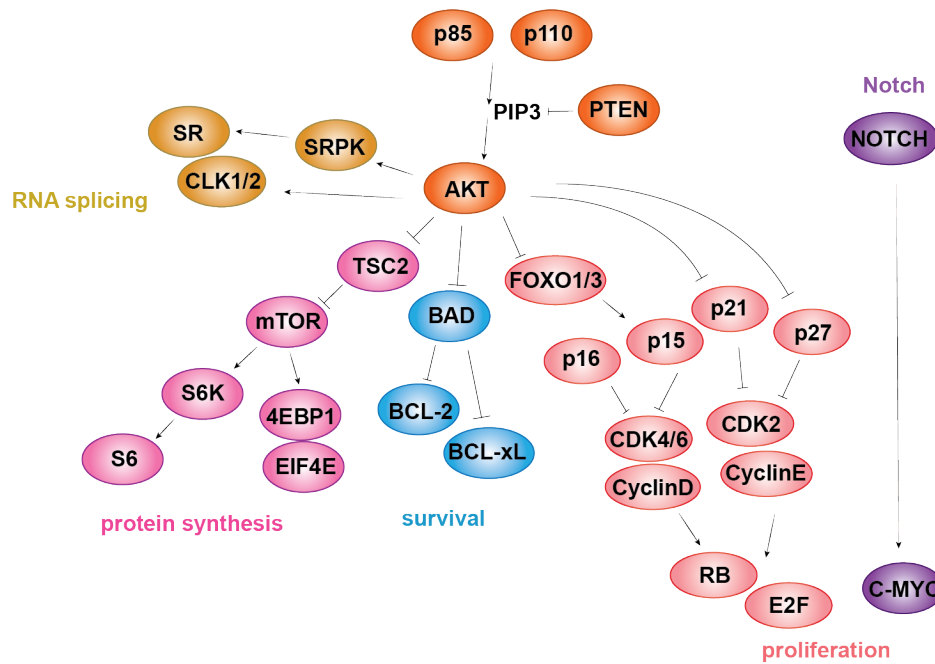


Figure 21. A proposed model summarizing the key nodes mediating resistance to Notch inhibition upon loss of *PIK3R1*.

Notch signaling (Dark purple); PI3K-AKT (Orange); Protein synthesis (Light purple); Cell proliferation (Pink); Pro-survival signaling (Blue); RNA splicing (Brown).

4.5. Pharmacological Notch inhibitors synergize with targeted therapies in human T-ALL cells *in vitro*

The advantage of using a CRISPR/Cas9 screen in T-ALL cells under drug selection is enables the identification of not only candidate genes that mediate drug resistance, such as *PIK3R1*, but also genes and pathways that are crucial for cell survival under drug selection. This opens avenues to identify novel combination therapies. Preferentially depleted sgRNAs in GSI- and CB-103-treated T-ALL cells pointed to well established signaling components within T-ALL, including components of the IL7/JAK pathway (IL7R, JAK1), regulators of the cell cycle machinery (CDK6:CCND3), and the key gene encoding the PI3K catalytic subunit (*PIK3CD*) (Figure 8B-C).

We validated these candidates using available FDA-approved inhibitors against CDK4/6 (PD-0332991), JAK1/2 (Ruxolitinib), and PIK3 δ (CAL-101). We first established *in vitro* sensitivity profiles, and observed that the single agent IC₅₀ of CB-103 for DND-41 cells was 4.3 μ M and 0.1 μ M for PD-0332991. We then tested a combination treatment administrating CB-103 and PD-0332991 at three fixed ratios of

their corresponding IC₅₀ (1:1, 1:2.5 and 1:0.5) and established dose response curves (Figure 22A). The combination treatment increased sensitivity of the cells to CB-103 by lowering its IC₅₀ to approximately 0.1 μM, which is 43-fold lower than single agent treatment (Figure 22A). Similarly, combination of PD-0332991 and GSI lowered the IC₅₀ of GSI approximately 100-fold (Figure 22B). The Combination Index¹⁴² (CI) was 0.06 for CB-103 plus PD-0332991 and 0.0183 for GSI plus PD-0332991, both of which are below 0.1 indicating very strong synergism (Figure 23).

In addition, combination treatment induces the downregulation of C-MYC, which is downstream of Notch and p-RB as key cell cycle regulator in two independent T-ALL cell lines (Figure 22C).

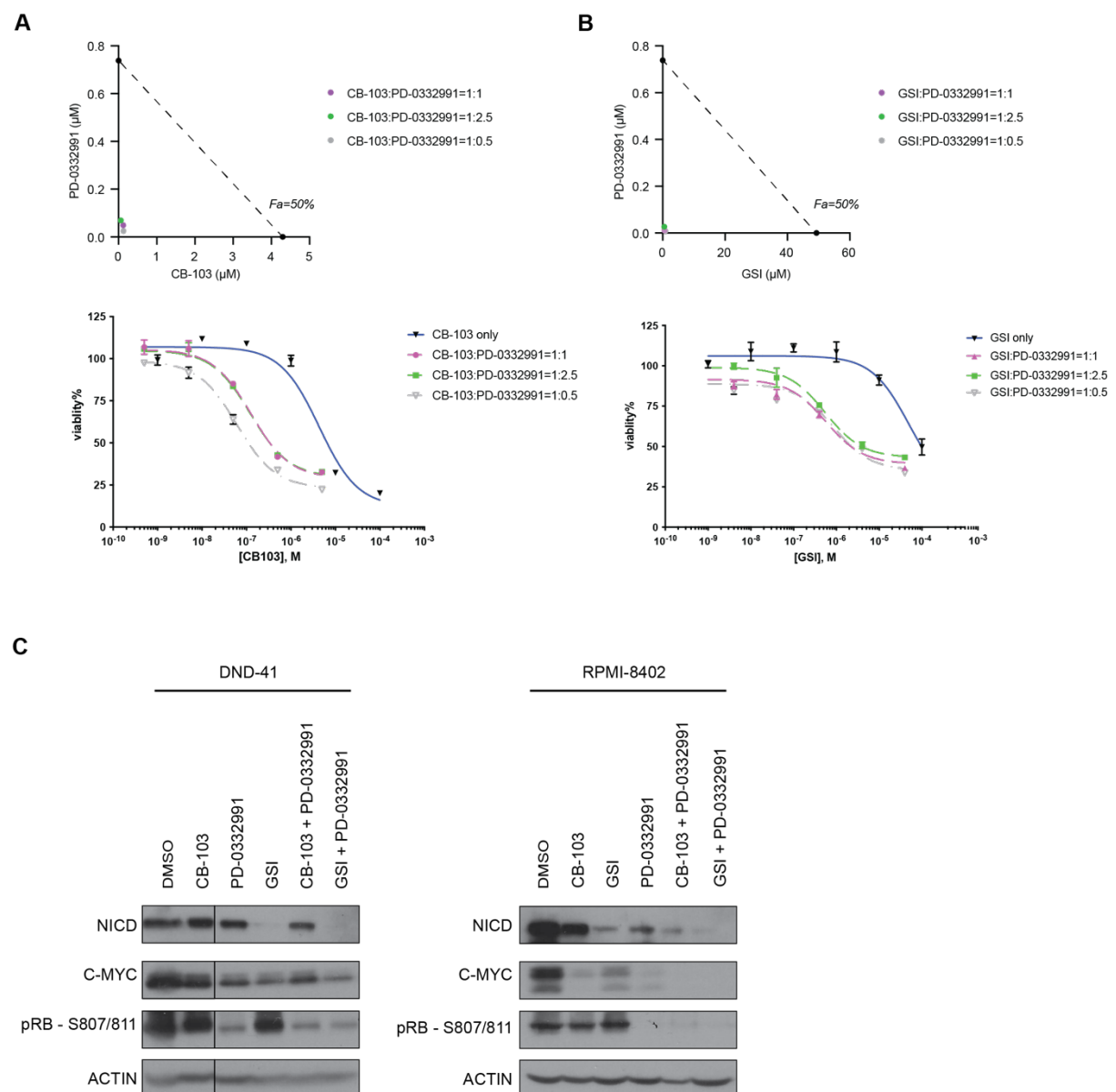


Figure 22. *In vitro* synergy between Notch inhibitors and a CDK4/6 inhibitor.

(A) Isobologram plots (upper panel) and cell survival assay (lower panel) of T-ALL cells in response to CB-103 alone (Blue), or in combination with PD-0332991 with corresponding ratios of each IC50 in decreasing doses for 3 days. Purple, ratio (Notch inhibitor: PD-0332991) = 1:1; Green, ratio = 1:2.5; Grey, ratio = 1:0.5. X-axis plotting concentration of CB-103. The values shown are mean \pm SD (n=4 biologically independent samples, two independent experiments performed). (B) Isobologram plots (upper panel) and cell survival assay (lower panel) of T-ALL cells in response to γ -secretase inhibitor (GSI) alone (Blue), or in combination with PD-0332991 with corresponding ratios of each IC50 in decreasing doses for 3 days. Purple, ratio (Notch inhibitor: PD-0332991) = 1:1; Green, ratio = 1:2.5; Grey, ratio = 1:0.5. X-axis plotting concentration of GSI. The values shown are mean \pm SD (n=4 biologically independent samples, two independent experiments performed). (C) Total protein levels of NICD and C-MYC as well as phosphorylation level of p-RB in DND-41 cells (left panel) and RPMI-8402 cells (right panel). Cells were treated with DMSO or corresponding single drugs or drug combinations for 24hrs. ACTIN was used as loading control.

Similarly, we observed very strong synergism combining Notch inhibitors with a JAK1/2 inhibitor or a PI3K δ inhibitor (Table 4).

Targets	CDK4/6:CCND3	JAK1/2	PI3K δ
Drugs	PD-0332991	Ruxolitinib	CAL-101
CI (CB-103)	0.06	0.064	0.624
CI (GSI)	0.0183	0.0177	0.0009

Table 4. *In vitro* synergy between Notch inhibitors and multiple targeted therapies identified from the CRISPR screen.

A table summarizing combination index (CI) of Notch inhibitors together with PD-0332991, Ruxolitinib or CAL-101.

These findings suggest that Notch inhibition in combination with FDA-approved compounds targeting CDK4/6, IL7R signaling, or PI3K/AKT pathway should be more efficacious compared to single agent treatment.

4.6. Pharmacological Notch inhibitors synergize with targeted therapies in a human T-ALL cell line xenografted model

These promising *in vitro* results prompted us to assess their efficacy in xenotransplantation assays. RPMI-8402 T-ALL cells expressing a luciferase reporter were transplanted into NSG mice to monitor tumor growth and progression of disease over time. Animals with established tumors were treated with single agent compounds (vehicle, CB-103, GSI, PD-0332991) or with combination therapies (CB-103 or GSI

plus PD-0332991) for two weeks (Figure 23A).

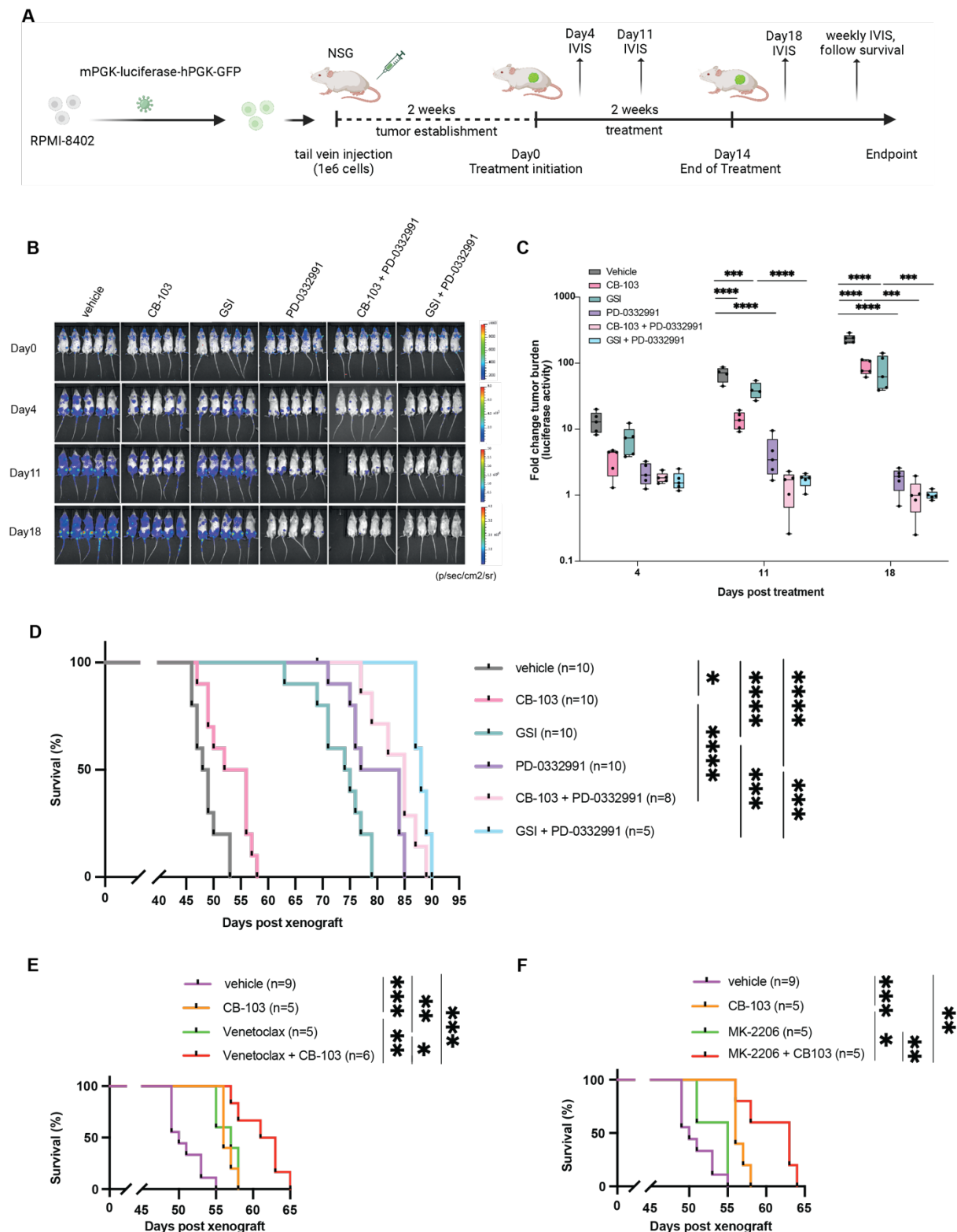


Figure 23. Combination of Notch inhibitors and multiple targeted therapies lead to decreased tumor burden and prolonged survival in a human T-ALL cell line xenograft model.

(A) Schematic representation of a human T-ALL cell line (RPMI-8402) xenograft model and drug treatment study. (B) Representative bioluminescence imaging at days indicated post treatment of each group. (C) Quantification of tumor burden measured by bioluminescent

signals at days indicated post treatment of each group, testing Notch inhibitors alone or in combination with PD-0332991. Y-axis shows \log_{10} fold change of signals on Day 11 or Day 18 post treatment comparing to initiation of treatment. Data are shown in box and whisker plots showing all data points. One-way ANOVA was performed. (D) Kaplan-Meier survival analysis of NSG mice within each treatment group testing Notch inhibitors, PD-0332991 or in combinations. (E) Kaplan-Meier survival analysis of NSG mice within each treatment group, testing CB-103, Venetoclax or in combination. (F) Kaplan-Meier survival analysis of NSG mice within each treatment group, testing CB-103, MK-2206 or in combination. Log-rank (Mantel-Cox) test, *P* value as indicated. **P* value < 0.0332, ***P* value < 0.0021, ****P* value < 0.0002, *****P* value < 0.0001.

The kinetics of tumor progression showed a moderate and statistically significant reduction in tumor burden for both single agent treatments of CB-103 or GSI compared to vehicle (Figure 23B-C).

Single agent treatment of PD-0332991 revealed a robust reduction in tumor burden. However, the strongest reduction in tumor burden was observed when mice were treated with combination of PD-0332991 and either CB-103 or GSI (Figure 23C).

To test whether combination treatment led to an increase in overall survival of experimental animals, treatment was ceased after 2 weeks and tumor relapse and survival rates were monitored. Despite the short treatment window, the dual agent treatment of GSI plus PD-033291 translated into significant prolonged overall survival compared to other treatment regimens (Figure 23D).

In light of increased BCL2 expression in our RNA-seq data and a recent report on complete clinical response of a relapsed and refractory T-ALL patient treated with the BCL2 inhibitor Venetoclax and CB-103¹⁰, we proceeded to assess the efficacy of combining CB-103 and Venetoclax in our model. Indeed, this combination treatment significantly extended overall survival compared to single agent treatment (Figure 23E).

The PI3K-AKT axis was identified as a main switch of downstream signaling events responsible for resistance to Notch inhibition in the CRSIPR/Cas screen, RNA-seq and proteomics data. Therefore, we also tested dual treatment of the AKT inhibitor (MK-2206) combined with CB-103 and observed significant prolongation of overall survival with combination compared to single agent therapy (Figure 23F).

Overall, the CRISPR/Cas9 screen in T-ALL cells unveiled potentially novel avenues of combination therapies.

5. Conclusion and discussion

5.1. Mutation loss of *PIK3R1* induces resistance to Notch inhibition in T-ALL

NGS analyses of primary T-ALL samples and cell lines have identified the *NOTCH1* as being amongst the most frequently mutated genes throughout different T-ALL subgroups^{67,68}. This, together with the identification of gain-of-function (GoF) mutations in other tumor entities⁶² highlights the Notch pathway as a therapeutic target for precision medicine. However, a major issue with personalized medicine is the establishment of resistance causing relapse.

Thus, we performed an unbiased genome-wide LoF CRISPR screen in a NOTCH1-driven T-ALL cell line (DND-41). We identified and validated that loss or downregulation of *PIK3R1* in several human T-ALL cell lines is responsible for resistance to both GSI- and CB-103-mediated Notch inhibition implicating a generic resistance mechanism.

Aberrant activation of the PI3K pathway has been demonstrated to contribute to various cancer types including T-ALL^{169–172}. 23% to 27% of T-ALL patients harbor mutations in PI3K pathway genes^{68,135,173}, raising the question whether all T-ALL patients with activating NOTCH1 mutations and aberrations within the PI3K signaling cascade might be resistant to Notch inhibitors.

A previous report linked PTEN, which negatively regulates PI3K/AKT signaling, in human T-ALL cell lines to GSI-resistance¹³². However, this conclusion is not consistent with observations that GSI sensitivity was comparable in Notch-driven T-ALL cells obtained from wild type and *Pten* deficient mice¹⁷⁴. Similarly, multiple human T-ALL cell lines carrying mutant *PTEN* alleles are sensitive to GSI¹⁷³. Thus, the loss of PTEN may not a priori be linked to resistance to pharmacological Notch inhibition but might be dependent on the time point amid the T-ALL transformation process. Thus, loss of *PIK3R1* or *PTEN* during drug-mediated selection in a fully established T-ALL may lead to rapid and high activation of the AKT pathway, resulting in continuous proliferation, survival and thus resistance to pharmacological Notch inhibitors, as observed and

validated in our genetic CRISPR-based screen. The hypothesis is supported by findings using a mouse model of Notch1-induced T-ALL with subsequent loss of the *Pten* gene once T-ALL has been established. In this model loss of *Pten* indeed resulted in the development of GSI resistance, -unlike the *Pten* knockout models, in which *Pten* was already lost at the onset of Notch mediated disease^{174,175}. Therefore, the prediction would be that T-ALL patients with LoF mutations of *PIK3R1*, *PTEN* or activating mutations in PI3K catalytic subunits at disease onset still respond to Notch inhibition. Nonetheless, individuals that acquire such mutations during treatment or at late-stage disease, are more likely to be resistant to pharmacological Notch inhibitors due to elevated activation of AKT signaling.

One way of analyzing driver mutation clonality is through the calculation of cancer cell fractions¹⁷⁶ (CCFs, percentage of tumor cells bearing mutations). A high CCF score indicates an early acquisition of a driver mutation, while a low CCF score suggests a later evolutionary occurrence. CCF analysis of 387 T-ALL samples revealed a medium CCF score for NOTCH1 mutations, while the CCF score for *PIK3R1*-LoF, *PTEN*-LoF and *AKT1* GoF mutations are low⁶⁷, suggesting that mutations in genes are acquired during the evolution of the leukemia, presumably after NOTCH1 mutations. Whether such subclones would indeed be resistant to pharmacological Notch inhibitors is currently unclear. The prediction is that resistance would be dependent on the extent of activated PI3K-AKT signaling within these subclones.

In this context, previous research has been mainly focused on characterizing the consequences of the aberrant activity of catalytic subunits of PI3Ks (P110s) and the development of corresponding inhibitors. Yet, increasing evidence has pointed to *PIK3R1* as key driver of tumorigenesis in ovarian cancer¹⁴¹, endometrial cancer¹⁶⁴ and breast cancer¹⁶⁵. Moreover, *PIK3R1* loss-of-function mutations in the SH2 domain were recently reported in pediatric T-ALL patients. Thus, it's of great clinical interest to consider not only the mutational status of PI3K catalytic partners, but also that of *PIK3R1*.

We further validated the growth advantage rendered by the loss of *PIK3R1* encountering Notch inhibition in three human T-ALL cell lines, and discovered that this is due to the protection from drug induced cell cycle arrest and apoptosis. Given the

above, the *PIK3R1* status should be considered as a potential biomarker of response in future clinical trials of Notch inhibitors in T-ALL treatment.

5.2. Increased PI3K/AKT signaling regulates the cell cycle and spliceosome machinery at the transcriptional and post-translational level

Global transcriptome analysis of *PIK3R1* deficient versus control T-ALL cells under drug selection, revealed upregulated gene expression of pro-survival and proliferation pathways including E2F targets, MYC targets, and G2M checkpoint signaling. These are consistent with the cell proliferation advantage and anti-apoptotic phenotype observed in the *PIK3R1* KO cells when challenged by Notch inhibitors.

Similarly, our phospho-proteomic analysis reveals that loss of *PIK3R1* leads to prominent phosphorylation changes in proteins involved in AKT signaling, cell proliferation, pro-survival and mTOR pathway. The changes in these mediators are highly agreeable with both downstream transcriptional profile changes and growth phenotype observed. Taken together, both transcriptomic and phospho-proteome analysis are consistent with the proliferative advantage and anti-apoptotic phenotype in *PIK3R1* knockout T-ALL cells under drug treatment.

Pharmacological inhibition of Notch signaling in Notch-driven T-ALL cells results in cell cycle arrest and apoptosis mostly through downregulation of *C-MYC* expression¹⁷⁷. Interestingly, although *MYC* transcript levels are downregulated similarly in CB-103-treated *PIK3R1* KO and NT control cells (Figure 15C), MYC protein levels of CB-103-treated *PIK3R1* KO cells were higher compared to NT control cells but lower compared to vehicle treated cells (Figure 19C-D) suggesting that increased AKT signaling maintains C-MYC protein levels at least partially.

Another interesting observation is that loss of *PIK3R1* leads to prominent phosphorylation changes in proteins involved in the spliceosome and RNA processing in cells treated with pharmacological Notch inhibitors. To the best of our knowledge, our study provides for the first time a comprehensive analysis of altered

phosphorylation modification on splicing factors (Figure 20A-B) upon altered PI3K signaling in response to Notch inhibition. The profound change in phosphorylation profile of splicing factors is associated with differential expression levels and exon usage profiles of transcripts (Figure 20C-E). In particular, cell cycle, anti-apoptotic and alternative splicing pathways were well-represented among differentially expressed transcripts events (Figure 20C-D).

PI3K-AKT pathway was demonstrated to regulate RNA splicing family proteins directly, or phosphorylate and modulate the activity of CLKs (CDC2-like protein kinases) and SRPKs (SRSF protein kinases)¹⁷⁸. Recently, oncogenic PI3K signaling was shown to induce expression of alternatively spliced transcripts linked to proliferation and metabolism in breast cancer¹⁶⁸. The question remains how the altered phosphorylation profile of splicing factors could cause transcript isoform alterations and specifically contribute to the resistance phenotype. One possible explanation is that the subcellular localization and activity of splicing factors might be phosphorylation-dependent and contribute to the expression of particular splice variants involved in key oncogenic pathways. Whether alternative splicing profiles can predict response to Notch inhibition in T-ALL and other cancer contexts requires future exploration.

Overall, we found that *PIK3R1* deficient cells regulate the cell cycle and spliceosome machinery at both the transcriptional and post-translational level in order to cope with Notch inhibition in T-ALL.

5.3. Pharmacological Notch inhibition synergizes with CDK4/6 inhibitors in T-ALL

To complement our discovery of a resistance mechanism to Notch inhibition in T-ALL, we also identified potential targets for combination therapies with pharmacological Notch inhibitors. Our CRISPR screen led to the identification of *PIK3CD*, *IL7R/JAK1*, and *CDK6:CCND3* as candidates (Figure 8B-C), which can be targeted together with Notch inhibition.

Unfavored loss of *PI3KCD* (encoding catalytic PI3K subunit P110 δ) was notable as its

activity is modulated by the negative regulatory subunit p85a, which we identified as a resistance-associated protein to Notch inhibition. It is noteworthy that 9% of T-ALL patients⁶⁹ as well as the cell line used for the screen harbor somatic GoF mutation in IL7R. IL7R mutation has been proved oncogenic in T-ALL via driving constitutive JAK1 signaling¹⁷⁹. Interestingly, in our CRISPR screen sgRNAs targeting *IL-7R* and the downstream mediator *JAK1* were both identified to be depleted in the presence of Notch inhibition. Similarly, CyclinD3 and CDK6 are additional candidates identified from our screen. Both proteins are interesting targets as CyclinD3-CDK4/6 complex is known to regulate the cell cycle during G1/S transition through RB1. Importantly, this complex has been demonstrated to be essential for initiation and maintenance of T-ALL^{180–182} and may serve a promising candidate to be targeted together with chemotherapy in T-ALL¹⁸³.

Thus, we explored a panel of FDA-approved inhibitors to target these candidates *in vitro*. We tested them first for their ability to function synergistically with CB-103 or GSI *in vitro*. Interestingly PD-0332991 (inhibiting CDK4/6), Ruxolitinib (inhibiting JAK1/2), and CAL-101 (inhibiting PIK3CD) appear to function synergistically with both CB-103 or GSI (Table 4) to inhibit the growth of Notch-driven T-ALL cells.

We further assessed both CB-103 and GSI in combination with PD-0332991 in xenotransplantation assays and demonstrated that the combination treatments showed reduced tumor burden as well as significant prolonged survival when compared to single Notch inhibitor treatment. Similarly, we observed beneficial overall survival when combining pharmacological Notch inhibitors with the AKT inhibitor MK-2206. Whether *PIK3R1* deficient T-ALL cells would benefit from a dual treatment with AKT and Notch inhibitors remains to be explored. Motivated by a case report in which a relapsed and refractory T-ALL patient showed a complete response when treated with CB-103 and BCL-2 inhibitor Venetoclax, we were also able to demonstrate that combination of these two targeted therapies resulted in extended overall survival compared to single agent treatment in a pre-clinical xenotransplantation assay. However, the best combination in terms of overall survival was obtained by combining PD-0332991 with GSI, suggesting that simultaneous inhibition of CDK4/6 together with Notch signaling might be worthwhile to be considered in future clinical combination trials.

Overall, we successfully identified regimens of blocking Notch signaling in combination with several other targeted therapies, providing a strong rationale for testing such combination therapies in refractory or relapsed T-ALL patients.

5.4. Limitations of this project

5.4.1. Identification of other potential biomarkers of response to Notch inhibition in clinics

The analysis of the CRISPR screen revealed several other candidate genes that when lost may render T-ALL cells resistant to Notch inhibition. However, due to time constraint and technical difficulties of generating KO clones in T-ALL cell lines for all candidates, I could not functionally validate more candidates systematically and thus focused on *PIK3R1*.

The list of these candidates includes several genes that encode galactosyltransferases and glycosyltransferases (*B4GALT7*, *B3GALT6*, *EXT1*, *EXTL3*). For example, *EXT1*, which encodes an endoplasmic reticulum-resident type II transmembrane glycosyltransferase, is involved in the chain elongation step of heparan sulfate biosynthesis. Mutations in *EXT1* cause the type I form of multiple exostoses¹⁸⁴ (benign bone tumors) and epigenetic silencing of this gene has been observed in ALL and acute promyelocytic leukemia (APL)¹⁸⁵.

Newly translated Notch protein is glycosylated in ER and Golgi. The glycosylation of Notch is considered to affect the strength of receptor-ligand binding and subsequently the strength of the signaling pathway^{186,187}, yet the detailed mechanism remains to be studied. The known regulators of such process are glycosyltransferases including POFUT-1 and Fringes in mammals²¹. It also remains to be explored if other galactosyltransferases (such as *B4GALT7*, *B3GALT6*) or glycosyltransferases (such as *EXT1*, *EXTL3*) are involved in regulating Notch signaling pathways such as ligand-receptor interaction and receptor turnover, and whether disturbance of this regulation might be involved in potential resistance mechanism to Notch inhibition in T-ALL.

Overall, it is an interesting aspect to test these additional candidates in future experiments for their potential implication in resistance mechanism to pharmacological Notch inhibitors. This may be of value and lead to the establishment of additional biomarkers for predicting response in future clinical trials of Notch inhibitors in T-ALL treatment.

5.4.2. Systematic analysis of alternative splicing upon increased PI3K signaling in T-ALL cells in response to Notch inhibition

We found differential phosphorylation profiles of splicing factors upon altered PI3K signaling from our proteomics data, and another recent study found a link between activated PI3K signaling and splicing alterations on the transcriptional level in breast cancer¹⁶⁸. We therefore re-purposed our RNA-seq (75nt, paired-end) data in search for evidence suggesting alternative splicing events in the T-ALL context.

We indeed were able to map differentially expressed transcript isoforms, which were associated with genes involved in cell cycle and apoptosis regulation. Moreover, we performed differential exon usage analysis with DEXSeq and identified 43 alternative exon usage events comparing *PIK3R1* deficient cells to NT cells in response to Notch inhibition. Yet, the sequencing depth (on average roughly 75million reads per sample) and length (75nt) is suboptimal for a typical systematic alternative splicing analysis which requires 100 million reads per sample and an average fragment length of 150nt.

In addition to DEXSeq, which detects differential exon usage, other analytical software packages can provide complementary views of splicing events. For example, JunctionSeq can be used to analyze differential splicing and exon usage¹⁸⁸. IncScore can predict coding potential of novel splicing junction transcripts¹⁸⁹ and SUPPA2 can identify alternative splicing and the types of splicing events¹⁹⁰. Currently, we were only able to perform DEXSeq analysis on our RNA-seq data. It remains to be seen if running other analyses on optimized sequencing reads can provide a more concrete landscape of alternative splicing events in our system.

As mentioned above, a recent report has established associations between oncogenic

PI3K signaling and alternatively spliced transcript isoforms linked to proliferation and metabolism in breast cancer¹⁶⁸. The PI3K-AKT pathway has been shown to regulate several proteins of the splicing machinery directly by phosphorylation, or modulating their activity and localization¹⁷⁸. Our finding identified a list of altered phosphorylation patterns of splicing factors including SF3B1, a key U2 spliceosome component. Understanding how exactly the altered phosphorylation profile of splicing factors can cause transcript isoform alterations and contribute to the resistance to Notch inhibition in T-ALL needs to be addressed in future experiments. This could provide a novel mechanistic insight into how PI3K signaling might regulate differential transcript isoform expression.

Inhibitors against SF3B1 have been shown to inhibit growth of T-ALL and other leukemias¹⁹¹. Whether SF3B1-inhibitor can re-sensitize *PIK3R1* deficient T-ALL cells to Notch inhibitors or simply kill T-ALL cells *per se* remains to be addressed.

Interestingly, a more recent study of pediatric T-ALL patients revealed genetic alterations in RNA processing factors (11 % all cases)⁶⁷, a key biological pathway not previously associated with ALL.

Understanding the relationship between PI3K signaling and the regulation of splicing factors provides us a deeper knowledge of fundamental biology. Importantly, uncovering the functional consequence of this link on expression and regulation of downstream transcripts might be clinically relevant in T-ALL. It also remains to be determined whether alternative splicing within tumors can be used as biomarker that predicts their responses to Notch inhibition in T-ALL and other cancer contexts.

5.4.3. Further exploration of molecular resistance mechanism by *PIK3R1* loss to Notch inhibition in T-ALL

Within this study, we were able to demonstrate that upon *PIK3R1* loss, increased PI3K/AKT signaling regulates the cell cycle and spliceosome machinery at both the transcriptional and post-translation level. Yet, unfortunately most of our multifactorial analysis remains correlative and the precise molecular resistance mechanism caused

by mutational loss of *PIK3R1* in response to pharmacological Notch inhibition in T-ALL requires further investigation.

Possible axes of future investigations include studies into how increased PI3K signaling may uncouple T-ALL cells from MYC addiction. We observed decreased MYC expression on the transcript level but less profound changes at the protein level upon *PIK3R1* loss in response to Notch inhibition. The exact mechanism of how altered PI3K signaling affects MYC expression dramatically on the protein level (and if this is crucial for the resistant phenotype to Notch inhibitions) remains to be explored.

We observed that upregulation of PI3K/AKT signaling lead to downstream mTOR and RB activation, anti-apoptosis signaling, as well as upregulation of cell cycle genes (for example E2F family genes). It therefore remains to be explored whether the AKT-RB-E2F axis is crucial for the Notch-resistant phenotype, and if perturbation of this axis can rescue the resistance phenotype.

5.4.4. Significance of *PIK3R1* loss to Notch inhibition in primary T-ALL cells.

Hotspot mutations of *PIK3R1* have been identified in T-ALL patients^{67,69}, yet there's no available clinical data demonstrating the response to Notch inhibition in these patients. Clonality analysis of T-ALL patient samples suggested that mutations in *PIK3R1* were acquired during the evolution of the leukemia possibly after NOTCH1 mutations⁶⁷. A Whole-genome sequencing study of diagnosis-relapse matched T-ALL patient samples provided insight into the T-ALL subclones dynamics under chemotherapy selection pressure¹²⁷. *PIK3R1* mutations occurred in two cases only in relapse samples and in two cases both in diagnosis and relapse samples¹²⁷. Yet, it remains unclear if *PIK3R1* deficient clones are indeed resistant to Notch inhibitors in patient samples.

It would certainly be interesting to gather a panel of primary human Notch-driven T-ALL samples and assess their *PIK3R1* status – or engineer *PIK3R1* mutational loss in these samples – and test their responses to Notch inhibition. We obtained several human PDX samples (with unknown *PIK3R1* status) but didn't manage to propagate

and assess them *in vivo* within the given timeframe.

Overall, it remains to be explored whether the resistant phenotype to Notch inhibition we observed in human *PIK3R1* deficient T-ALL cell lines translates to the primary T-ALL disease context.

5.5. Future Perspectives

5.5.1. Further exploration of the mechanism how loss of *PIK3R1* may cause resistance to Notch inhibitor in T-ALL

1. Examine the consequence of *PIK3R1* loss on spliceosome machinery post-translational regulation, by validating key altered phosphorylation events comparing *PIK3R1* deficient cells to NT cells in response to Notch inhibition, which were revealed from phospho-proteomics data.
2. Explore splicing alterations systematically upon *PIK3R1* loss in response to Notch inhibition, by performing long-read RNA-sequencing and subsequent alternative splicing analysis and isoform-specific gene expression analysis.
3. Dissect in details how altered phosphorylation of splicing factors upon *PIK3R1* loss translates to isoform alterations on transcriptional level, and subsequently contributes to the resistance phenotype to Notch inhibition in T-ALL.

One possible experiment is to examine if the subcellular localization and activity of splicing factors are phosphorylation-dependent (phosphorylation modifications from point 1). Furthermore, it's worthwhile to test if ablation of certain phosphorylation modifications can reverse particular splicing alterations involved in key oncogenic pathways and whether this contributes to rescuing the resistance phenotype.

4. Identify a panel of key splicing events as Splicing Signatures that can correlate with response to Notch inhibition in T-ALL and other cancer contexts.
5. Examine if inhibition of spliceosome factor (for example SF3B1) can resensitize the

PIK3R1 deficient cells to Notch inhibition or simply kill T-ALL cells *per se*, and furthermore if the combination of spliceosome factor inhibitor with Notch inhibitor is good strategy to efficiently treat T-ALL.

5.5.2. Further exploration of the consequence of *PIK3R1* loss to Notch inhibitor resistance in primary T-ALL cells.

1. Gather human primary T-ALL cells with and without *PIK3R1* mutational loss, and examine their responses to Notch inhibition *in vitro* or *in vivo*.
2. Alternatively, gather human T-ALL PDX samples and genetically engineer the *PIK3R1* locus to explore WT and *PIK3R1* deficient T-ALL PDX samples for their responses to Notch inhibition in xenograft models.
3. Additionally, gather data from T-ALL patients in current cohort of phase I/II trial for CB-103, and explore the correlation between the sensitivity to Notch inhibition with the *PIK3R1* status among patients.

6. Annex

Annexed Table 5. List of oligos used in this study

Name	sequence (5'->3')
PIK3R1 sgRNA_1F	CAC CGA CTG AGC TAG AGA TTC ATT C
PIK3R1 sgRNA_1R	AAACGAATGAATCTCTAGCTCAGTC
PIK3R1 sgRNA_2F	CACCGCGCTTTCAAACGCTATCTCC
PIK3R1 sgRNA_2R	AAACGGAGATAGCGTTTGAAAGCGC
NT_sgRNA_1F	CACCGCTGAAAAAGGAAGGAGTTGA
NT_sgRNA_1R	AAACTCAACTCCTTCCTTTTTTCAGC
PIK3R1 crRNA_1	rArCrUrGrArGrCrUrArGrArGrArUrUrCrArUrUrCrGrUrUrUrArGrArGrCrUr ArUrGrCrU
PIK3R1 crRNA_2	rCrGrCrUrUrUrCrArArArCrGrCrUrArUrCrUrCrGrUrUrUrArGrArGrCrUr ArUrGrCrU
PIK3R1-sh3F	AGCGATTCAACCACAGA AACTGAAGGAATAGTGAAGCCACAGATGTATT CCTTCAGTTCTGTGGTTGAAT
PIK3R1-sh3R	GGCAATTCAACCACAGA AACTGAAGGAATACATCTGTGGCTTCACTATT CCTTCAGTTCTGTGGTTGAAT
PIK3R1_sh4F	AGCGATGTCTTCTCATGATGGGAATAGTGAAGCCACAGATGTATTCCC ATCATGAGAAGACAT
PIK3R1_sh4R	GGCAATGTCTTCTCATGATGGGAATACATCTGTGGCTTCACTATTCCCA TCATGAGAAGACAT
PIK3R1_sh5F	AGCGGCGGTACAGCAAAGAATACATAATAGTGAAGCCACAGATGTATTA TGATTCTTTGCTGTACCGC
PIK3R1_sh5R	GGCAGCGGTACAGCAAAGAATACATAATACATCTGTGGCTTCACTATTA TGATTCTTTGCTGTACCGC
PIK3R1_sh6F	AGCGCCGAGCCCTATAACTTGTACAAATAGTGAAGCCACAGATGTATTT GTACAAGTTATAGGGCTCGG
PIK3R1_sh6R	GGCACCGAGCCCTATAACTTGTACAAATACATCTGTGGCTTCACTATTT GTACAAGTTATAGGGCTCGG
scr_F	AGCGTAGCGACTAAACACATCAA AATAGTGAAGCCACAGATGTATTTTG ATGTGTTTAGTCGCTA
scr_R	GGCATAGCGACTAAACACATCAA AATACATCTGTGGCTTCACTATTTTG ATGTGTTTAGTCGCTA
NGS-Lib-Fwd-1	AATGATACGGCGACCACCGAGATCTA CACTCTTTCCCTACACGACGCTCTTCC GATCTTAAGTAGAGGCTTTATATATCT TGTGGAAAGGACGAAACACC
NGS-Lib-Fwd-2	AATGATACGGCGACCACCGAGATCTA CACTCTTTCCCTACACGACGCTCTTCC GATCTATCATGCTTAGCTTTATATATC TTGTGGAAAGGACGAAACACC

NGS-Lib-Fwd-3	AATGATACGGCGACCACCGAGATCTA CACTCTTTCCCTACACGACGCTCTTCC GATCTGATGCACATCTGCTTTATATAT CTTGTGGAAAGGACGAAACACC
NGS-Lib-Fwd-4	AATGATACGGCGACCACCGAGATCTA CACTCTTTCCCTACACGACGCTCTTCC GATCTCGATTGCTCGACGCTTTATATA TCTTGTGGAAAGGACGAAACACC
NGS-Lib-Fwd-5	AATGATACGGCGACCACCGAGATCTA CACTCTTTCCCTACACGACGCTCTTCC GATCTTCGATAGCAATTCGCTTTATAT ATCTTGTGGAAAGGACGAAACACC
NGS-Lib-Fwd-6	AATGATACGGCGACCACCGAGATCTA CACTCTTTCCCTACACGACGCTCTTCC GATCTATCGATAGTTGCTTGCTTTATA TATCTTGTGGAAAGGACGAAACACC
NGS-Lib-Fwd-7	AATGATACGGCGACCACCGAGATCTA CACTCTTTCCCTACACGACGCTCTTCC GATCTGATCGATCCAGTTAGGCTTTAT ATATCTTGTGGAAAGGACGAAACACC
NGS-Lib-Fwd-8	AATGATACGGCGACCACCGAGATCTA CACTCTTTCCCTACACGACGCTCTTCC GATCTCGATCGATTTGAGCCTGCTTTA TATATCTTGTGGAAAGGACGAAACAC C
NGS-Lib-Fwd-9	AATGATACGGCGACCACCGAGATCTA CACTCTTTCCCTACACGACGCTCTTCC GATCTACGATCGATACGATCGCTTT ATATATCTTGTGGAAAGGACGAAACA CC
NGS-Lib-Fwd-10	AATGATACGGCGACCACCGAGATCTA CACTCTTTCCCTACACGACGCTCTTCC GATCTTACGATCGATGGTCCAGAGCTT TATATATCTTGTGGAAAGGACGAAAC ACC
NGS-Lib-KO-Rev-1	CAAGCAGAAGACGGCATAACGAGATTCGCCTTGGTACTGGAGTTCAG ACGTG TGCTCTTCCGATCTCCGACTCGGTGCC ACTTTTTCAA
NGS-Lib-KO-Rev-2	CAAGCAGAAGACGGCATAACGAGATATAGCGTCGTGACTGGAGTTCAG ACGTG TGCTCTTCCGATCTCCGACTCGGTGCC ACTTTTTCAA
NGS-Lib-KO-Rev-3	CAAGCAGAAGACGGCATAACGAGATGAAGAAGTGTGACTGGAGTTCAG ACGTG TGCTCTTCCGATCTCCGACTCGGTGCC ACTTTTTCAA
NGS-Lib-KO-Rev-4	CAAGCAGAAGACGGCATAACGAGATATTCTAGGGTACTGGAGTTCAGA CGTG TGCTCTTCCGATCTCCGACTCGGTGCC ACTTTTTCAA
NGS-Lib-KO-Rev-5	CAAGCAGAAGACGGCATAACGAGATCG

	TTACCAGTGACTGGAGTTCAGACGTG TGCTCTTCCGATCTCCGACTCGGTGCC ACTTTTTCAA
NGS-Lib-KO-Rev-6	CAAGCAGAAGACGGCATACGAGATGTCTGATGGTGACTGGAGTTCAG ACGTG TGCTCTTCCGATCTCCGACTCGGTGCC ACTTTTTCAA
NGS-Lib-KO-Rev-7	CAAGCAGAAGACGGCATACGAGATTTACGCACGTGACTGGAGTTCAG ACGTG TGCTCTTCCGATCTCCGACTCGGTGCC ACTTTTTCAA
NGS-Lib-KO-Rev-8	CAAGCAGAAGACGGCATACGAGATTTGAATAGGTGACTGGAGTTCAG ACGTG TGCTCTTCCGATCTCCGACTCGGTGCC ACTTTTTCAA
NGS-Lib-KO-Rev-9	CAAGCAGAAGACGGCATACGAGATCGAGTAATGTGACTGGAGTTCAG ACGTG TGCTCTTCCGATCTCCGACTCGGTGCC ACTTTTTCAA
NGS-Lib-KO-Rev-10	CAAGCAGAAGACGGCATACGAGATAATGAGCGGTGACTGGAGTTCAG ACGTG TGCTCTTCCGATCTCCGACTCGGTGCC ACTTTTTCAA
GeCKO-F1	AATGGACTATCATATGCTTACCGTAACTTGAAAGTATTTCCG
GeCKO-R1	CTTTAGTTTGTATGTCTGTTGCTATTATGTCTACTATTCTTTCC

Annexed Table 6. List of antibodies used in this study

Target	Company	Clone #	Catalog #	RRID #
pAKT(T308)	Cell Signaling	D25E6	13038s	AB_2629447
pAKT(S473)	Cell Signaling	D9E	4060s	AB_2315049
pAKT(T450)	Cell Signaling	polyclonal	9267s	AB_823676
AKT	Cell Signaling	polyclonal	9272s	AB_329827
NICD (V1744)	Cell Signaling	D3B8	4147s	AB_2153348
c-MYC	Abcam	Y69	ab32072	AB_731658
P85	Cell signaling	19H8	4257	AB_659889
pS6K (T421/S424)	Cell Signaling	polyclonal	9204s	AB_2265913
pS6K (T389)	Cell Signaling	polyclonal	9205s	AB_330944
p70 S6K	Cell Signaling	polyclonal	9202s	AB_331676
pS6 Ribosomal protein (S235/236)	Cell Signaling	polyclonal	2211s	AB_331679
S6 Ribosomal protein	Cell Signaling	54D2	2317s	AB_2238583
CRISPR-CAS9	Abcam	7A9-3A3	ab191468	AB_2692325
BCL-xL	Abcam	polyclonal	ab98143	AB_10674728
BCL2	Cell Signaling	polyclonal	2872T	AB_10693462
TATA binding protein TBP	Abcam	mAbcam 51841	ab51841	AB_945758
p-Tuberin/TSC2 (S939)	Cell Signaling	polyclonal	3615T	AB_2207796
Tuberin/TSC2	Cell Signaling	D93F12	4308T	AB_10547134
pBAD (S136)	Cell Signaling	D25H8	4366T	AB_10547878
BAD	Cell Signaling	D24A9	9239T	AB_2062127

pRB (S807/811)	Cell Signaling	D20B12	8516S	<i>AB_11178658</i>
pRB (S780)	Cell Signaling	polyclonal	9307T	<i>AB_330015</i>
pRB (S795)	Cell Signaling	unknown	9301T	<i>AB_330013</i>
RB	Abcam	EPR17512	ab181616	<i>AB_2848193</i>
ACTIN	Abcam	mAbcam8226	ab8226	<i>AB_306371</i>
mouse IgG, HPR-linked	Cell Signaling	polyclonal	7076S	<i>AB_330924</i>
anti-rabbit IgG, HPR-linked	Cell Signaling	polyclonal	7074S	<i>AB_2099233</i>

Annexed Table 7. List of drugs used in this study

Name	Target	CAS	Provider	Catalog #	Delivery
Palbociclib	CDK4/6	827022-32-2	Chemietek	CT-PD2991	Oral Gavage
Ruxolitinib	JAK1/2	941678-49-5	Selleck Chemicals	S1378	<i>in vitro</i>
Venetoclax	BCL2	1257044-40-8	LuBioScience	HY-15531	Oral Gavage
MK-2206	AKT	1032349-77-1	LuBioScience	HY-10358	Oral Gavage
Idelalisib	PI3K δ	870281-82-6	LuBioScience	S2226	<i>in vitro</i>
CB-103	Notch	218457-67-1	Chemie Brunschwig AG	CBLSS-5069	intraperitoneal
LY3039478	Notch	1421438-81-4	SpiroChem	S7169	intraperitoneal
DAPT	Notch	208255-80-5	Selleck Chemicals	S2215	<i>in vitro</i>

7. Bibliography

1. Galloway, J. L. & Zon, L. I. 3 Ontogeny of hematopoiesis: Examining the emergence of hematopoietic cells in the vertebrate embryo. in *Current Topics in Developmental Biology* vol. 53 139–158 (Elsevier, 2003).
2. Yamane, T. Mouse Yolk Sac Hematopoiesis. *Front. Cell Dev. Biol.* **6**, 80 (2018).
3. Canu, G. & Ruhrberg, C. First blood: the endothelial origins of hematopoietic progenitors. *Angiogenesis* **24**, 199–211 (2021).
4. Palis, J. & Yoder, M. C. Yolk-sac hematopoiesis. *Exp. Hematol.* **29**, 927–936 (2001).
5. de Bruijn, M. F. T. R. Definitive hematopoietic stem cells first develop within the major arterial regions of the mouse embryo. *EMBO J.* **19**, 2465–2474 (2000).
6. Lewis, K., Yoshimoto, M. & Takebe, T. Fetal liver hematopoiesis: from development to delivery. *Stem Cell Res. Ther.* **12**, 139 (2021).
7. Gao, X., Xu, C., Asada, N. & Frenette, P. S. The hematopoietic stem cell niche: from embryo to adult. *Development* **145**, dev139691 (2018).
8. Belyavsky, A., Petinati, N. & Drize, N. Hematopoiesis during Ontogenesis, Adult Life, and Aging. *Int. J. Mol. Sci.* **22**, 9231 (2021).
9. Pinho, S. & Frenette, P. S. Haematopoietic stem cell activity and interactions with the niche. *Nat. Rev. Mol. Cell Biol.* **20**, 303–320 (2019).
10. Cite This Page - Wikimedia Commons.
[https://commons.wikimedia.org/w/index.php?id=718431935&page=File%3AHematop
oiesis_%28human%29_diagram.png&title=Special:CiteThisPage&wpFormIdentifier=titl
eform.](https://commons.wikimedia.org/w/index.php?id=718431935&page=File%3AHematop%20oiesis_%28human%29_diagram.png&title=Special:CiteThisPage&wpFormIdentifier=titleform)
11. Morrison, S. J. & Weissman, I. L. The long-term repopulating subset of hematopoietic stem cells is deterministic and isolatable by phenotype. *Immunity* **1**, 661–673 (1994).

12. Pucella, J. N., Upadhaya, S. & Reizis, B. The Source and Dynamics of Adult Hematopoiesis: Insights from Lineage Tracing. *Annu. Rev. Cell Dev. Biol.* **36**, 529–550 (2020).
13. Weissman, I. L. Stem Cells. *Cell* **100**, 157–168 (2000).
14. Sun, J. *et al.* Clonal dynamics of native haematopoiesis. *Nature* **514**, 322–327 (2014).
15. Zavidij, O. *et al.* Stable Long-Term Blood Formation by Stem Cells in Murine Steady-State Hematopoiesis. *Stem Cells* **30**, 1961–1970 (2012).
16. Ganuza, M. *et al.* The global clonal complexity of the murine blood system declines throughout life and after serial transplantation. *Blood* **133**, 1927–1942 (2019).
17. Cheng, H., Zheng, Z. & Cheng, T. New paradigms on hematopoietic stem cell differentiation. *Protein Cell* **11**, 34–44 (2020).
18. Laurenti, E. & Göttgens, B. From haematopoietic stem cells to complex differentiation landscapes. *Nature* **553**, 418–426 (2018).
19. Hosokawa, H. & Rothenberg, E. V. How transcription factors drive choice of the T cell fate. *Nat. Rev. Immunol.* **21**, 162–176 (2021).
20. Curiel, T. J. Tregs and rethinking cancer immunotherapy. *J. Clin. Invest.* **117**, 1167–1174 (2007).
21. Kopan, R. & Ilagan, M. X. G. The Canonical Notch Signaling Pathway: Unfolding the Activation Mechanism. *Cell* **137**, 216–233 (2009).
22. Bray, S. J. Notch signalling: a simple pathway becomes complex. *Nat. Rev. Mol. Cell Biol.* **7**, 678–689 (2006).
23. Yatim, A. *et al.* NOTCH1 Nuclear Interactome Reveals Key Regulators of Its Transcriptional Activity and Oncogenic Function. *Mol. Cell* **48**, 445–458 (2012).
24. Siebel, C. & Lendahl, U. Notch Signaling in Development, Tissue Homeostasis, and Disease. *Physiol. Rev.* **97**, 1235–1294 (2017).

25. Wahi, K., Bochter, M. S. & Cole, S. E. The many roles of Notch signaling during vertebrate somitogenesis. *Semin. Cell Dev. Biol.* **49**, 68–75 (2016).
26. Buas, M. F. & Kadesch, T. Regulation of skeletal myogenesis by Notch. *Exp. Cell Res.* **316**, 3028–3033 (2010).
27. Fish, J. E. & Wythe, J. D. The molecular regulation of arteriovenous specification and maintenance. *Dev. Dyn. Off. Publ. Am. Assoc. Anat.* **244**, 391–409 (2015).
28. Luxán, G., D'Amato, G., MacGrogan, D. & de la Pompa, J. L. Endocardial Notch Signaling in Cardiac Development and Disease. *Circ. Res.* **118**, e1–e18 (2016).
29. Lammert, E., Brown, J. & Melton, D. A. Notch gene expression during pancreatic organogenesis. *Mech. Dev.* **94**, 199–203 (2000).
30. Hadland, B. K. *et al.* A requirement for Notch1 distinguishes 2 phases of definitive hematopoiesis during development. *Blood* **104**, 3097–3105 (2004).
31. Radtke, F. *et al.* Deficient T Cell Fate Specification in Mice with an Induced Inactivation of Notch1. *Immunity* **10**, 547–558 (1999).
32. Pui, J. C. *et al.* Notch1 Expression in Early Lymphopoiesis Influences B versus T Lineage Determination. *Immunity* **11**, 299–308 (1999).
33. Knust, E. & Campos-Ortega, J. A. The molecular genetics of early neurogenesis in *Drosophila melanogaster*. *BioEssays News Rev. Mol. Cell. Dev. Biol.* **11**, 95–100 (1989).
34. Estrach, S., Cordes, R., Hozumi, K., Gossler, A. & Watt, F. M. Role of the Notch ligand Delta1 in embryonic and adult mouse epidermis. *J. Invest. Dermatol.* **128**, 825–832 (2008).
35. Miyajima, A., Tanaka, M. & Itoh, T. Stem/progenitor cells in liver development, homeostasis, regeneration, and reprogramming. *Cell Stem Cell* **14**, 561–574 (2014).
36. Owens, G. K., Kumar, M. S. & Wamhoff, B. R. Molecular regulation of vascular smooth muscle cell differentiation in development and disease. *Physiol. Rev.* **84**, 767–801 (2004).

37. van Es, J. H. *et al.* Notch/ γ -secretase inhibition turns proliferative cells in intestinal crypts and adenomas into goblet cells. *Nature* **435**, 959–963 (2005).
38. Carraro, G. & Stripp, B. R. A New Notch for Lung Stem Cells. *Cell Stem Cell* **16**, 107–109 (2015).
39. Hozumi, K. *et al.* Delta-like 4 is indispensable in thymic environment specific for T cell development. *J. Exp. Med.* **205**, 2507–2513 (2008).
40. Schmitt, T. M. & Zúñiga-Pflücker, J. C. Induction of T Cell Development from Hematopoietic Progenitor Cells by Delta-like-1 In Vitro. *Immunity* **17**, 749–756 (2002).
41. Zhou, W. *et al.* Single-Cell Analysis Reveals Regulatory Gene Expression Dynamics Leading to Lineage Commitment in Early T Cell Development. *Cell Syst.* **9**, 321-337.e9 (2019).
42. Yui, M. A. & Rothenberg, E. V. Developmental gene networks: a triathlon on the course to T cell identity. *Nat. Rev. Immunol.* **14**, 529–545 (2014).
43. Hosoya, T. *et al.* GATA-3 is required for early T lineage progenitor development. *J. Exp. Med.* **206**, 2987–3000 (2009).
44. Weber, B. N. *et al.* A critical role for TCF-1 in T-lineage specification and differentiation. *Nature* **476**, 63–68 (2011).
45. Germar, K. *et al.* T-cell factor 1 is a gatekeeper for T-cell specification in response to Notch signaling. *Proc. Natl. Acad. Sci.* **108**, 20060–20065 (2011).
46. Hosokawa, H. *et al.* Bcl11b sets pro-T cell fate by site-specific cofactor recruitment and by repressing Id2 and Zbtb16. *Nat. Immunol.* **19**, 1427–1440 (2018).
47. De Obaldia, M. E. *et al.* T cell development requires constraint of the myeloid regulator C/EBP- α by the Notch target and transcriptional repressor Hes1. *Nat. Immunol.* **14**, 1277–1284 (2013).
48. Washburn, T. *et al.* Notch Activity Influences the $\alpha\beta$ versus $\gamma\delta$ T Cell Lineage Decision. *Cell*

- 88**, 833–843 (1997).
49. Reedijk, M. *et al.* High-level coexpression of JAG1 and NOTCH1 is observed in human breast cancer and is associated with poor overall survival. *Cancer Res.* **65**, 8530–8537 (2005).
 50. Ho, A. S. *et al.* The mutational landscape of adenoid cystic carcinoma. *Nat. Genet.* **45**, 791–798 (2013).
 51. Jackstadt, R. *et al.* Epithelial NOTCH Signaling Rewires the Tumor Microenvironment of Colorectal Cancer to Drive Poor-Prognosis Subtypes and Metastasis. *Cancer Cell* **36**, 319–336.e7 (2019).
 52. Bailey, P. *et al.* Genomic analyses identify molecular subtypes of pancreatic cancer. *Nature* **531**, 47–52 (2016).
 53. Bonfiglio, F. *et al.* Genetic and phenotypic attributes of splenic marginal zone lymphoma. *Blood* **139**, 732–747 (2022).
 54. Tardivon, D. *et al.* Notch signaling promotes disease initiation and progression in murine chronic lymphocytic leukemia. *Blood* **137**, 3079–3092 (2021).
 55. Weng, A. P. *et al.* Activating Mutations of *NOTCH1* in Human T Cell Acute Lymphoblastic Leukemia. *Science* **306**, 269–271 (2004).
 56. Nowell, C. S. & Radtke, F. Notch as a tumour suppressor. *Nat. Rev. Cancer* **17**, 145–159 (2017).
 57. Wang, N. J. *et al.* Loss-of-function mutations in Notch receptors in cutaneous and lung squamous cell carcinoma. *Proc. Natl. Acad. Sci. U. S. A.* **108**, 17761–17766 (2011).
 58. Agrawal, N. *et al.* Exome sequencing of head and neck squamous cell carcinoma reveals inactivating mutations in NOTCH1. *Science* **333**, 1154–1157 (2011).
 59. George, J. *et al.* Comprehensive genomic profiles of small cell lung cancer. *Nature* **524**, 47–

- 53 (2015).
60. Zhou, B. *et al.* Notch signaling pathway: architecture, disease, and therapeutics. *Signal Transduct. Target. Ther.* **7**, 95 (2022).
61. Aster, J. C., Pear, W. S. & Blacklow, S. C. Notch Signaling in Leukemia. *Annu. Rev. Pathol. Mech. Dis.* **3**, 587–613 (2008).
62. Aster, J. C., Pear, W. S. & Blacklow, S. C. The Varied Roles of Notch in Cancer. *Annu. Rev. Pathol. Mech. Dis.* **12**, 245–275 (2017).
63. Brenner, H. *et al.* Long-term survival of children with leukemia achieved by the end of the second millennium. *Cancer* **92**, 1977–1983 (2001).
64. Mody, R. *et al.* Twenty-five-year follow-up among survivors of childhood acute lymphoblastic leukemia: a report from the Childhood Cancer Survivor Study. **111**, 10 (2008).
65. Greaves, M. A causal mechanism for childhood acute lymphoblastic leukaemia. *Nat. Rev. Cancer* **18**, 471 (2018).
66. Cordo', V., van der Zwet, J. C. G., Canté-Barrett, K., Pieters, R. & Meijerink, J. P. P. T-cell Acute Lymphoblastic Leukemia: A Roadmap to Targeted Therapies. *Blood Cancer Discov.* **2**, 19–31 (2021).
67. Brady, S. W. *et al.* The genomic landscape of pediatric acute lymphoblastic leukemia. *Nat. Genet.* **54**, 1376–1389 (2022).
68. Ma, X. *et al.* Pan-cancer genome and transcriptome analyses of 1,699 paediatric leukaemias and solid tumours. *Nature* **555**, 371–376 (2018).
69. Liu, Y. *et al.* The genomic landscape of pediatric and young adult T-lineage acute lymphoblastic leukemia. *Nat. Genet.* **49**, 1211–1218 (2017).
70. Ellisen, L. W. *et al.* TAN-1, the human homolog of the *Drosophila* Notch gene, is broken by

- chromosomal translocations in T lymphoblastic neoplasms. *Cell* **66**, 649–661 (1991).
71. Ferrando, A. A. The role of NOTCH1 signaling in T-ALL. *Hematology* **2009**, 353–361 (2009).
 72. Ferrando, A. NOTCH mutations as prognostic markers in T-ALL. *Leukemia* **24**, 2003–2004 (2010).
 73. Petit, A. *et al.* Oncogenetic mutations combined with MRD improve outcome prediction in pediatric T-cell acute lymphoblastic leukemia. *Blood* **131**, 289–300 (2018).
 74. Breit, S. *et al.* Activating NOTCH1 mutations predict favorable early treatment response and long-term outcome in childhood precursor T-cell lymphoblastic leukemia. *Blood* **108**, 1151–1157 (2006).
 75. Park, M.-J. *et al.* FBXW7 and NOTCH1 mutations in childhood T cell acute lymphoblastic leukaemia and T cell non-Hodgkin lymphoma. *Br. J. Haematol.* **145**, 198–206 (2009).
 76. Asnafi, V. *et al.* NOTCH1/FBXW7 mutation identifies a large subgroup with favorable outcome in adult T-cell acute lymphoblastic leukemia (T-ALL): a Group for Research on Adult Acute Lymphoblastic Leukemia (GRAALL) study. *Blood* **113**, 3918–3924 (2009).
 77. Mansour, M. R. *et al.* Prognostic implications of NOTCH1 and FBXW7 mutations in adults with T-cell acute lymphoblastic leukemia treated on the MRC UKALLXII/ECOG E2993 protocol. *J. Clin. Oncol. Off. J. Am. Soc. Clin. Oncol.* **27**, 4352–4356 (2009).
 78. Clappier, E. *et al.* NOTCH1 and FBXW7 mutations have a favorable impact on early response to treatment, but not on outcome, in children with T-cell acute lymphoblastic leukemia (T-ALL) treated on EORTC trials 58881 and 58951. *Leukemia* **24**, 2023–2031 (2010).
 79. Inaba, H. & Mullighan, C. G. Pediatric acute lymphoblastic leukemia. *Haematologica* **105**, 2524–2539 (2020).
 80. Raetz, E. A. & Teachey, D. T. T-cell acute lymphoblastic leukemia. *Hematology* **2016**, 580–

- 588 (2016).
81. Wu, Y. *et al.* Therapeutic antibody targeting of individual Notch receptors. *Nature* **464**, 1052–1057 (2010).
 82. Yen, W.-C. *et al.* Targeting Notch signaling with a Notch2/Notch3 antagonist (tarextumab) inhibits tumor growth and decreases tumor-initiating cell frequency. *Clin. Cancer Res. Off. J. Am. Assoc. Cancer Res.* **21**, 2084–2095 (2015).
 83. Chiorean, E. G. *et al.* A Phase I First-in-Human Study of Enoticumab (REGN421), a Fully Human Delta-like Ligand 4 (Dll4) Monoclonal Antibody in Patients with Advanced Solid Tumors. *Clin. Cancer Res. Off. J. Am. Assoc. Cancer Res.* **21**, 2695–2703 (2015).
 84. Takebe, N., Nguyen, D. & Yang, S. X. Targeting notch signaling pathway in cancer: clinical development advances and challenges. *Pharmacol. Ther.* **141**, 140–149 (2014).
 85. Samon, J. B. *et al.* Preclinical analysis of the γ -secretase inhibitor PF-03084014 in combination with glucocorticoids in T-cell acute lymphoblastic leukemia. *Mol. Cancer Ther.* **11**, 1565–1575 (2012).
 86. A Study of LY3039478 in Combination With Dexamethasone in Participants With T-ALL/T-LBL - Study Results - ClinicalTrials.gov. <https://clinicaltrials.gov/ct2/show/results/NCT02518113>.
 87. Bristol-Myers Squibb. *Phase 1 Ascending Multiple-Dose Study to Evaluate the Safety, Pharmacokinetics (PK) and Pharmacodynamics (PD) of BMS-906024 in Subjects With Relapsed/Refractory T-cell Acute Lymphoblastic Leukemia or T-cell Lymphoblastic Lymphoma*. <https://clinicaltrials.gov/ct2/show/NCT01363817> (2019).
 88. Habets, R. A. *et al.* Safe targeting of T cell acute lymphoblastic leukemia by pathology-specific NOTCH inhibition. *Sci. Transl. Med.* **11**, eaau6246 (2019).
 89. Lehal, R. *et al.* Pharmacological disruption of the Notch transcription factor complex. *Proc.*

- Natl. Acad. Sci.* **117**, 16292–16301 (2020).
90. Stoeck, A. *et al.* Discovery of Biomarkers Predictive of GSI Response in Triple-Negative Breast Cancer and Adenoid Cystic Carcinoma. *Cancer Discov.* **4**, 1154–1167 (2014).
91. Robinson, D. R. *et al.* Functionally recurrent rearrangements of the MAST kinase and Notch gene families in breast cancer. *Nat. Med.* **17**, 1646–1651 (2011).
92. Cellectia Biotech AG. *A Phase I/IIA, Multi-Centre, Open-Label, Dose-Escalation Study With Expansion Arms to Assess the Safety, Tolerability, Pharmacokinetics and Preliminary Efficacy of CB-103 Administered Orally in Adult Patients With Locally Advanced or Metastatic Solid Tumours and Haematological Malignancies Characterised by Alterations of the NOTCH Signalling Pathway.* <https://clinicaltrials.gov/ct2/show/NCT03422679> (2022).
93. M, M. *et al.* CB-103: A novel CSL-NICD inhibitor for the treatment of NOTCH-driven T-cell acute lymphoblastic leukemia: A case report of complete clinical response in a patient with relapsed and refractory T-ALL. *EJHaem* **3**, (2022).
94. Bride, K. L. *et al.* Preclinical efficacy of daratumumab in T-cell acute lymphoblastic leukemia. *Blood* **131**, 995–999 (2018).
95. Krejcik, J. *et al.* Daratumumab depletes CD38+ immune regulatory cells, promotes T-cell expansion, and skews T-cell repertoire in multiple myeloma. *Blood* **128**, 384–394 (2016).
96. Moreno, L. *et al.* The Mechanism of Action of the Anti-CD38 Monoclonal Antibody Isatuximab in Multiple Myeloma. *Clin. Cancer Res. Off. J. Am. Assoc. Cancer Res.* **25**, 3176–3187 (2019).
97. Sanofi. *Open-label, Single-arm Trial to Evaluate Antitumor Activity, Safety, and Pharmacokinetics of Isatuximab Used in Combination With Chemotherapy in Pediatric Patients From 28 Days to Less Than 18 Years of Age With Relapsed/Refractory B or T*

- Acute Lymphoblastic Leukemia or Acute Myeloid Leukemia in First or Second Relapse.*
<https://clinicaltrials.gov/ct2/show/NCT03860844> (2022).
98. Janssen Research & Development, LLC. *An Open-label, Multicenter, Phase 2 Study Evaluating the Efficacy and Safety of Daratumumab in Pediatric and Young Adult Subjects ≥ 1 and ≤ 30 Years of Age With Relapsed/Refractory Precursor B-cell or T-cell Acute Lymphoblastic Leukemia or Lymphoblastic Lymphoma.*
<https://clinicaltrials.gov/ct2/show/NCT03384654> (2022).
99. Ofran, Y. *et al.* Daratumumab for eradication of minimal residual disease in high-risk advanced relapse of T-cell/CD19/CD22-negative acute lymphoblastic leukemia. *Leukemia* **34**, 293–295 (2020).
100. Trinquand, A. *et al.* Triggering the TCR Developmental Checkpoint Activates a Therapeutically Targetable Tumor Suppressive Pathway in T-cell Leukemia. *Cancer Discov.* **6**, 972–985 (2016).
101. Rouce, R. *Phase 1 Therapy With Manufactured Autologous T-Cells Expressing a Second Generation Chimeric Antigen Receptor (CAR) for Treatment of T-Cell Malignancies Expressing CD5 Antigen.* <https://clinicaltrials.gov/ct2/show/NCT03081910> (2022).
102. Hill, L. *Cell Therapy for High Risk T-cell Malignancies Using CD7-Specific CAR Expressed on Non-Edited T Cells (CRIMSON-NE).* <https://clinicaltrials.gov/ct2/show/NCT03690011> (2022).
103. DeVita, V. T. *et al.* Curability of advanced Hodgkin's disease with chemotherapy. Long-term follow-up of MOPP-treated patients at the National Cancer Institute. *Ann. Intern. Med.* **92**, 587–595 (1980).
104. Bosl, G. J. *et al.* VAB-6: an effective chemotherapy regimen for patients with germ-cell tumors. *J. Clin. Oncol. Off. J. Am. Soc. Clin. Oncol.* **4**, 1493–1499 (1986).

105. Bonadonna, G. *et al.* Combination chemotherapy as an adjuvant treatment in operable breast cancer. *N. Engl. J. Med.* **294**, 405–410 (1976).
106. Labrie, M., Brugge, J. S., Mills, G. B. & Zervantonakis, I. K. Therapy resistance: opportunities created by adaptive responses to targeted therapies in cancer. *Nat. Rev. Cancer* **22**, 323–339 (2022).
107. Vasan, N., Baselga, J. & Hyman, D. M. A view on drug resistance in cancer. *Nature* **575**, 299–309 (2019).
108. Fisher, B., Slack, N. H., Bross, I. D. F., & Cooperating Investigators. Cancer of the breast: Size of neoplasm and prognosis. *Cancer* **24**, 1071–1080 (1969).
109. Norton, L., Simon, R., Brereton, H. D. & Bogden, A. E. Predicting the course of Gompertzian growth. *Nature* **264**, 542–545 (1976).
110. Norton, L. & Simon, R. Growth curve of an experimental solid tumor following radiotherapy. *J. Natl. Cancer Inst.* **58**, 1735–1741 (1977).
111. Early Breast Cancer Trialists' Collaborative Group (EBCTCG). Increasing the dose intensity of chemotherapy by more frequent administration or sequential scheduling: a patient-level meta-analysis of 37 298 women with early breast cancer in 26 randomised trials. *Lancet Lond. Engl.* **393**, 1440–1452 (2019).
112. Corcoran, R. B. *et al.* EGFR-mediated re-activation of MAPK signaling contributes to insensitivity of BRAF mutant colorectal cancers to RAF inhibition with vemurafenib. *Cancer Discov.* **2**, 227–235 (2012).
113. Prahallad, A. *et al.* Unresponsiveness of colon cancer to BRAF(V600E) inhibition through feedback activation of EGFR. *Nature* **483**, 100–103 (2012).
114. Azam, M., Seeliger, M. A., Gray, N. S., Kuriyan, J. & Daley, G. Q. Activation of tyrosine kinases by mutation of the gatekeeper threonine. *Nat. Struct. Mol. Biol.* **15**, 1109–1118

- (2008).
115. Juric, D. *et al.* Convergent loss of PTEN leads to clinical resistance to a PI(3)K α inhibitor. *Nature* **518**, 240–244 (2015).
 116. Mu, P. *et al.* SOX2 promotes lineage plasticity and antiandrogen resistance in TP53- and RB1-deficient prostate cancer. *Science* **355**, 84–88 (2017).
 117. Minchinton, A. I. & Tannock, I. F. Drug penetration in solid tumours. *Nat. Rev. Cancer* **6**, 583–592 (2006).
 118. Jain, R. K. Normalization of tumor vasculature: an emerging concept in antiangiogenic therapy. *Science* **307**, 58–62 (2005).
 119. Rini, B. I. *et al.* Pembrolizumab plus Axitinib versus Sunitinib for Advanced Renal-Cell Carcinoma. *N. Engl. J. Med.* **380**, 1116–1127 (2019).
 120. Makker, V. *et al.* Lenvatinib plus pembrolizumab in patients with advanced endometrial cancer: an interim analysis of a multicentre, open-label, single-arm, phase 2 trial. *Lancet Oncol.* **20**, 711–718 (2019).
 121. Lopes-Coelho, F., Martins, F., Pereira, S. A. & Serpa, J. Anti-Angiogenic Therapy: Current Challenges and Future Perspectives. *Int. J. Mol. Sci.* **22**, 3765 (2021).
 122. Zhang, J., Huang, D., Saw, P. E. & Song, E. Turning cold tumors hot: from molecular mechanisms to clinical applications. *Trends Immunol.* **43**, 523–545 (2022).
 123. Zaretsky, J. M. *et al.* Mutations Associated with Acquired Resistance to PD-1 Blockade in Melanoma. *N. Engl. J. Med.* **375**, 819–829 (2016).
 124. Merck Sharp & Dohme LLC. *A Randomized, Double-Blind, Phase III Study of Platinum+Pemetrexed Chemotherapy With or Without Pembrolizumab (MK-3475) in First Line Metastatic Non-squamous Non-small Cell Lung Cancer Subjects (KEYNOTE-189).* <https://clinicaltrials.gov/ct2/show/NCT02578680> (2023).

125. Merck Sharp & Dohme LLC. *A Randomized, Double-Blind, Phase III Study of Pembrolizumab (MK-3475) Plus Chemotherapy vs Placebo Plus Chemotherapy for Previously Untreated Locally Recurrent Inoperable or Metastatic Triple Negative Breast Cancer - (KEYNOTE-355)*. <https://clinicaltrials.gov/ct2/show/NCT02819518> (2022).
126. Waanders, E. *et al.* Mutational Landscape and Patterns of Clonal Evolution in Relapsed Pediatric Acute Lymphoblastic Leukemia. *Blood Cancer Discov.* **1**, 96–111 (2020).
127. Li, B. *et al.* Therapy-induced mutations drive the genomic landscape of relapsed acute lymphoblastic leukemia. *Blood* **135**, 41–55 (2020).
128. Wandler, A. M. *et al.* Loss of glucocorticoid receptor expression mediates in vivo dexamethasone resistance in T-cell acute lymphoblastic leukemia. *Leukemia* **34**, 2025–2037 (2020).
129. Barz, M. J. *et al.* Subclonal NT5C2 mutations are associated with poor outcomes after relapse of pediatric acute lymphoblastic leukemia. *Blood* **135**, 921–933 (2020).
130. Li, Y. *et al.* IL-7 Receptor Mutations and Steroid Resistance in Pediatric T cell Acute Lymphoblastic Leukemia: A Genome Sequencing Study. *PLOS Med.* **13**, e1002200 (2016).
131. Delgado-Martin, C. *et al.* JAK/STAT pathway inhibition overcomes IL7-induced glucocorticoid resistance in a subset of human T-cell acute lymphoblastic leukemias. *Leukemia* **31**, 2568–2576 (2017).
132. Palomero, T. *et al.* Mutational loss of PTEN induces resistance to NOTCH1 inhibition in T-cell leukemia. *Nat. Med.* **13**, 1203–1210 (2007).
133. Herranz, D. *et al.* Metabolic reprogramming induces resistance to anti-NOTCH1 therapies in T cell acute lymphoblastic leukemia. *Nat. Med.* **21**, 1182–1189 (2015).
134. Sanchez-Martin, M. *et al.* Synergistic antileukemic therapies in NOTCH1 -induced T-ALL. *Proc. Natl. Acad. Sci.* **114**, 2006–2011 (2017).

135. Mendes, R. D., Cante-Barrett, K., Pieters, R. & Meijerink, J. P. P. The relevance of PTEN-AKT in relation to NOTCH1-directed treatment strategies in T-cell acute lymphoblastic leukemia. *Haematologica* **101**, 1010–1017 (2016).
136. Trinquand, A. *et al.* Toward a *NOTCH1/FBXW7/RAS/PTEN* –Based Oncogenetic Risk Classification of Adult T-Cell Acute Lymphoblastic Leukemia: A Group for Research in Adult Acute Lymphoblastic Leukemia Study. *J. Clin. Oncol.* **31**, 4333–4342 (2013).
137. Paganin, M. *et al.* The presence of mutated and deleted PTEN is associated with an increased risk of relapse in childhood T cell acute lymphoblastic leukaemia treated with AIEOP-BFM ALL protocols. *Br. J. Haematol.* **182**, 705–711 (2018).
138. Knoechel, B. *et al.* An epigenetic mechanism of resistance to targeted therapy in T cell acute lymphoblastic leukemia. *Nat. Genet.* **46**, 364–370 (2014).
139. Cordo', V. *et al.* Phosphoproteomic profiling of T cell acute lymphoblastic leukemia reveals targetable kinases and combination treatment strategies. *Nat. Commun.* **13**, 1048 (2022).
140. Barde, I., Salmon, P. & Trono, D. Production and Titration of Lentiviral Vectors. in *Current Protocols in Neuroscience* (eds. Crawley, J. N. *et al.*) ns0421s53 (John Wiley & Sons, Inc., 2010). doi:10.1002/0471142301.ns0421s53.
141. Li, X. *et al.* Deregulated Gab2 phosphorylation mediates aberrant AKT and STAT3 signaling upon PIK3R1 loss in ovarian cancer. *Nat. Commun.* **10**, 716 (2019).
142. Chou, T.-C. Drug Combination Studies and Their Synergy Quantification Using the Chou-Talalay Method. *Cancer Res.* **70**, 440–446 (2010).
143. Li, W. *et al.* MAGeCK enables robust identification of essential genes from genome-scale CRISPR/Cas9 knockout screens. *12* (2014).
144. Subramanian, A. *et al.* Gene set enrichment analysis: A knowledge-based approach for

- interpreting genome-wide expression profiles. *Proc. Natl. Acad. Sci.* **102**, 15545–15550 (2005).
145. Yu, G., Wang, L.-G., Han, Y. & He, Q.-Y. clusterProfiler: an R Package for Comparing Biological Themes Among Gene Clusters. *OMICS J. Integr. Biol.* **16**, 284–287 (2012).
146. Liberzon, A. *et al.* The Molecular Signatures Database Hallmark Gene Set Collection. *Cell Syst.* **1**, 417–425 (2015).
147. Dolgalev I (2022). msigdbr: MSigDB Gene Sets for Multiple Organisms in a Tidy Data Format. R package version 7.5.1.
148. Kim, D., Paggi, J. M., Park, C., Bennett, C. & Salzberg, S. L. Graph-based genome alignment and genotyping with HISAT2 and HISAT-genotype. *Nat. Biotechnol.* **37**, 907–915 (2019).
149. Soneson, C., Love, M. I. & Robinson, M. D. Differential analyses for RNA-seq: transcript-level estimates improve gene-level inferences. *F1000Research* **4**, 1521 (2016).
150. Tarazona, S. *et al.* Data quality aware analysis of differential expression in RNA-seq with NOISeq R/Bioc package. *Nucleic Acids Res.* gkv711 (2015) doi:10.1093/nar/gkv711.
151. Robinson, M. D., McCarthy, D. J. & Smyth, G. K. edgeR: a Bioconductor package for differential expression analysis of digital gene expression data. *Bioinformatics* **26**, 139–140 (2010).
152. McCarthy, D. J., Chen, Y. & Smyth, G. K. Differential expression analysis of multifactor RNA-Seq experiments with respect to biological variation. *Nucleic Acids Res.* **40**, 4288–4297 (2012).
153. Love, M. I., Huber, W. & Anders, S. Moderated estimation of fold change and dispersion for RNA-seq data with DESeq2. *Genome Biol.* **15**, 550 (2014).
154. Ritchie, M. E. *et al.* limma powers differential expression analyses for RNA-sequencing and microarray studies. *Nucleic Acids Res.* **43**, e47–e47 (2015).

155. Waardenberg A (2022). consensusDE: RNA-seq analysis using multiple algorithms. R package version 1.14.0.
156. Kulak, N. A., Pichler, G., Paron, I., Nagaraj, N. & Mann, M. Minimal, encapsulated proteomic-sample processing applied to copy-number estimation in eukaryotic cells. *Nat. Methods* **11**, 319–324 (2014).
157. Dorfer, V. *et al.* MS Amanda, a Universal Identification Algorithm Optimized for High Accuracy Tandem Mass Spectra. *J. Proteome Res.* **13**, 3679–3684 (2014).
158. Kong, A. T., Leprevost, F. V., Avtonomov, D. M., Mellacheruvu, D. & Nesvizhskii, A. I. MSFragger: ultrafast and comprehensive peptide identification in mass spectrometry-based proteomics. *Nat. Methods* **14**, 513–520 (2017).
159. R Core Team (2020). R: A language and environment for statistical computing. R Foundation for Statistical Computing, Vienna, Austria.
160. Plubell, D. L. *et al.* Extended Multiplexing of Tandem Mass Tags (TMT) Labeling Reveals Age and High Fat Diet Specific Proteome Changes in Mouse Epididymal Adipose Tissue. *Mol. Cell. Proteomics* **16**, 873–890 (2017).
161. Benjamini, Y. & Hochberg, Y. Controlling the False Discovery Rate: A Practical and Powerful Approach to Multiple Testing. *J. R. Stat. Soc. Ser. B Methodol.* **57**, 289–300 (1995).
162. Szklarczyk, D. *et al.* The STRING database in 2021: customizable protein–protein networks, and functional characterization of user-uploaded gene/measurement sets. *Nucleic Acids Res.* **49**, D605–D612 (2021).
163. Shalem, O. *et al.* Genome-Scale CRISPR-Cas9 Knockout Screening in Human Cells. *Science* **343**, 84–87 (2014).
164. Cheung, L. W. T. *et al.* High Frequency of *PIK3R1* and *PIK3R2* Mutations in Endometrial

- Cancer Elucidates a Novel Mechanism for Regulation of PTEN Protein Stability. *Cancer Discov.* **1**, 170–185 (2011).
165. Chen, L. *et al.* Characterization of PIK3CA and PIK3R1 somatic mutations in Chinese breast cancer patients. *Nat. Commun.* **9**, 1357 (2018).
166. Olsen, J. V. *et al.* Global, In Vivo, and Site-Specific Phosphorylation Dynamics in Signaling Networks. *Cell* **127**, 635–648 (2006).
167. Franciosa, G. *et al.* Proteomics of resistance to Notch1 inhibition in acute lymphoblastic leukemia reveals targetable kinase signatures. *Nat. Commun.* **12**, 2507 (2021).
168. Ladewig, E. *et al.* The Oncogenic PI3K-Induced Transcriptomic Landscape Reveals Key Functions in Splicing and Gene Expression Regulation. *Cancer Res.* **82**, 2269–2280 (2022).
169. Gutierrez, A. *et al.* High frequency of PTEN, PI3K, and AKT abnormalities in T-cell acute lymphoblastic leukemia. *Blood* **114**, 647–650 (2009).
170. Aziz, S. A. *et al.* Phosphatidylinositol-3-Kinase as a Therapeutic Target in Melanoma. *Clin. Cancer Res.* **15**, 3029–3036 (2009).
171. Yuan, T. L. & Cantley, L. C. PI3K pathway alterations in cancer: variations on a theme. *Oncogene* **27**, 5497–5510 (2008).
172. Dillon, R. L., White, D. E. & Muller, W. J. The phosphatidyl inositol 3-kinase signaling network: implications for human breast cancer. *Oncogene* **26**, 1338–1345 (2007).
173. Zuurbier, L. *et al.* The significance of PTEN and AKT aberrations in pediatric T-cell acute lymphoblastic leukemia. *Haematologica* **97**, 1405–1413 (2012).
174. Medyouf, H. *et al.* Acute T-cell leukemias remain dependent on Notch signaling despite PTEN and INK4A/ARF loss. *Blood* **115**, 1175–1184 (2010).
175. Hagenbeek, T. J. *et al.* Murine Pten^{-/-} T-ALL requires non-redundant PI3K/mTOR and DLL4/Notch1 signals for maintenance and γ c/TCR signals for thymic exit. *Cancer Lett.* **346**,

- 237–248 (2014).
176. Dentro, S. C., Wedge, D. C. & Van Loo, P. Principles of Reconstructing the Subclonal Architecture of Cancers. *Cold Spring Harb. Perspect. Med.* **7**, a026625 (2017).
177. Palomero, T. *et al.* NOTCH1 directly regulates *c-MYC* and activates a feed-forward-loop transcriptional network promoting leukemic cell growth. *Proc. Natl. Acad. Sci.* **103**, 18261–18266 (2006).
178. Naro, C. & Sette, C. Phosphorylation-Mediated Regulation of Alternative Splicing in Cancer. *Int. J. Cell Biol.* **2013**, 1–15 (2013).
179. Zenatti, P. P. *et al.* Oncogenic IL7R gain-of-function mutations in childhood T-cell acute lymphoblastic leukemia. *Nat. Genet.* **43**, 932–939 (2011).
180. Jena, N. *et al.* CDK6-mediated repression of CD25 is required for induction and maintenance of Notch1-induced T-cell acute lymphoblastic leukemia. *Leukemia* **30**, 1033–1043 (2016).
181. Choi, Y. J. *et al.* The Requirement for Cyclin D Function in Tumor Maintenance. *Cancer Cell* **22**, 438–451 (2012).
182. Sawai, C. M. *et al.* Therapeutic Targeting of the Cyclin D3:CDK4/6 Complex in T Cell Leukemia. *Cancer Cell* **22**, 452–465 (2012).
183. Pikman, Y. *et al.* Synergistic Drug Combinations with a CDK4/6 Inhibitor in T-cell Acute Lymphoblastic Leukemia. *Clin. Cancer Res.* **23**, 1012–1024 (2017).
184. Wuyts, W. & Van Hul, W. Molecular basis of multiple exostoses: mutations in the EXT1 and EXT2 genes. *Hum. Mutat.* **15**, 220–227 (2000).
185. Ropero, S. *et al.* Epigenetic loss of the familial tumor-suppressor gene exostosin-1 (EXT1) disrupts heparan sulfate synthesis in cancer cells. *Hum. Mol. Genet.* **13**, 2753–2765 (2004).

186. Stanley, P. Regulation of Notch signaling by glycosylation. *Curr. Opin. Struct. Biol.* **17**, 530–535 (2007).
187. Haines, N. & Irvine, K. D. Glycosylation regulates Notch signalling. *Nat. Rev. Mol. Cell Biol.* **4**, 786–797 (2003).
188. Hartley, S. W. & Mullikin, J. C. Detection and visualization of differential splicing in RNA-Seq data with JunctionSeq. *Nucleic Acids Res.* gkw501 (2016) doi:10.1093/nar/gkw501.
189. Zhao, J., Song, X. & Wang, K. IncScore: alignment-free identification of long noncoding RNA from assembled novel transcripts. *Sci. Rep.* **6**, 34838 (2016).
190. Trincado, J. L. *et al.* SUPPA2: fast, accurate, and uncertainty-aware differential splicing analysis across multiple conditions. *Genome Biol.* **19**, 40 (2018).
191. Han, C. *et al.* SF3B1 homeostasis is critical for survival and therapeutic response in T cell leukemia. *Sci. Adv.* **8**, eabj8357 (2022).

Acknowledgements

First and foremost, I would like to express my sincere gratitude to Freddy, for giving me the opportunity to work on my thesis and for continuously guiding me through my projects all these years. As an academic mentor, he offers fantastic scientific support and advice. As a loving supervisor, his genial understanding and cordial encouragement is crucial for my PhD career. I'm blessed to have him on this journey!

I wish to thank Gustavo and Nadine, who have provided excellent bioinformatic analyses, great discussions and scientific inputs throughout this project. I want to thank Yuanlong, who has offered generous help on bioinformatic analyses. I would like to thank the EPFL core facilities: FCCF, BSF, HCF, BIOP, CPG, and in particular Bastien and Elisa from GECF, and Romain, Florence and Maria from PCF. They have continuously offered fantastic technical supports, great discussions and scientific inputs.

I would like to thank all members of the Jury: Dr. Elisa Oricchio, Dr. Jules Meijerink, Dr. Andreas Trumpp, Dr. Bart Deplancke for their time and insightful comments.

I wish to thank my mentor Dr. Joerg Huelsken for his kind support and great discussions.

I would like to thank Ute, our lab mom, for her tremendous mental support and compassion, scientific discussions and supervisions. Thanks to Marianne and Pasqualina, for their kindness and wonderful technical supports in the lab. I want to thank the past members of Radtke Lab: Alain, Markus, for welcoming me in the bay and their generous advice; Tara for her kindness; Christelle, Charlotte, Michele, for being always amiable and cheerful; Delphine, for always available to share her experience; Mateusz, for sharing this journey with me through many years; Jessica and Erta, for their energy and charms. I want to thank my current lab members: Jelena, for always being considerate, supportive and warm; Amber, for always radiating positivity and eagerness to help; Morgane, for always full of vibrancy and kindness; Anita, for always being gentle and understanding; Joaquim, Elia, Mariia, Mario, Erhan, for their vigor and wisdom, and joy to interact with and learn from.

I want to thank past and present colleagues Qiqun, Yuqing, Gerard, Elena, Maria, Aaron, Valentina, Patrick, Natalya, Kannu, Pierre and many more, who I have had the opportunity to interact with, learn from and share this journey with.

I wish to thank Dr. L., Dr. S., Dr. B., for supporting me all these years.

I would like to thank my friends. Big hugs to all YiYanBaDing members, it's amazing to share with you everything despite time-zone differences. Thanks to Li and Xiaojing, for your great support and company. Thanks to Jing, Yueyun, Qianhui, Dong, Jiabin, Ruxandra, for knocking on my door and for holding me in the ups and downs in Lausanne. Thanks to Elisa and Giovanni, it's simply a privilege to have you in my life.

Last but not least, I wish to thank my family from the bottom of my heart. Thanks Anne, Sophie, for being there for me. Thanks Hulu, you are an angel. 非常感谢爸爸妈妈, 你们对我的爱、无私抚育和培养、无限鼓励和支持, 使我走到今天并将一直进行下去。 Thanks Fabien, for making me complete, and Felix, for showing me what a miracle is. And thanks to that me a few years back, for simply going on.

CV

Linlin CAO

Chinese | Swiss work permit B | Married
Allée du Rionzi 6, 1028 Préverenges, Switzerland
+41 78 638 45 28 | Lynncaoccc@gmail.com
ORCID: 0000-0002-8667-1571 | [linkedin.com/in/linlin-cao-2205162a](https://www.linkedin.com/in/linlin-cao-2205162a)

Education

- 11.2016 – Present **Ecole Polytechnique Fédérale de Lausanne (EPFL), Switzerland**
Ph.D student, Molecular Life Sciences
- 2008 – 2012 **Tsinghua University, China**
B.S., Biological Science and Technology

Research Experience

- 11.2016 – 03.2023 **EPFL, Lausanne, Switzerland - Doctoral Student**
- Discovered the resistance mechanism to Notch inhibition and designed novel combination therapy in human T-cell leukemia.
 - Discovered the varying sensitivities and kinetics of response to a novel Notch inhibitor CB-103 which is currently in Phase I/II clinical trial.
- 07.2012 – 05.2015 **Memorial Sloan Kettering Cancer center, NYC, USA - Graduate Research Assistant**
- Identified candidate genes that lead to the discovery of NRF2 activation as a mechanism of resistance to eIF4A inhibitors in cancer therapy
 - Established the translational profile that leads to the discovery of acute immune translational response program in CD8 memory T lymphocytes upon activation
 - Investigated murine models for Mantle Cell Lymphomagenesis
- 10.2009 – 01.2012 **Tsinghua Stem Cell Center, Beijing, China - Research Assistant**
- Investigated the differentiation of Germline Stem Cell in Drosophila
 - Investigated the regulation of aging and lifespan in Drosophila

Professional Experience

- 02.2016 – 06.2016 **China Center for Disease Control and Prevention (CDC), Beijing, China - Intern**
- Performed SAS analysis on China Nutritional and Health Survey database & reviews and reports
 - Developed "Potato Intake Intervention" projects in collaboration with Chinese Ministry of Agriculture
 - Translated and edited Report of China National Nutrition and Health Survey
- 02.2016 – 06.2016 **TiP Lab Ltd., Shanghai, China - IP Analyst (Part-time)**
Established analysis on Cancer Immunotherapy Patents and Industry Trend study

Publications

Salloum D., Singh K., Davidson N. R., **Cao L.**, [...], Wendel H.G.
A Rapid Translational Immune Response Program in CD8 Memory T Lymphocytes.
The Journal of Immunology (2022).

Sanghvi V. R., Mohan P., Singh K., **Cao L.**, [...], Wendel H.G.
NRF2 Activation Confers Resistance to eIF4A Inhibitors in Cancer Therapy.
Cancers (2021).

Lehal R., Zaric J., Vigolo M., Urech C., Frismantas V., Zangger N., **Cao, L.**, [...], Radtke F.
Pharmacological disruption of the Notch transcription factor complex.
Proceedings of the National Academy of Sciences (2020).

Cao L., Buendia G.A.R., Fournier N., Liu Y., Armand F., Hamelin R., Pavlou M., Radtke F.
Resistance mechanism to Notch inhibition and combination therapy in human T cell acute lymphoblastic leukemia.
Leukemia, Under review

Skills

Language: English (Full professional proficiency), Mandarin (Native proficiency), French (Elementary proficiency)

Software and programming: FlowJo, Prism, ImageJ, QuPath, Cytoscape, IGV, MS Office; R, Python

Molecular and Cell Biology techniques: whole genome CRISPR-Cas9 screens; sample preparation for DNA- and RNA-seq, SLAM-seq, Ribo-seq, LC-MS (phosphor-) proteomics; molecular cloning; immunoblotting; PCR, RT-qPCR; cell culture; Fetal liver stem cell/HSC harvesting and engineering; Primary T cell harvesting and activation assay; genome editing; CRISPR knockout cell line generation; drug screening; multicolor flow cytometry; proliferation assay; cell viability assay; cell cycle assay; immunofluorescence assay and immunohistochemical analysis.

Mouse: mouse handling, intraperitoneal injection, intravenous injection, subcutaneous injection, oral gavage, *in vivo* imaging, tumor harvesting. (Licensed for mouse experimentation in Switzerland)

Transferable skills: experimental design, literature review, data interpretation, analytic reasoning, critical thinking, problem solving, flexibility and adaptability, communication skills (presentations in internal and external meetings, seminars, conferences), teamwork and collaboration outreach, writing skills (annual reports, manuscript), project management.

Awards

11.2011 **Silver Prize - International Genetically Engineered Machine (iGEM) competition**

2010 – 2012 **Scholarship for Tsinghua Xuetang Talented Program for academic excellence**

Training courses

2021 Single-cell Transcriptomics (SIB)

NGS - Quality control, Alignment, Visualisation (SIB)

Advanced Technical Presentation (Thoughtstream)

2019 Python Bootcamp (EPFL)

2018 R programming (Coursera)

Transcriptomics Analysis: RNA-seq (SIB)

2017 Python for Life Scientists (SIB)

Academic Writing for Doctoral Students level C2 (EPFL)

2017 RESAL module I (FELASA)

Presentations

08.2021 **ISREC-SCCL Symposium “Hallmarks of Cancer – 21 Years On”, Lausanne, Switzerland**
Poster presentation

11.2019 **ISREC Retreat 2019, Lausanne, Switzerland**
Poster presentation

06.2019 **Stem Cell Retreat 2019, Basel, Switzerland**
Oral presentation

Teaching

BIOENG-433 Biotechnology Lab (3 semesters), EPFL

BIO-205 Cellular and molecular biology I (1 semester), EPFL